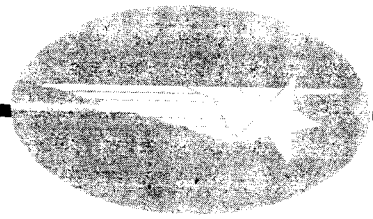

[redacted]

[redacted]

GPO PRICE $ _____

OTS PRICE(S) $ _____

Hard copy (HC) 4.00

Microfiche (MF) 1.00

LMSC M-50-65-1

26 March 1965

Eight-Month Progress Report For Period 27 June 1964 to 27 February 1965

SOLAR-RADIATION-INDUCED DAMAGE TO OPTICAL PROPERTIES OF ZnO-TYPE PIGMENTS

NAS 8-11266

Project Leader: L. A. McKellar

LOCKHEED MISSILES & SPACE COMPANY

A GROUP DIVISION OF LOCKHEED AIRCRAFT CORPORATION

SUNNYVALE, CALIFORNIA

FOREWORD

This report was prepared by the Research Laboratories of Lockheed Missiles & Space Company, for the George C. Marshall Space Flight Center of the National Aeronautics and Space Administration. The work was performed under contract NAS 8-11266. The contract was administered by the Research Projects Laboratory of Marshall Space Flight Center.

This Eight-Month Progress Report describes work performed from 27 June 1964 to 27 February 1965.

PERSONNEL

The following personnel are responsible for the work described in this report.

L. A. McKellar
J. S. Blakemore
K. F. Cuff
S. A. Greenberg
C. D. Kuglin
H. F. MacMillan
A. F. Sklensky
W. E. Spicer
E. R. Washwell
L. R. Williams

The program is being carried out under the direction of L. A. McKellar. Critical review of the literature was performed primarily by J. S. Blakemore. The theoretical and experimental studies of bulk properties were carried out by K. F. Cuff, J. S. Blakemore, E. R. Washwell, and L. R. Williams. Preparation and characterization of particulate samples were performed by S. A. Greenberg. Design and construction of the bi-directional reflectance apparatus and the in situ measurements were performed by H. F. MacMillan and A. F. Sklensky, assisted by consultation with R. E. Rolling and D. J. Ballegeer; R. A. Breuch initially conceived the apparatus.

The band structure calculations were carried out by C. D. Kuglin. General advice on band structure calculations were provided by F. Herman. Review, evaluating, and intercomparison of data and information obtained from the studies of particulate

and single crystal samples was performed primarily by K. F. Cuff, S. A. Greenberg, W. E. Spicer, and E. R. Washwell. General consultation on all aspects of the program was provided by W. E. Spicer.

CONTENTS

ILLUSTRATIONS

TABLES

Section 1
INTRODUCTION

Successful operation of space vehicles demands that components be maintained within their designed temperature limits. Control of temperatures on an operational spacecraft is based on the exchange of radiant energy with the vehicle's environment, and therefore, with the optical properties of the exterior surfaces. Design requirements often dictate the use of a surface with a low ratio of solar absorptance (α_s) to emittance (ϵ). These surfaces are generally susceptible to damage by natural or induced radiation in space, resulting in an increase in α_s.

Of all sources of radiation encountered in space, both natural and induced, the ultraviolet portion of the solar spectrum is the most important source of damage to low α_s/ϵ surfaces. In general, ultraviolet-induced damage is at least as great as that due to other forms of radiation. In addition, all space vehicles are exposed to high fluxes of solar radiation. In contrast, all vehicles do not experience high doses of Van Allen, nuclear, or other forms of high-energy radiation.

Over the past five years a large body of data on the effects of simulated solar ultraviolet radiation in vacuum on low α_s/ϵ thermal control surfaces has been generated by various agencies concerned with spacecraft (Refs. 1 – 12). Time requirements necessitated concentration on the achievement of relatively crude engineering design data. Available information on solar-radiation-induced damage to thermal control surfaces is virtually entirely empirical. Since complete environmental simulation is never achieved in the laboratory, precise prediction of behavior in space from the existing laboratory testing data is not possible. This problem is demonstrated by the comparison of laboratory and spacecraft data shown in Ref. 13.

This report documents the activities and progress of an investigation into the mechanisms of solar-radiation-induced damage to the optical properties of zinc oxide. The first eight months of effort are reported.

Central to the investigation is an experimental study of the optical behavior of particulate samples of zinc oxide; particle size is essentially that of the pigment in a low α_s white paint. Carefully prepared particulate samples are exposed to radiation of wavelengths between 0.2 and 2.6 microns (μ). Parameters being varied in both initial exposures and studies of damage reversibility are the flux density, spectrum, and time of exposure, and the sample temperature and gaseous environment. Selected exposures are being performed in which the bi-directional spectral reflectance of the sample is monitored during exposure (in situ). The in situ measurements provide the key to comprehensive detailed knowledge of optical damage to particulate samples. In addition, static ultraviolet tests with before- and after-exposure measurements have been carried out to supplement the slower, more thorough tests with in situ measurements.

A parallel theoretical and experimental program to describe the pertinent bulk and surface properties of zinc oxide is underway; the goal of these parallel efforts is a comprehensive explanation of phenomena observed in the particulate samples. The extensive and often contradictory literature on zinc oxide is being critically evaluated and related to the observed optical damage. Selected measurements of optical and transport properties of zinc oxide single crystals are being performed, when required, to formulate a coherent picture of zinc oxide optical behavior, or to resolve contradictions and fill voids in the open literature. Electronic energy band structure calculations for the ideal crystal have been performed as a point of departure for the understanding of electronic behavior in real crystals.

The study is directed toward identification of the primary mechanisms involved in solar-radiation-induced damage to the optical properties of ZnO-type semiconductor pigments, as exemplified by ZnO itself.

Knowledge of the damage mechanisms would greatly simplify the problem by providing a rational basis both for the design of environmental tests and for interpretation of the resulting data. Ultimately, such knowledge would guide materials specialists in the development of optimum materials.

The type of low α_s/ϵ surface usually employed on spacecraft is a white coating made up of a pigment dispersed in a binder. A definitive understanding of the changes in the spectra of such systems is impossible unless the behavior of each component alone is first understood. A detailed study has been undertaken to better understand the behavior of the pigment itself. If this study is to produce positive results, it must concentrate on one pigmenting material. The ideal material would possess the following attributes:

- Simple, well-defined chemical and electronic structure.
- Data available on optical, electrical, and related physical properties.
- Representative of a class of stable white pigments.
- In use in promising thermal control coatings.

Zinc oxide possesses each of the above characteristics to a greater degree than does any other single material. ZnO is the most widely quoted example of a metal excess (n-type) semiconductor, and a great deal of work has been done with sintered material as well as single crystals. Considerable progress has been made in characterizing the electrical and optical properties of ZnO, although it is by no means completely understood. Furthermore, its properties are similar to those of titanium dioxide, zinc sulfide, and stannic oxide; ZnO, TiO_2, ZnS, and SnO_2 are all in use as pigments in promising white thermal control surfaces. Study of ZnO, then, is a logical starting point for investigation of the mechanisms involved in solar-radiation-induced damage to low α_s/ϵ surfaces.

2.0 ZINC OXIDE PROPERTIES AFFECTING OPTICAL BEHAVIOR

2.1 INTRODUCTION

ZnO is a II-VI compound semiconductor which crystallizes in the hexagonal wurtzite structure (B_4-type). The binding is largely polar, but there is also significant covalent binding; ZnO stands somewhat between the polar alkali halides and the covalent bonded group IV semiconductors.

The energy gap of ZnO is 3.2 eV (0.38μ) at 300°K and appears to be a direct gap located at the center of the Brillouin zone. The optical absorption coefficient has the characteristic steep rise at this energy and reaches a value greater than 2×10^5 cm^{-1} at photon energies greater than the band gap. The ultraviolet reflection spectra (Ref. 14) is just beginning to receive serious attention and will play a strong role in elucidating the overall band structure of ZnO (see Section 5). Infrared studies on single crystals have revealed the characteristic lattice absorption spectra of ZnO, and also distinct free carrier absorption effects. Electron paramagnetic resonance, visible and infrared absorption, photoconductivity and luminescence studies have provided some information on the details of the impurity levels in ZnO.

ZnO is an n-type semiconductor; hole conductivity has not been observed to date. The conduction band has an effective mass of 0.27 m_o and an electron mobility of 60 cm^2/volt-sec at 300°K (Ref. 15). The resistivity of ZnO crystals can be varied over a wide range by doping; from about 10^{-2} ohm-cm to greater than 10^{11} ohm-cm at 300°K. Extensive transport studies have been carried out on ZnO and many of its basic semiconducting properties have been characterized.

Because ZnO has been rather thoroughly studies, there is a relatively large amount of information concerning its transport, optical, photoconductive and catalytic properties. In the following sections (2.2 to 2.5) some of these

properties of ZnO which have a direct bearing on the formulation of the ultraviolet damage mechanism are discussed in detail. Finally, in Section 2.6, a working degradation model is formulated.

2.2 SURFACE PHENOMENA

Before discussing photoconduction and degradation effects in ZnO, it is important to point out some of the pertinent phenomena which occur at semiconductor surfaces. For simplicity, we will consider an n-type semiconductor as is the case for ZnO. In Fig. 2-1a we have indicated a semiconductor surface with a net negative charge and in Fig. 2-1b a surface with a net positive charge.

A negative surface charge will, of course, repel electrons near the surface creating a depletion region (depleted of electrons) with a net positive charge near the surface due to ionized donors. The potential barrier height V_s is produced at the surface, bending both the conduction and valence bands upwards (with respect to the bands in the volume of the crystal). It should be noted that in this case holes in the depletion region are strongly attracted to the surface.

A positive surface charge on the other hand, will attract electrons toward the surface causing an accumulation layer of electrons adjacent to the surface. In this instance the bands bend downward at the surface with respect to the bulk; holes in the valence band are repelled from the surface.

Without developing the relationship between the donor density, barrier heights, surface charge and space charge dimension ℓ, it is important simply to point out the magnitudes of these quantities expected in ZnO crystals and pigments (for a full treatment see G. Heiland (Ref. 16)). The maximum surface charge density (as would exist in an atmosphere of air) will be approximately 10^{12} - 10^{13} charges per cm^2. In vacuum the surface charge density will in general be much less than this. At this maximum surface charge density and with donor concentrations in the range of 10^{16} to 10^{18} cm^3, the barrier height V_s will be in the range of 0.1 to 1.0 ev and the depletion region depth will be of the order of 100 to 1000 Å. The important point here is that these are the magnitude of the effects to be expected in the pigments under investigation in this contract.

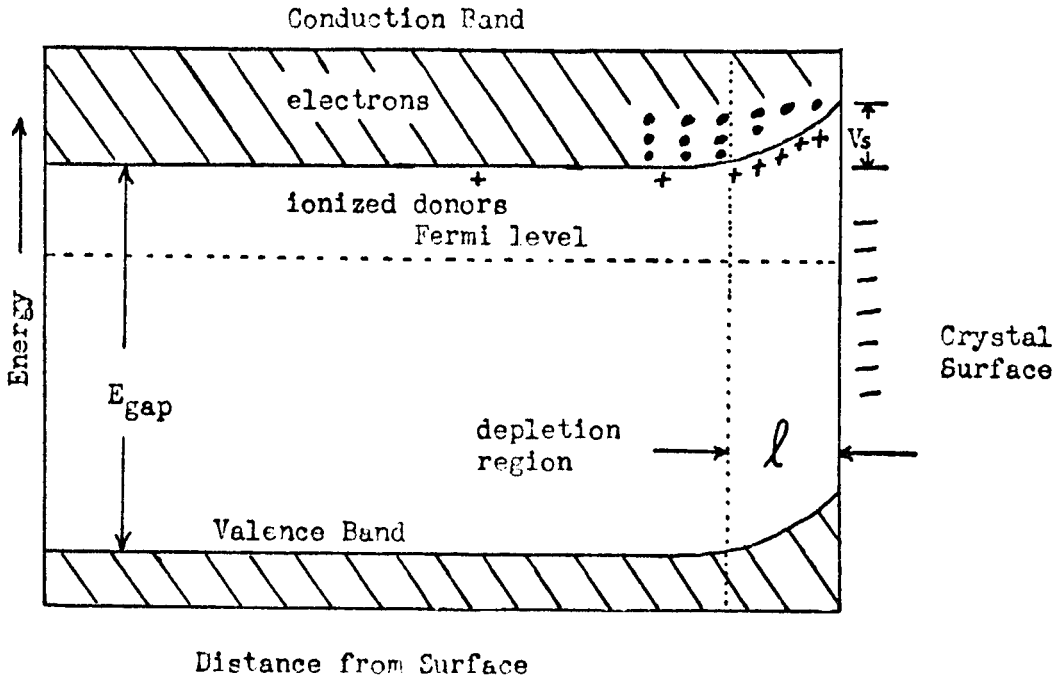

2-1a Surface Band Bending In Depletion Region

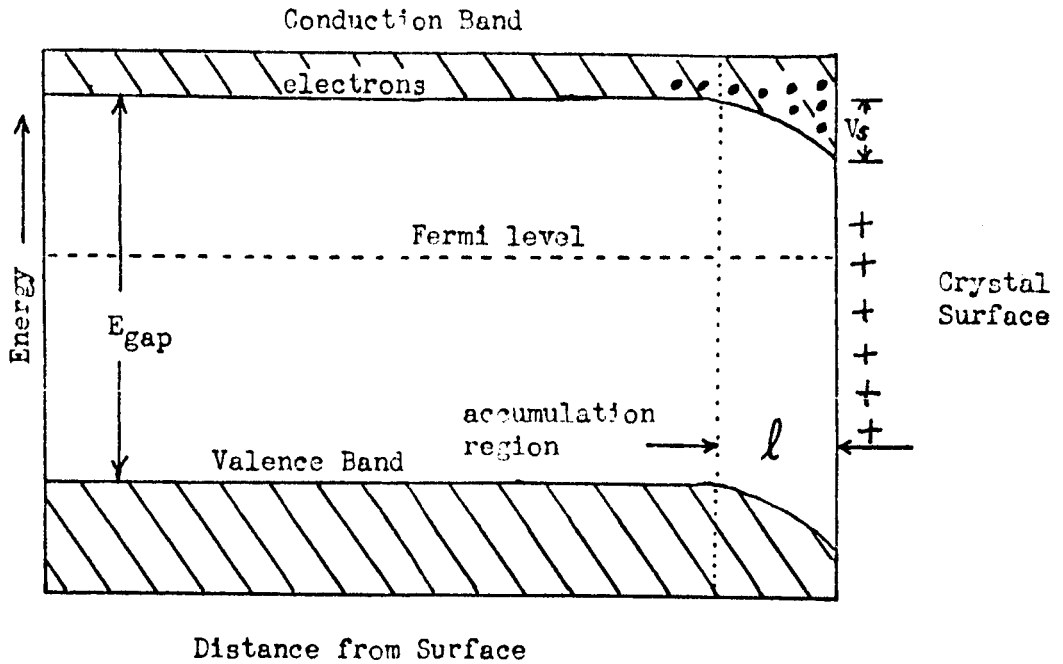

2-1b Surface Band Bending In Accumulation Region

The phenomena of surface conduction in a ZnO crystal occurs, for example, when the surface has been reduced; say with hydrogen or excess zinc. This will produce the band bending shown in Fig. 2-1b where the electron conduction now occurs predominately in the accumulation region near the crystal surface. The enhanced conductivity which is observed when surface conduction occurs is the result of donors diffusing inward to provide additional free carriers. The diffusion distance does not have to be any greater than the accumulation layer depth which is relatively small (approximately 100-1000 $\mathring{A}$).

Another important feature to bear in mind is the relationship between the Fermi level in the crystal and the location of the surface states in energy in determining the type and degree of band bending at the surface. First let us consider a negative surface-charge state with a sufficiently small density ($<<10^{12}/cm^2$) such that the Fermi level is not pinned at the surface state. Then if the Fermi level is above the energy level of the surface state, that surface state will contain electrons and provide a negative surface charge. If the Fermi level is below the surface state, it must be depleted of electrons, and no negative surface charge will exist. This model is shown in Fig. 2-2 for the two cases, where it will be noted that the usual depletion region and upward band bending occurs in the first case and no band bending occurs in the second case. By appropriate doping of the ZnO crystal, the Fermi level in the bulk can be lowered; e.g., down to approximately midway between conduction and valence bands by Li substitutional impurites. It is then possible to control the band bending at the surface by changing the volume characteristics of the crystallites. If the surface charge density is sufficiently large, however, then the Fermi level at the surface will be anchored at the surface impurity level, regardless of the position of the Fermi level in the bulk of the crystal. Therefore, it can be seen that modification of the position of the Fermi level in the bulk of the crystallites can produce marked changes in its surface properties such as its photoadsorption-desorption characteristics.

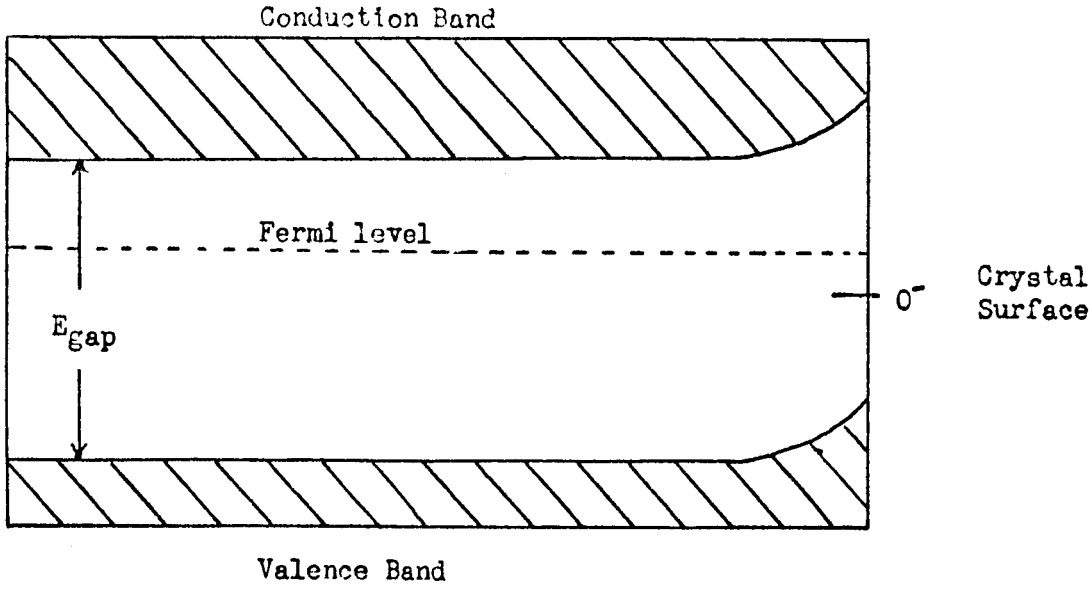

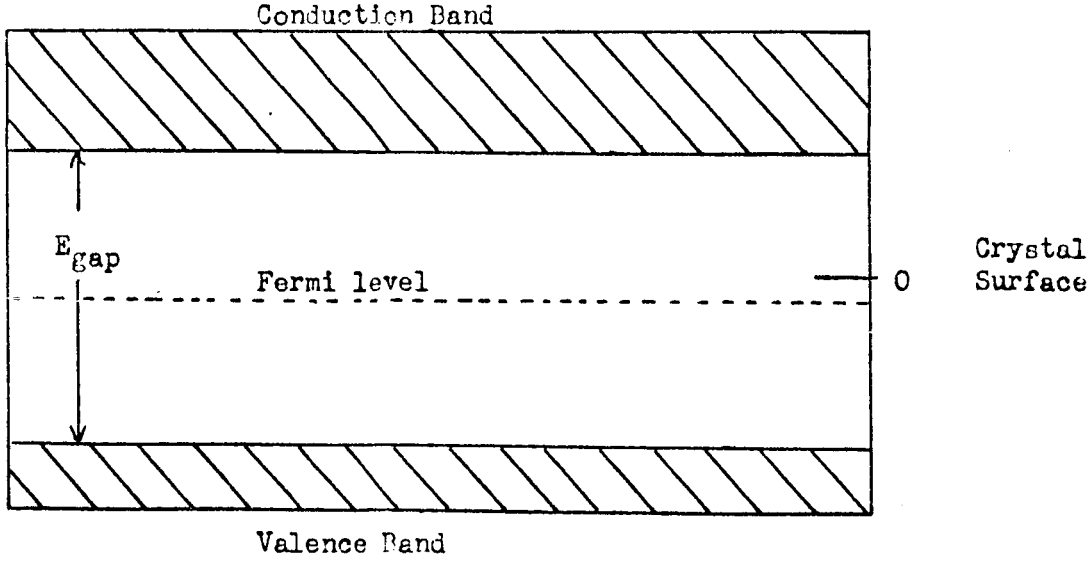

2-2 Effect of Fermi level on Surface State Occupancy

2.3 BULK IMPURITY STATES

Donors

The known donor states are interstitial Zn, and interstitial Li and Cu when added as impurities. Also Group III elements such as Ga and In when incorporated substitutionally act as donors. These levels, which are singly ionized, exist approximately 0.05 eV below the conduction band and appear to take the form of simple hydrogen-like impurity levels. It should be noted that an electron in a hydrogen-like impurity state near a band edge will have a binding energy of

$$E = \frac{13.6\ m^*}{K^2} \quad \text{ev}$$

where m* is the effective mass of an electron in the band in question and K is the static dielectric constant (K = 8.5 for ZnO). As an example, for an electron in or "near" the conduction band of ZnO we have m* = 0.27 (Ref.15) and therefore

$$E = \frac{(1.36)(0.27)}{72} \sim 0.05 \quad \text{ev}$$

in reasonable agreement with the singly ionized states observed. Oxygen vacancies can also exist; the singly ionized vacancy having the binding energy of approximately that of the singly ionized interstitial donors and the doubly ionized vacancy being approximately 0.8 ev below the conduction band edge. The doubly ionized state has definitely been observed in electron paramagnetic resonance work (Ref. 17) and being doubly ionized can act as an electron trap. In fact, the 2.4 ev luminescence of ZnO has been ascribed to the radiative transition between this level and the valence band.

Acceptors

Monovalent Cu and Li act as acceptors in ZnO, when they substitute for Zn in the lattice. The level of the Cu acceptor from the valence band is somewhat uncertain; however the Li acceptor level appears to exist ~0.85 ev

above the valence band. These acceptor centers have a net negative charge in the lattice when ionized, which is generally the case; i.e., the acceptor levels lie beneath the Fermi level.

The impurity levels are summarized in Fig. 2-3.

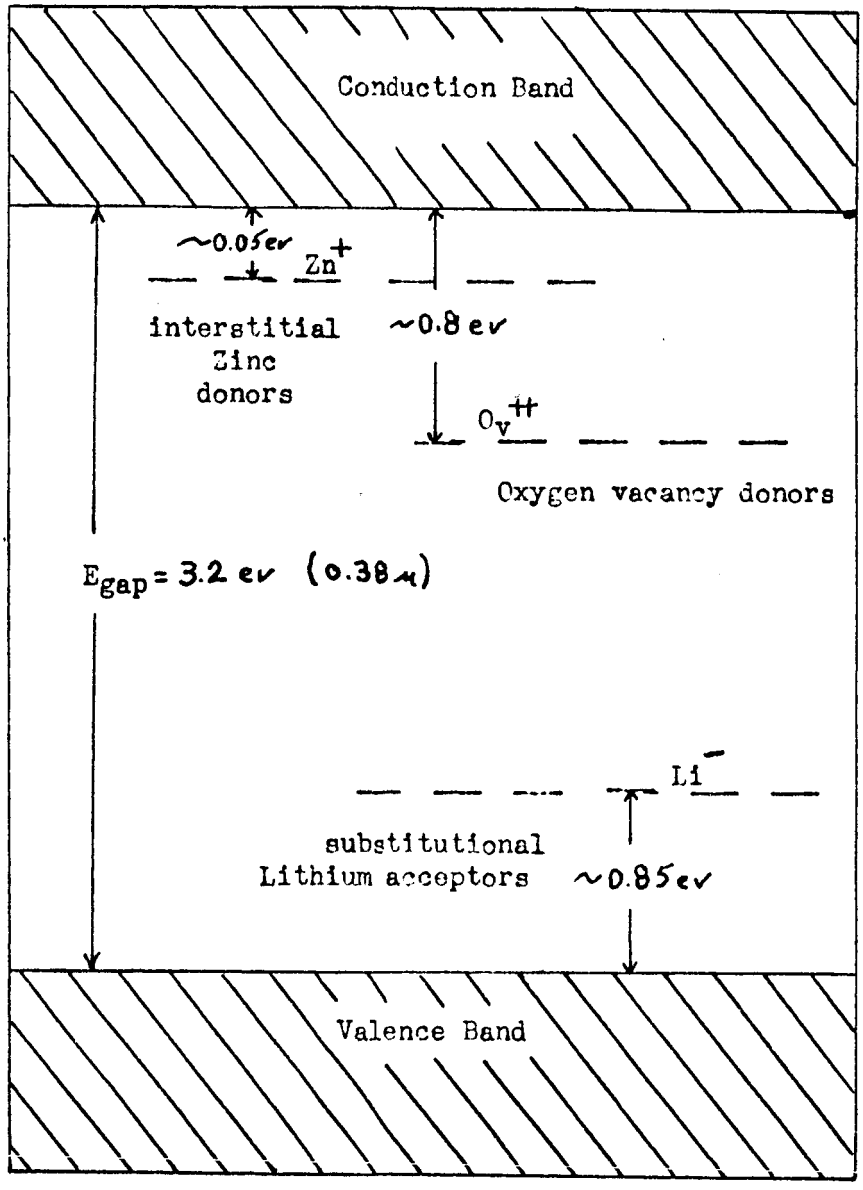

2-3 Bulk Impurity States

2.4 FAST PHOTOCONDUCTIVITY AND TRAPPING

As far as determination of the nature and energy spectrum of the carrier trapping states in ZnO is concerned, the most comprehensive work was done by Hieland (Ref. 18). In this work he investigated both field effect and photoconductivity in the surface conduction region of single crystals. Basically, the field effect will determine the effective mobility of the electrons in the space charge region which is determined by the density of states distribution for the electron traps, and the photoconductivity determines the density of states for the hole traps. The essential results of these studies can be summarized as follows:

(1) The trapping of excess holes or electrons is not determined by the dark surface conductivity, that is by the density of surface charges.

(2) The electron mobility increases and the photoconductivity decreases with increasing intensity of radiation with energy greater than or equal to the band gap. This says that electron trapping (from field effect) and hole trapping (from photoconductivity) decreases with increasing illumination.

(3) Both of the above results would occur if the quasi Fermi levels for the electron and holes (each quasi Fermi level approaches the corresponding band edge with increasing illumination) are moving through a continuum of trapping states. A quasi-Fermi level is used to describe electron and hole distributions under steady state non-thermal-equilibrium conditions. In the case of photoconductivity the quasi-Fermi levels describe the separate distribution functions of the electron and hole densities produced by illumination.

(4) The density of states of trapping levels for electrons and holes obtained in Heiland's work is shown in Fig. 2-4. The important point to note here is the preponderance of trapping levels found near the conduction and valence band edges. It is difficult to interpret from his results alone what the actual spectrum of trapping states is

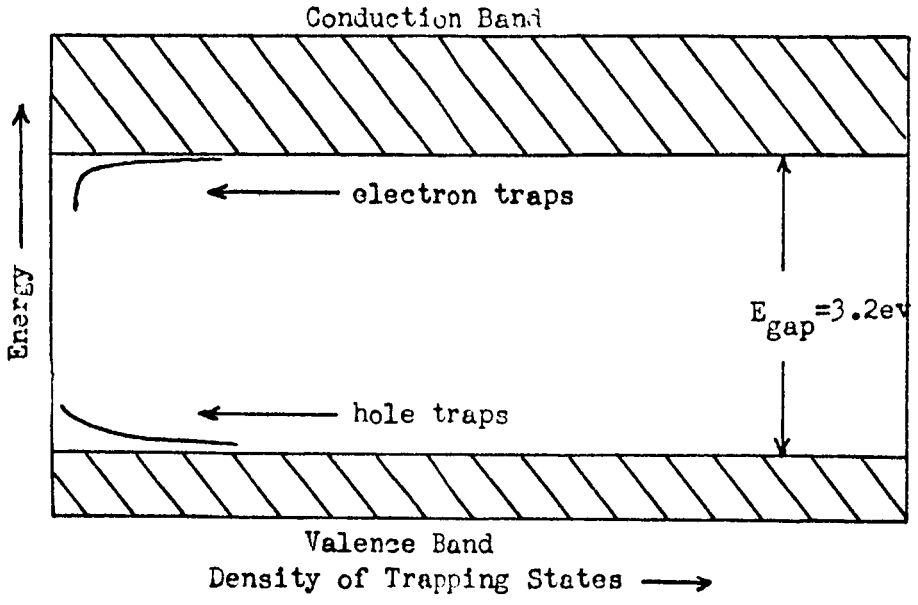

2-4 Density of Hole and Electron Trapping States

because of the complexities of the situation at the crystal surface. In fact, the spectrum he finds can be reasonably accounted for simply by assuming that the quasi-Fermi level passes through a single trapping level in the region near the surface where the bands are bent. It should be mentioned that this observed density of states could also be the result of a single level which crosses the Fermi level inside the space charge layer because of band bending.

(5) The electron traps are located at the surface or in the space charge region and they are not effective in recombination. Also the traps for electrons must be located near the traps for holes with regard to the distribution of charge; a spatial separation of the two levels of traps would result in bending of the bands and great changes in the surface conductivity which is not observed.

(6) The hole trapping effects indicate that the holes are protected against recombination with electrons; that is, the hole traps have a double negative charge in the trapping state. Oxygen ions ($O^{=}$) at the surface can satisfy this requirement, but the hole trap density has been shown to be independent of the coverage of the surface with adsorbed oxygen (over four orders of magnitude). Therefore the oxygen bound in the lattice may provide hole traps at the surface or additionally in the bulk.

2.5 SLOW PHOTOCONDUCTIVITY

In addition to the fast photoconductive process which is electronic in origin, there is a slow photoconductive process which is related to the adsorption and desorption of oxygen from the surface. This process is characterized by a sluggish rise (minutes to days) of the conductance during irradiation and a similar decay upon cessation of the irradiation. The general characteristics of this photoconductivity, such as its time-dependence and saturation level, depend on the experimental conditions such as light intensity, temperature, and ambient pressure. The general features of the experimental results can be understood in terms of the photoadsorption-desorption mechanism discussed below.

This slow process is irreversible in a vacuum to the extent that although there is a slow decay of the conductivity after the irradiation is stopped, the initial conductivity is not regained. However, admission of air accelerates the decay and, eventually, the initial conductivity is regained. It has been noted that there is an attendant pressure rise in the system when the ZnO is irradiated and a corresponding decrease in the pressure when the irradiation is stopped. The kinetics of this photodesorptive and photoadsorptive process have been extensively investigated. The results clearly show that the kinetics of the slow photoconductance behavior are determined by the kinetics of the photoadsorption-desorption process. Studies of the photocatalytic behavior and surface potential measurements of ZnO give a further clue to the processes involved. In particular, it has been shown that oxygen is adsorbed both physically and chemically, the chemisorbed form resulting in a negative surface charge. The exact species involved have not been conclusively determined, but the most likely chemisorbed forms are O^- and $O^=$. Their activation energies lie in the range 0.5 ev to 1.5 ev; the physically adsorbed species about 0.05 ev. Reduced ZnO, on the other hand, has been shown to have a positive surface charge. As an example, heating ZnO in an atmosphere of H_2 at elevated temperatures results in a positive surface charge. Also, changes in the surface charge of ZnO have been brought about by variations in the Fermi level as a result of

bulk doping of the crystal. Doping with Li, for instance (which is an acceptor when incorporated substitutionally) lowers the surface charge by emptying the negatively charged surface states as a result of the lower Fermi level.

With this background information we are in a position to discuss a mechanism which best relates these observations. The negatively charged surface resulting from the adsorption of oxygen on ZnO is considered to consist of negative oxygen ions which have been formed by the transfer of conduction electrons to the adsorbed species. If adsorbed at low temperatures O^- is considered to be the predominant specie and if adsorbed at high temperatures (above 200°C) $O^=$ is more likely. In addition to these chemisorbed species, physically adsorbed oxygen is also present. The adsorption of oxygen on the surface thus gives rise to a decrease in conductivity by removing electrons from the conduction band. This electron transfer creates a compensating space charge layer of ionized donors and a Schottky barrier is formed, i.e., the negative charge on the surface gives rise to an upward band-bending at the surface. This is the normal configuration of a ZnO surface in air.

The adsorbed ions can be desorbed by illuminating the surface with band-gap light in the following way. When band gap light is incident on an oxidized ZnO surface, i.e., one that has a negatively charged oxygen surface layer, an electron-hole pair is created and the holes will be accelerated by the field to the surface where they neutralize a negative charge on the oxygen. The oxygen is now only physically adsorbed. The electron created by the action of the light is weakly attracted to this physically adsorbed oxygen and is available for conduction only after the oxygen is desorbed. Thus the rate of increase in photoconductivity is determined by the rate of desorption of the physically adosrbed oxygen. Therefore, it can be seen that the photoconductive response will increase at a rate which is initially relatively independent of the ambient oxygen pressure. However, the saturation value of the photoconductivity will depend on the ambient oxygen pressure such that in a vacuum the photoconductivity will show a gradual increase which will

ultimately saturate at much higher levels than the corresponding level in an oxygen atmosphere.

When the irradiation is stopped, the decay time of the photoconductivity is essentially determined by the rate at which electrons can overcome the surface barrier to create chemisorbed oxygen from the physical adsorbed oxygen. When oxygen is admitted to this system, the rate of decay is increased because there are more physically adosrbed oxygen sites to accommodate the electrons.

In general, these processes appear to dominate the slow photoconductive effects. However, the situation is in fact much more complicated. As an example, during the slow process diffusion of such species as oxygen vacancies and excess zinc may occur. This diffusion not only would modify the rate of the observed effects but through electron trapping can modify the electron mobility in the space charge region and consequently the magnitude of the photoconductive effects.

2.6 WORKING DEGRADATION MODEL

Obviously, the degradation of the optical properties of ZnO by ultraviolet radiation is a complicated phenomenon. However, in this section, we would like to outline a degradation model in a general sense and then point out those features which are uncertain at the present time. For this outline, we will first start with a ZnO particle in an oxygen atmosphere. The surface (as shown in Fig. 2-1A) should take on a net negative charge due to electrons bound to the oxygen atoms at the surface. The potential barrier produced at the surface is such that electrons will be repelled and holes will be attracted to the surface within the space charge layer. The volume near the surface will therefore be a depletion region because ZnO is an n-type semiconductor.

When ultraviolet radiation of energy greater than the intrinsic energy gap (3.2 ev) is incident on the sample, electron-hole pairs are created within the bulk of the crystal or particle; the absorption depth for the radiation is a tenth of a micron or less. The electrons have difficulty in getting to the surface but the holes will be accelerated to the surface by the action of the strong electric field in the space charge region. The holes recombine with the O^- at the surface and change the oxygen from the chemi-sorbed to the physically adsorbed form which then can leave the surface with relative ease. The activation energy for physical adsorption is roughly 0.05 ev. This process results in oxygen leaving the surface which becomes Zn rich. Furthermore, this Zn rich surface layer gives a positive contribution to surface charge, thus decreasing the band bending and potential barrier at the surface. As the degradation proceeds the surface charge will tend to change to a net positive charge and the bands at the surface will begin to bend down (see Fig. 2-1B). Under this condition the holes have a retarding potential at the surface to overcome and the rate of charge neutralization slows down severely. Thus the degradation process (loss of oxygen) proceeds initially at a rate largely determined by the rate of evolution of adsorbed oxygen and eventually

at a rate limited by the arrival of holes through the retarding potential of the positive surface charge.

With this general trend outlined, the next step is to ascertain what changes produced by this oxygen loss manifest themselves as the permanent damage observed in various spectral regions of the reflectivity from pigments. Two general consequences are expected to result from the oxygen loss. Changes in the band-bending can be expected to modify the availability for optical absorption of the impurity states already present in the ZnO crystallites because of changes in the relative positions of the impurity states and the Fermi level. Diffusion of defects and impurities is also expected to occur and would give rise to additional absorption.

There is insufficient information at this time to specify the exact nature of the impurity states giving rise to the optical absorption observed in the damaged ZnO pigments. We can, however, make some comments as to the impurities to be expected. With the loss of oxygen from the surface both interstitial Zn and oxygen vacancies can be expected to diffuse into the material. It should be pointed out that the problem of predicting diffusion rates in the pigments is very difficult. Even if the diffusion rates of the impurities were well known in single crystals — and there is much contradiction in this area — the complexities of the interactions near the surface of the crystallites prevents realistic estimates of these diffusion rates in the pigments with our present information. However, assuming interstitial Zn and oxygen vacancies as the impurities we can indicate some of the consequences. Interstitial Zn provides rather shallow (~0.05 eV) donor states and oxygen vacancies provide donor states about 0.8 eV below the conduction band. At the densities of impurities expected in the degraded material these levels are expected to be considerably broadened; thus if these levels were present, significant absorption should be observed in the material for photon energies from about 2.1 eV to 3.2 eV; that is, over the wavelength interval of .38 to .6 μ.

In the infrared two types of absorption can occur as a result of the degradation. First, the existence of levels with energies up to 1 eV below the conduction band can provide absorption for wavelengths longer than 1 μ. Also, since Zn interstitial and oxygen vacancies are donors, the electron density in the bulk of the crystal can be increased, which would result in increased free carrier scattering absorption. It should again be emphasized that the data presently available does not allow an unambiguous assignment of the levels giving rise to the optical absorption observed in the degraded material.

There is one consequence of the degradation model which should be pointed out. The model would predict that the photodesorption rate of oxygen from the surface should be significantly retarded if the Fermi level in the bulk of the crystallities can be lowered sufficiently. This should occur regardless of whether the Fermi level is pinned at the surface state energy or not. If it is not pinned and the Fermi level can be lowered beneath the surface state energy the surface charges will be depleted of electrons (see Section 2.2) and the photodesorption rate should be decreased. If the Fermi level is pinned at the surface (which will occur at large surface coverage) a lower Fermi level in the bulk of the crystallites will decrease the band bending. It can even cause the bands to turn down at the surface depending upon the relative level of the bulk Fermi level and the surface state energy. This decreased band bending will also tend to decrease the photodesorption rate.

The lowering of the Fermi level in the bulk of the crystallites can be accomplished by Cu or Li substitutional doping. However, doping the pigments with Cu or Li will tend to give added optical absorption in the energy region just below the band gap, such that the overall visible reflectivity may be slightly lower than that for an undoped pigment. Thus, with doping, the pigment might start out slightly degraded but subsequent ultraviolet degradation may be greatly reduced if not eliminated.

The specific application of this model to the experimental results of the degradation effects observed in ZnO pigments will be discussed in Section 6.

3.0 SINGLE CRYSTAL MEASUREMENTS

The single crystal measurements reported in this section were carried out to obtain certain fundamental information about the fast photoconductive process and impurity levels in ZnO. This work was undertaken to provide information which was not adequately covered in previous investigations of ZnO and which we felt was important in ultimately formulating the ultraviolet degradation mechanism in ZnO pigments.

3.1 SPECTRAL DEPENDANCE OF ABSORPTION AND PHOTOCONDUCTIVITY

The optical absorption data on an undoped ZnO crystal (excess Zn) and a Li doped crystal were taken on a Cary 14 (double-beam grating spectrometer) from 0.35μ to 2.8μ. Samples are described in Table 3-1. The results are shown in Fig. 3-1a and 3-1b. The first point to note is the apparent shift of the fundamental absorption edge to lower energy (a shift of ~0.04 eV) with the Li addition. This shift is either the result of a high density of shallow acceptor states or a deformation of the lattice itself due to the high impurity concentration. Our absorption data does not go to high enough values of the absorption coefficient to resolve this. The most noteworthy feature is the broad absorption tail in the Li-doped sample which extends to about 0.75 microns.

Before discussing this absorption in greater detail we should first discuss the spectral dependence of the photoconductivity. The measurements were carried out at room temperature in air on the Li-doped crystal. Radiation from a Xenon compact arc source was passed through a Perkin Elmer-112 monochromator and then brought to a focus on the sample. The chopping frequency of 1 kc was chosen to insure that only the fast photoconductive process was being observed. The observed photoconductive signal is shown in Figure 3-1a as a function of wavelength. The measurements were carried out to 6 microns but no other photoconductive signals were detected. The photoconductive response and the absorption edge data on the Li-doped sample are compared in Figure 3-1. The essential feature is that the photoconductivity which we are observing is a bulk as opposed to a surface phenomenon. The following argument supports this statement. It is to be noted that the photoconductive signal decreases as the absorption coefficient increases sharply due to the band-to-band absorption (the fundamental band edge). The sample surface was purposely not etched, thus providing a surface with a high recombination rate. Therefore, in these experiments radiation which is absorbed

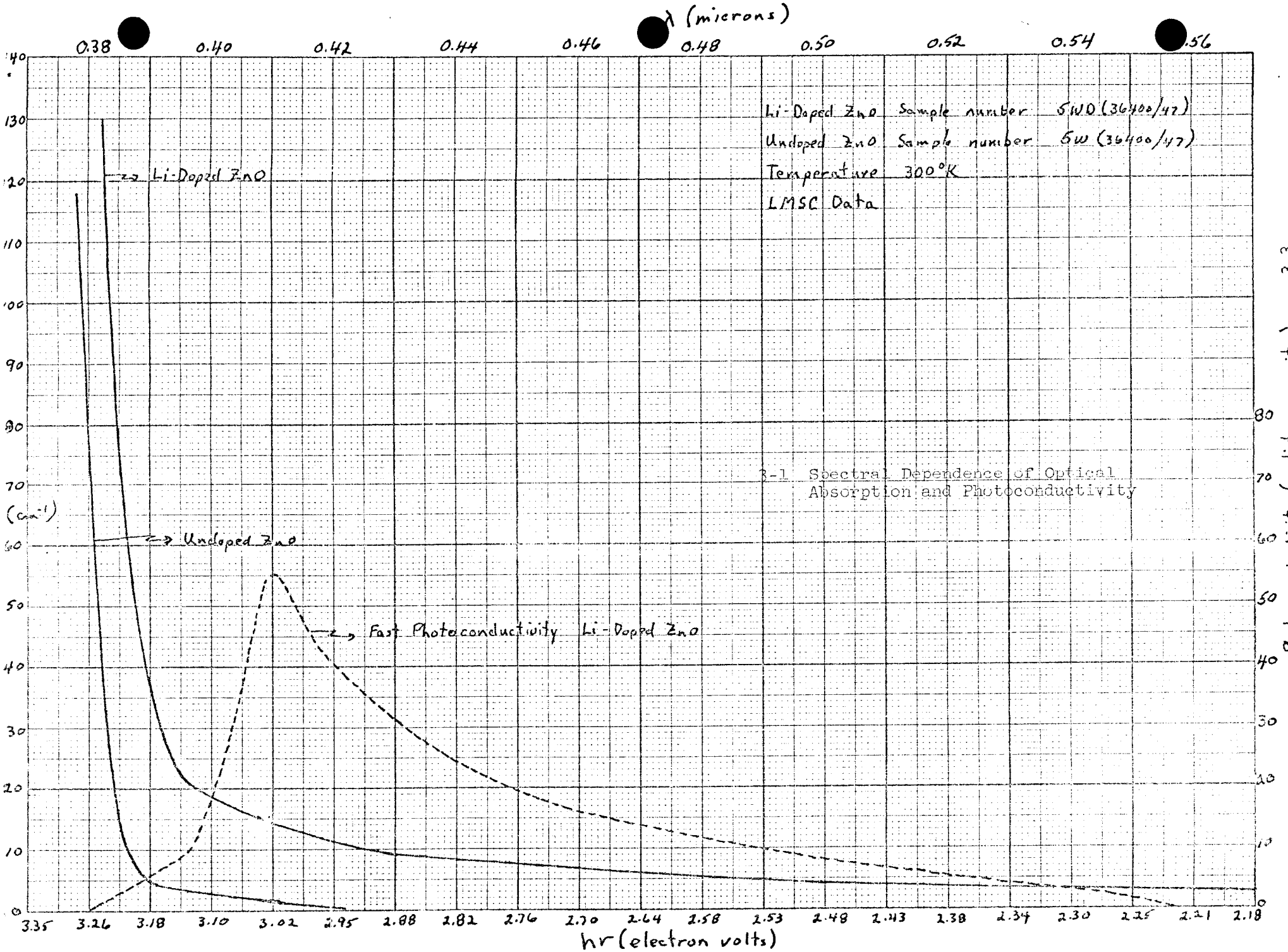

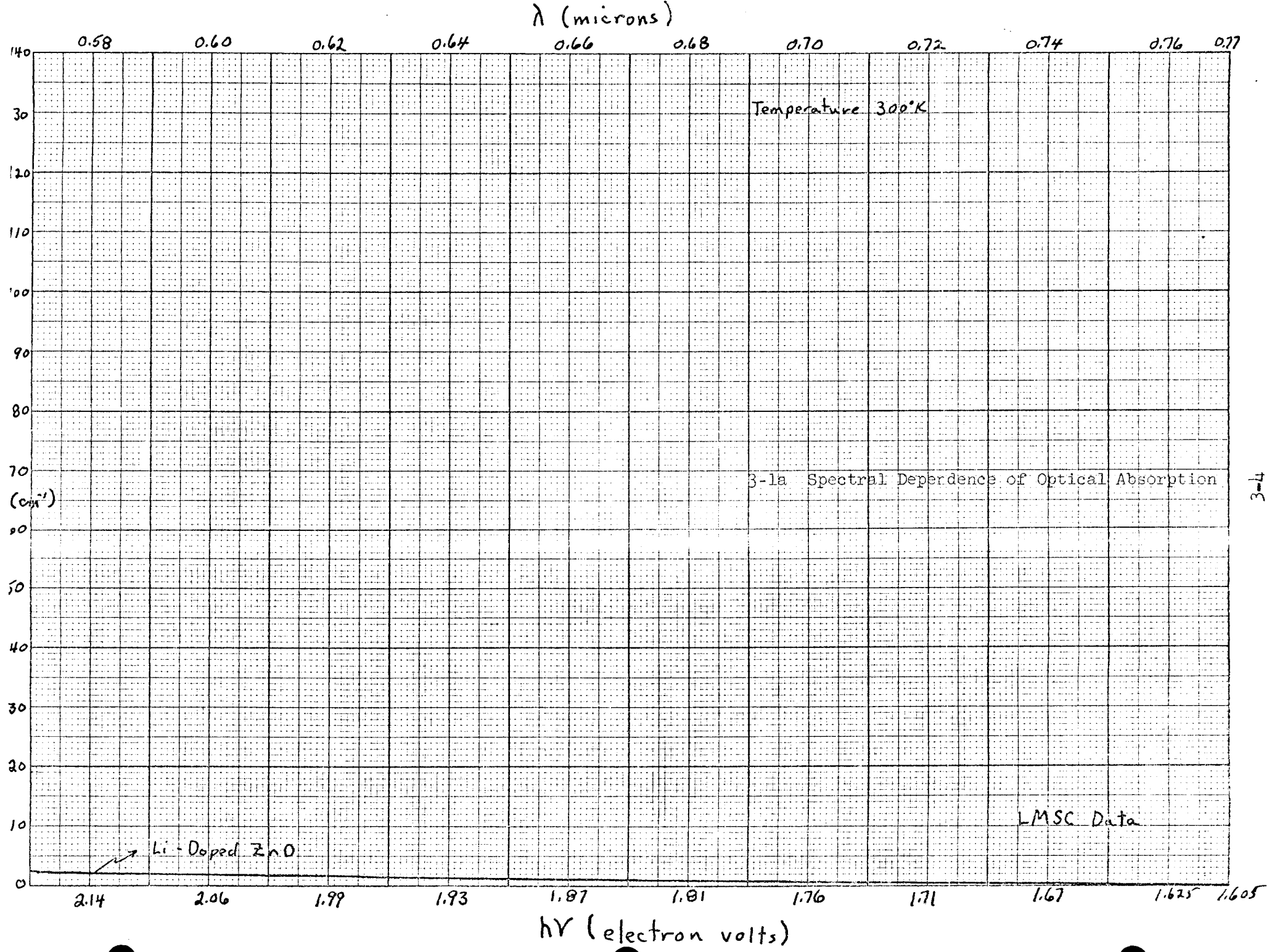

very close to the surface (high absorption coefficient) does not give rise to a photoconductive signal. The next feature to note is that the signal peaks at that wavelength for which the absorption coefficient corresponds approximately to the reciprocal of the sample thickness (~ 0.04 cm). At longer wavelengths an increasing amount of the incident energy is transmitted through the sample, due to the decreasing absorption coefficient. The photoconductive response decreases proportionately. Consequently, it is clear that the observed photoconductive effect is a bulk phenomena.

Since ZnO shows only n-type conduction, the photoconductive spectral response must be associated with the excitation of electrons from acceptor levels to the conduction band. The photoconductive response turns on at 2.25 eV, thus indicating that the acceptor levels involved are located about 0.95 eV above the valence band. This is in good agreement with previous assignments of the Li acceptor level (approximately 0.85 eV). Referring to Fig. 3-1b it will be noted that the optical absorption of Li doped single crystals begins at approximately 1.6 eV. This is certainly a much lower energy than that required to cause photoconductivity, and thus indicates that we are looking at additional absorption due to transitions from the valence band to donor levels above the middle of the energy gap. To determine if this is reasonable we first must establish that the Fermi level is at least this far below the conduction band, because only then will states above the Fermi level be available for optical transitions from the valence band.

The electrical resistivity and thermoelectric power were measured at room temperature on a Li-doped single crystal in an attempt to establish the Fermi level. These measurements were done in air and with an experimental arrangement designed to minimize surface conduction effects. The measured resistivity ($\rho \simeq 10^{10}$ ohm cm) and Seebeck coefficient ($Q = 1.9$ mV/°C) would both indicate that the Fermi level in the volume of the crystal was approximately 0.7 eV below the conduction band. When these measurements were carried out in vacuum,

surface conduction effects were quite evident. The resistivity and Seebeck coefficient measured in vacuum both indicate the Fermi level was much closer to the conduction band in the surface conduction region than in the measurements carried out at atmospheric pressure. The reason for pointing this out is that even in air, surface conduction effects could predominate and the true bulk resistivity can be far higher than was measured. Therefore, the bulk Fermi level may be quite a bit farther from the conduction band than the 0.7 eV which was measured. Landers (Ref. 19) carried out resistivity measurements on Li doped single crystals at much higher temperatures to minimize the effect of surface conduction (the bulk resistivity decreases by orders of magnitude at higher temperatures). He found that the Fermi level could be as low as 1.5 eV below the conduction band. We plan to carry out our own resistivity measurements to higher temperatures to unambiguously establish the Fermi level in our own crystals. If the Fermi level is indeed this deep, then the observation of absorption down to photon energies of 1.6 eV indicates the existence of rather deep impurity states of a significant density even in these relatively pure single crystals.

There is an alternative explanation for the 1.6 eV turn on of absorption which we feel, however, is not too probable. This would involve transitions between the Li acceptor levels and perhaps the oxygen vacancy level beneath the conduction band; the energy difference between these two levels being approximately 1.6 eV. For this to be an observable transition the acceptor and donor states would have to be spatially intimate. However, even in this case the transition probability between two impurity states is not as strong as between a band and impurity state and for this reason we feel that this explanation is not likely to be applicable.

3.2 TRANSIENT PHOTOCONDUCTIVITY

The transient behavior of the photoconductivity in Li doped single crystals was investigated with the apparatus described in Appendix D. A short light pulse (0.5 μsec) irradiates the sample causing an immediate rapid rise and then an immediate rapid decay of the photoconductivity. This is followed by a relatively longer decay process (milliseconds) which can provide information on the trapping processes in the crystal. This experimental arrangement has been designed to provide information on the trapping processes in ZnO, and we will now outline the preliminary results of this work.

To date these photoconductivity experiments have only been carried out near room temperature, and photoconductivity has been observed only in the Li-doped samples. The first point to note is that the photoconductivity observed is the fast photoconductive effect which is determined by the carrier recombination processes in the crystal and is not determined by adsorption or desorption of oxygen at the surface. The second point to note is that the response observed in the transient behavior is a bulk and not a surface effect. This can be established as follows. The transient behavior is completely independent of the surrounding atmosphere whether it be vacuum, oxygen or hydrogen. Furthermore, when a ZnO filter was placed between the light source and the ZnO photoconductor, no essential change was detected in either the magnitude of the photoconductivity or its decay time. Therefore, the fact that the filter did not alter the photoconductive characteristics indicate that photon energies less than the band gap gives rise to this photoconductive response. The spectral dependence of the absorption constant and the photoconductive response previously mentioned indicate that the transient photoconductivity observed is indeed a bulk effect. Furthermore, several different semiconductor filters, which cut off in the range of 1.5 to 3.0 eV were placed in front of the pulsed light source. The observed behavior further substantiated the fact that the transient photoconductivity has the same origin as the photoconductivity

observed in the spectral dependence measurements carried out on the Perkin-Elmer; i.e., the qualitative spectral dependence of the photoconductivity was the same as that of Fig. 3-1.

Since the photoconductive current is carried by electrons, the photoconductive decay will be determined by the length of time the electron is free in the conduction band once it has been excited. The electron will remain free as long as the accompanying hole remains trapped; once the hole becomes untrapped, electron-hole recombination occurs very rapidly. Thus the rate of photoconductive decay is determined by the rate at which holes can be freed from their trapping states.

To gain some information on the nature and position of the hole traps two experiments were carried out. In the first experiment, the decay time was observed as a function of temperature in the absence of any background illumination; the results are indicated in Fig. 3-2 and show that with increasing temperature the decay time decreases. The functional dependence of the decreasing decay time with increasing temperature was approximately

$$\tau = \tau_0 \exp\left(0.15/\frac{kT}{e}\right)$$

In the second experiment the decay time as a function of background illumination was investigated (Fig. 3-3). The background illumination light source was a tungsten lamp and the photoconductive decay time was observed to decrease with increased background illumination. Also using several semiconductor cutoff filters, including ZnO itself, it was established that the photon energy which produced the decrease in the decay time was slightly below the band gap value (within several tenths of an eV).

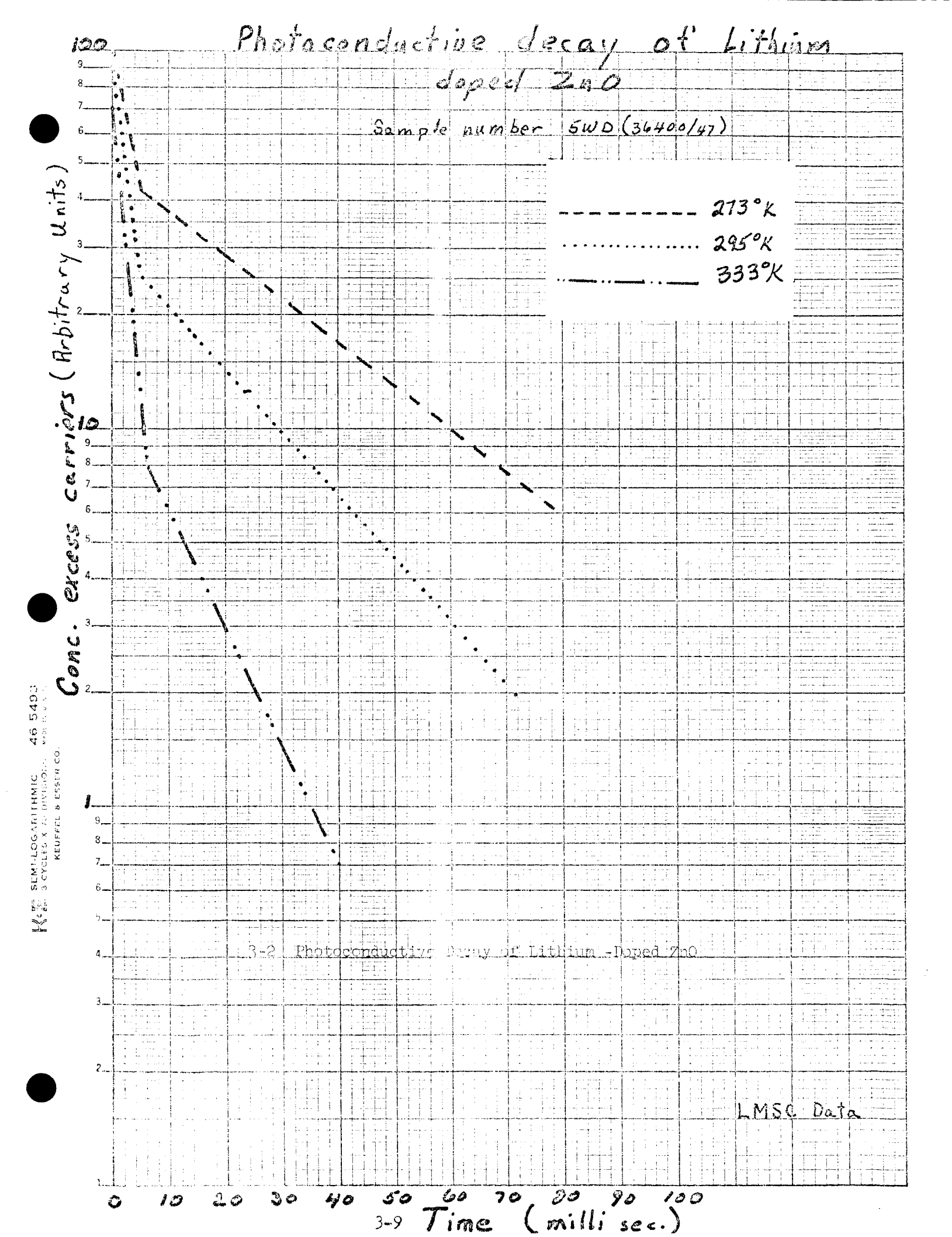

3-2 Photoconductive Decay of Lithium -Doped ZnO

Photoconductive Response of Lithium doped ZnO

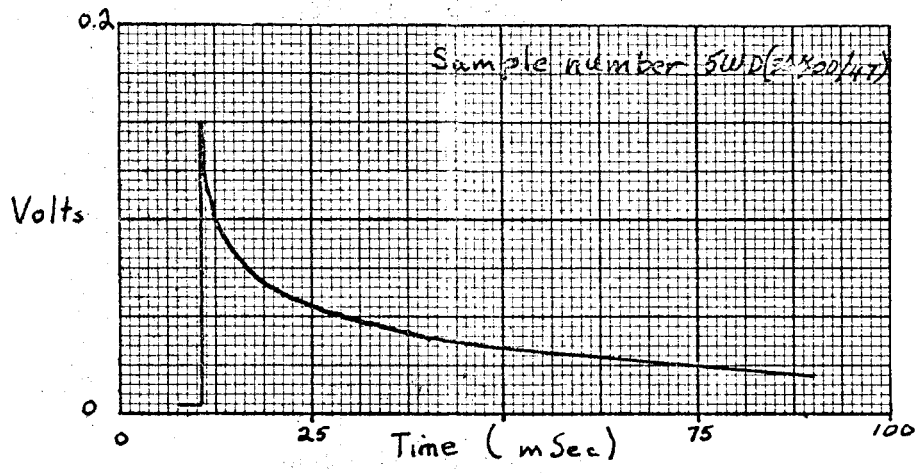

A. Without background illumination

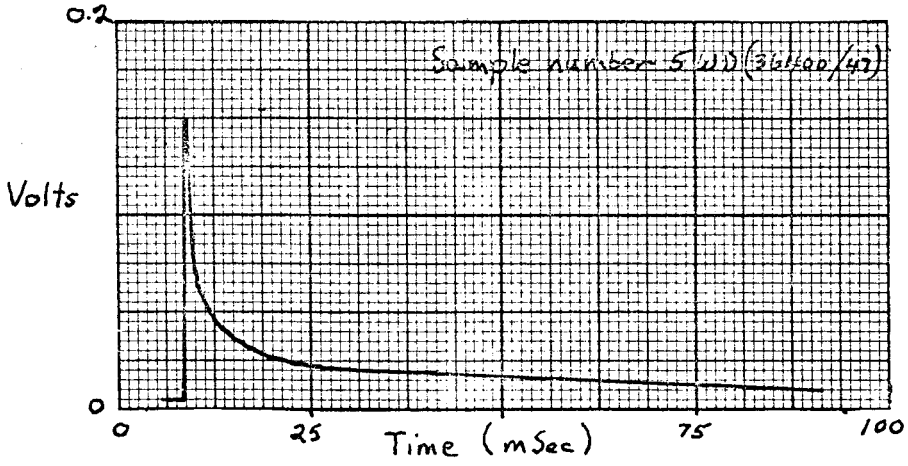

B. With background illumination

3-3 Effect of Background Illumination on Photoconductive Response

LMSC Data

The tentative interpretation of the last two experimental results is as follows. The exponential decrease of the observed decay time with temperature would indicate a hole trapping level approximately .15 eV above the valence band. As the temperature is increased fewer holes remain trapped and consequently the electron-hole pairs can recombine more readily. Also, with increasing background illumination the hole quasi-Fermi level will tend to move down through the trapping level decreasing its effectiveness as a hole trap; thus decreasing the electron-hole recombination time. The hole trap should be a doubly negative charged site; its form is uncertain, but it may be a Zn vacany or $O^{=}$ in the lattice.

Table 3-1

SINGLE CRYSTAL SAMPLES

Sample Number	Dopant	Resistivity (300°K)	Carrier Concentration	Thickness	Length and Width	Electrode Material	Supplier
SW (36400 /47)	Excess Zinc (as grown)	4 Ω cm	2.5×10^{16} cm^{-3}	1 mm	5 mm	Gallium or Silver Paste	Minnesota Mining and Manufacturing Co.
SWD (36400 /47)	Lithium	$\sim 10^{10}$ Ω cm	10^{7} cm^{-3}	1 mm	5 mm	Gallium or Silver Paste	Minnesota Mining and Manufacturing Co.

Section 4

STUDIES ON PARTICLES

4.0 GENERAL

The major portion of the experimental program has been concerned with studies of particulate samples of zinc oxide. The emphasis on this type of sample is especially appropriate in view of the particulate nature of the pigments incorporated into thermal control paints. Since this program is concerned with the effects of solar radiation on the optical properties of the pigment exclusively, it has been necesssary to devise methods of sample preparation which preserve the integrity of the zinc oxide particles without significantly altering the original properties of the pigment. Samples prepared by controlled pressing and sintering of zinc oxide powder have been found to adequately meet these requirements as discussed in Sections 4.1 and 4.2.

Studies of the effects of solar radiation on particulate samples have been performed in two modes: static ultraviolet exposures and in situ measurements. The details of these experiments are discussed in Sections 4.3 and 4.4. The static experiments are useful for collecting a relatively large amount of data in a routine manner. The in situ method permits detailed investigation of such factors as recovery and the influence of temperature and pressure, while maintaining the samples under the irradiation conditions. Both types of data are necessary for the formulation of a coherent model of the damage processes.

In all of the studies involving particulate samples, the primary index of damage was taken to be changes in the reflection spectra. The initial reflectance spectra of all samples were measured using a Cary Model 14 double beam spectrophotometer with an integrating sphere attachment. In some cases, where data extending out to 2.5 microns was required, a Backman DK-2 spectrophotometer equipped with an integrating sphere was employed. The spectra obtained from the two instruments were found to be substantially the same.

4.1 Sample Preparation

All particulate samples (except those specifically indicated) were prepared from the same material: zinc oxide powder, supplied by Merck & Co., batch number 52319. An analysis of the material, indicating the maximum impurities, is shown below.

Arsenic	0.0002%
Calcium and Magnesium	0.010
Iron	0.001
Lead	0.005
Manganese	0.0005
Insoluble in H_2SO_4	0.01
Chloride	0.001
Nitrate	0.003
Phosphate	0.001
Sulfur Compounds	0.01
Maximum total impurities	0.0417%

On the basis of this analysis, the zinc oxide utilized throughout this program has a purity of better than 99.9%. In addition, samples were prepared from New Jersey Zinc Co. SP 500, which has a nominal stated purity of 99.90%. In respect to initial optical properties and behavior under static ultraviolet exposure, the samples prepared from the two materials were identical within the limits of the measurements, as shown in Section 4.4.

The parameters involved in the preparation of the pressed particulate samples include forming pressure, sintering temperature and sintering atmosphere. The precise regulation of these parameters has been shown to be of considerable importance for the preparation of samples with reproducible optical properties. The method used for the preparation of zinc oxide samples throughout the course of this program is as follows: Three gram aliquots of the ZnO powder are weighed out, deposited in a one-inch diameter stainless steel pellet die, pressed at the requisite forming pressure, removed from the die, sintered under appropriate conditions, cooled, and stored.

The major conceptual problem involved in the sample preparation procedure is the production of reproducible, mechanically stable samples, composed of ZnO particles. It is felt that the zinc oxide in the composed samples should be identical to the original powder material from which they are formed. Unfortunately, loose powder samples are not amenable to handling and have no structural integrity. In this regard, pressed and sintered samples provide an adequate compromise. Under mild forming conditions the particles contained in the sintered samples have been shown to retain their original geometry to a large extent.

The effect of forming pressure has been investigated in an effort to ascertain the minimum pressure necessary for adequate compaction, as well as to examine the effect of mechanical damage on the zinc oxide samples. Experimentally, it was found that a minimum pressure of 10,000 lbs./sq. in. was required for the formation of stable pellets, in the absence of any binding additives. This forming pressure was used for the majority of the samples. At higher pressures, a pronounced yellowing of the zinc oxide throughout the bulk of the samples was found to occur. Figures 4-9 and 4-10 show the effect of forming pressure on the reflectance spectrum of zinc oxide pellets, before and after irradiation, respectively. It can be seen that the reflectance changes in an approximately linear fashion with forming pressure. It is of particular interest that the changes in

reflectance induced by mechanical damage (pressure) bear a marked resemblance to the ultraviolet induced spectral changes, indicating that the damage processes may be intimately related.

The forming pressure also has a pronounced affect on the specularity of the samples. Sample pressed at 10,000 lbs/sq. in. appear highly diffuse, while those formed at higher pressures assume a more specular appearance.

As the program progressed, it became of interest to study particulate samples doped with copper. Zinc oxide doped with a nominal 0.1% copper was prepared by coprecipitation as the mixed carbonate.

$$0.999\ Zn(NO_3)_2 + 0.001\ CuCl_2 + Na_2CO_3 \longrightarrow Zn_{.999}Cu_{.001}CO_3\ (\text{solid})$$

$$+ 1.998\ NaNO_3 + 0.002\ NaCl$$

The precipitate was washed three times with distilled water to free it of dissolved salts, and heated at 400 °C for six hours to decompose the carbonate.

$$Zn(Cu)CO_3 \xrightarrow{400^\circ C} Zn(Cu)O + CO_2$$

In order to study the effects of the copper doping on the zinc oxide powder, material was prepared in a similar manner without the added copper.

All particulate sample investigated are described in Table 4-1.

4.2 Sintering Studies

Although the pressing operation performed on the zinc oxide powder forms the material into pellets, they do not have appreciable mechanical stability unless they are sintered. The effects of sintering temperature, time and atmosphere have been investigated in an attempt to determine the mildest conditions compatible with adequate sample integrity. The criterion by which the extent of sintering was determined was surface area, as measured

by nitrogen adsorption using the standard Brunauer-Emmett - Teller (B.E.T.) technique. The surface area of the unsintered zinc oxide was found to be 3.54 m^2/gram, corresponding to an average particle diameter of 0.3 microns.

The effect of sintering temperature was determined by measuring the final surface areas of samples sintered in air at various temperatures in the range 500-1000°C, for times varying between 5 minutes and two hours. Sintering at the higher temperatures resulted in a yellow discoloration of the material, and pronounced distortion of the initial sample geometry. The minimum temperature at which sintering could be detected was found to be 600 °C. Sintering of the pressed samples at 600 °C for 15 minutes was found to be the optimum combination of conditions. Surface area measurements on six samples prepared in this manner indicated that the material had a specific surface area of 3.2 ± 0.1 m^2/gram. This corresponds to a reduction of 10% in the surface area. These results indicate that in terms of geometry, the material in sintered form is essentially the same as the unsintered ZnO. Therefore, it can be expected that effects related to the particle surfaces should not be altered by this sintering procedure. The reproducibility of the sample preparation technique, as manifested by the optical properties of the individual samples, is good. Reflection spectra of samples prepared under the same conditions routinely agree to within 1%.

Experiments relating to the effect of ambient oxygen on the optical properties of the sintered material have demonstrated the importance this parameter. Although samples sintered at 600 °C in one atmosphere of air, nitrogen and argon show similar reflection spectra, vacuum sintered ZnO shows drastically different properties. Pressed pellets of zinc oxide sintered at 600 °C for 15 minutes at a pressure of 10^{-3} Torr appeared dark gray with evidence of a substantial amount of free zinc on the surface. In addition, metallic zinc was found to deposit on the cool portion of the glass chamber containing the samples, (See Section 4.4).

These vacuum sintered samples were stored in vacuum in the dark until used.

The primary index of sample characterization throughout this program has been the reflectance spectra of the samples. Although characterization of particulate samples by means of electrical measurements (conductivity, Hall Effect, Seebeck coefficients, etc.) was considered, it was felt that this approach would be unfruitful due to the idiosyncrasies of non-single-crystal samples. Measurements of this type appear to be risky, at best, and provide relatively little insight into the properties of the bulk material.

Table 4-1

PARTICULATE ZINC OXIDE SAMPLES

Thermophysics Sample Number	Figure Number	Preparation*		Other Remarks	Optical Measurement Wavelength Range (microns)	Ultraviolet Exposure Conditions				Other Remarks	Difference between reflectance spectrum before and after irradiation
		Forming Pressure (1000 psi)	Sintering Atmosphere			Pressure (Torr)	Distance From A-H6 (in.)	Irradiation Time (hrs)	Nominal Sample Temperature (°F)		
14218		20	air		0.3 to 1.8	3×10^{-6} to 8×10^{-7}	3	45	100 – 125		Visible and infrared lowered
14507 A		12	air		0.3 to 2.6	6×10^{-6} to 4×10^{-7}	3	61.5	100 – 125		Visible and infrared lowered
AA	4-6	12	air		0.3 to 2.6	6×10^{-6} to 4×10^{-7}	3	61.5	100 – 125		Visible and infrared lowered
AB	4-6	12	air		0.3 to 2.6	4×10^{-6} to 2×10^{-7}	3.9	100	100 – 125		Visible and infrared lowered
AC		12	air		0.3 to 2.4	atmospheric	3	60	100 – 125	BDR**	No change
14671 A		101.6	air		0.3 to 2.6	4×10^{-6} to 2×10^{-7}	3.9	100	100 – 125		Higher forming pressure gave lower reflectance in the visible and infrared; ultraviolet exposure produced additional decrease in visible and infrared reflectance.
AA	4-5, 4-10	101.6	air		0.3 to 2.6	4×10^{-6} to 2×10^{-7}	3.9	100	100 – 125		
AB	4-5, 4-10	76.2	air		0.3 to 2.6	4×10^{-6} to 2×10^{-7}	3.9	100	100 – 125		
AC		76.2	air		0.3 to 2.6	4×10^{-6} to 2×10^{-7}	3.9	100	100 – 125		
AD		76.2	air		0.3 to 2.6	4×10^{-6} to 2×10^{-7}	3.9	100	100 – 125		
AE	4-9, 4-10	50.8	air		0.3 to 2.6	4×10^{-6} to 2×10^{-7}	3.9	100	100 – 125		
AF		50.8	air		0.3 to 2.6	4×10^{-6} to 2×10^{-7}	3.9	100	100 – 125		
AG		50.8	air		0.3 to 2.6	4×10^{-6} to 2×10^{-7}	3.9	100	100 – 125		
AH		25.4	air		0.3 to 2.6	4×10^{-6} to 2×10^{-7}	3.9	100	100 – 125		
AI	4-9, 4-10	25.4	air		0.3 to 2.6	4×10^{-6} to 2×10^{-7}	3.9	100	100 – 125		
B		25.4	air		0.3 to 2.6	4×10^{-6} to 2×10^{-7}	3.9	100	100 – 125		
14690 A		12	air	Stored in water 18 hours	0.3 to 2.6	4×10^{-6} to 2×10^{-7}	3.9	100	100 – 125		Different initial spectrum due to adsorbed water. Same post-exposure reflectance as irradiated standard sample
AA		12	air		0.3 to 2.6	4×10^{-6} to 2×10^{-7}	3.9	100	100 – 125		
14691 A	4-10	10	air		0.3 to 2.6	4×10^{-6} to 2×10^{-7}	3.9	100	100 – 125		Visible and infrared lowered
AA		10	air		0.3 to 2.6	4×10^{-6} to 2×10^{-7}	3.9	100	100 – 125		
14701 A		10	air		0.3 to 2.0						
14804 A		10	nitrogen		0.3 to 1.8						
AA		10	nitrogen		0.3 to 1.8						
AB		10	10 microns pressure		0.3 to 1.8						
AC		10	10 microns pressure		0.3 to 1.8						
14805 A	4-1	10	air		0.3 to 2.4	10^{-5} to 10^{-6}				BDR**	
AB		10	air		0.3 to 2.4	10^{-5} to 10^{-6}				BDR**	

Table 4-1 (Cont.)

Thermophysics Sample Number	Figue Number	Preparation* Forming Pressure (1000 psi)	Preparation* Sintering Atmosphere	Other Remarks	Optical Measurement Wavelength Range (microns)	Ultraviolet Exposure Conditions: Pressure (Torr)	Distance From A-H6 (in.)	Irradiation Time (hrs)	Nominal Sample Temperature (°F)	Other Remarks	Difference between reflectance spectrum before and after irradiation
14852		10	air		0.3 to 2.4	10^{-5} to 10^{-6}				BDR**	
14858		10	air	SP500	0.3 to 1.8	atmospheric	3.9	88	100 – 125		No change
14859 A		10	air		0.3 to 1.8	atmospheric	3.9	88	100 – 125	No	No change
AA		10	air		0.3 to 1.8	atmospheric	3.9	88	100 – 125	filter	No change
AB		10	air		0.3 to 1.8	atmospheric	3.9	88	100 – 125	0.4 cutoff	No change
AC		10	air		0.3 to 1.8	atmospheric	3.9	88	100 – 125	filter	No change
AD		10	air		0.3 to 1.8	atmospheric	3.9	88	100 – 125	0.3 cutoff	No change
AE		10	air		0.3 to 1.8	atmospheric	3.9	88	100 – 125	filter	No change
14860 A	4-11	10	10 microns		0.3 to 1.8	atmospheric	3.9	88	100 – 125		Increase large
AA		10	pressure		0.3 to 1.8	atmospheric	3.9	88	100 – 125		in visible, less in infrared
14861	4-2, 4-3	10	air		0.3 to 2.4	10^{-5} to 2×10^{-7}	3.9	54	490	BDR**	Visible and infrared lowered
14863 A	4-5	10	air	0.050 in. thick, vapor deposited gold backed	0.2 to 2.0						
AA	4-5			0.020 in. thick, applied as slurry to aluminum substrate	0.2 to 2.0						
14872 AB	4-8	10	air		0.3 to 1.8	10^{-4} to 2×10^{-7}	3.9	67	100 – 125	No	Lowered in visible and infrared
AE		10	air		0.3 to 1.8	10^{-4} to 2×10^{-7}	3.9	67	100 – 125	filter	
A	4-8	10	air		0.3 to 1.8	10^{-4} to 2×10^{-7}	3.9	67	100 – 125	0.3 cutoff	Slight visible damage, greater
AC		10	air		0.3 to 1.8	10^{-4} to 2×10^{-7}	3.9	67	100 – 125	filter	infrared damage
AA	4-8	10	air		0.3 to 1.8	10^{-4} to 2×10^{-7}	3.9	67	100 – 125	0.4 cutoff	No damage in visible slight in
AD		10	air		0.3 to 1.8	10^{-4} to 2×10^{-7}	3.9	67	100 – 125	filter	infrared
14873 A		10	air	SP500	0.3 to 1.8	10^{-4} to 2×10^{-7}	3.9	67	100 – 125		Same as standard sample exposed
AA		10	air	SP500	0.3 to 1.8	10^{-4} to 2×10^{-7}	3.9	67	100 – 125		simultaneously
14874 A	4-13	10	air	copper	0.3 to 1.8	10^{-4} to 2×10^{-7}	3.9	67	100 – 125		Lower initial reflectance than
AA		10	air	doped							standard samples; less damage

Table 4-1 (Cont.)

Thermophysics Sample Number	Figure Number	Preparation*		Other Remarks	Optical Measurement Wavelength Range (microns)	Ultraviolet Exposure Conditions					Difference between reflectance spectrum before and after irradiation
		Forming Pressure (1000 psi)	Sintering Atmosphere			Pressure (Torr)	Distance From A-H6 (in.)	Irradiation Time (hrs)	Nominal Sample Temperature (° F)	Other Remarks	
14875 A	4-12	10	1 micron pressure		0.3 to 1.8	10^{-4} to 2×10^{-7}	3.9	67	100 – 125		Visible and infrared increased; a large amount of zinc was evolved
AA		10	micron pressure		0.3 to 1.8	10^{-4} to 2×10^{-7}	3.9	67	100 – 125		
14876 A		10	argon		0.3 to 1.8	10^{-4} to 2×10^{-7}	3.9	67	100 – 125		Same as standard before and after irradiation
AA		10	argon		0.3 to 1.8	10^{-4} to 2×10^{-7}	3.9	67	100 – 125		
14507 A	4-4	10	air		0.3 to 2.4	3×10^{-7} to 8×10^{-7}	3.5	54	150	BDR**	Slightly lowered in visible and infrared
AA		10			0.3 to 2.4	3×10^{-7} to 8×10^{-7}	3.5	54	150		
14503	4-13	10	air	precipitated ZnO	0.3 to 1.8						

*All samples are formed in air and sintered at 960° C for 15 minutes.
For further sample preparation information see Section 4.1.
**BDR signifies in situ bi-directional reflectance measurements.

4.3 ULTRAVIOLET EXPOSURES WITH IN SITU MEASUREMENTS

Ultraviolet irradiation tests on sintered zinc oxide with in situ bi-directional reflectance measurements were conducted in an apparatus constructed for that purpose under this contract. To our knowledge, this is the first apparatus devised with the capability for measuring spectral reflectance during ultraviolet irradiation in vacuum. The apparatus is described in detail in Appendix B. Reflectance, either bi-directional or normal, is taken as the criterion for optical property damage. For the region 0.3 to 2.0 microns, the standard particulate samples are thick enough (~0.070") to be opaque. Hence, a change in reflectance is necessarily a change in absorptance, not transmittance. The tests are performed on standard particulate zinc oxide discs, formed at 10,000 psi and sintered at 600°C in air (Sec. 4.1). The samples are irradiated in vacuum at a lamp-to-sample distance of 3.5 in. for nominally 50 hours. The sample temperature is controlled and maintained nearly constant. Temperatures from -300°F to 500°F may be achieved. Under this contract, zinc oxide samples are to be exposed to ultraviolet radiation at three or more temperatures distributed over this range.

To date a complete test has been performed on a sample maintained at 500°F during irradiation. These data are reported herein. A test was completed at room temperature, but suspected instrumental errors (due to possible movement of the optical system during part of the run) have thrown doubt on some of the data obtained. However, the in situ data on damage recovery in air, following the irradiation, are valid. These data are also discussed.

Complete tests on samples maintained at room temperature and near liquid nitrogen temperature will be conducted and reported in a forthcoming addendum report.

Sample Temperature Effects

Measurement and control of sample temperature throughout the test period, including the time before and after irradiation, are important in the *in situ* evaluation of optical property changes. Zinc oxide in vacuum exhibits a decrease in visible and infrared reflectance with increasing temperature. In addition, there is the well-known shift in the absorption band edge to longer wavelengths with increasing temperature. In order to determine the ultraviolet-induced changes in spectral reflectance of a sample at a given temperature, one must also determine the spectral reflectance of the sample at the same temperature but without irradiation. The first problem in this determination is the measurement of sample temperature, particularly during irradiation. The approach taken is discussed in detail in Appendix B. The method used to control sample temperature is also discussed.

The A-H6 lamp subjects the sample to high incident heat fluxes. As a result, the most reliable method for bringing the sample to 500°F or maintaining it at room temperature is as follows. The A-H6 is started with the sample initially at room temperature; the sample table heater (or coolant flow) is regulated to produce the desired steady state sample temperature. Once steady state is reached bi-directional reflectance measurements are made. The change in reflectance due to ultraviolet irradiation is taken as the difference between the measured reflectance and that measured on another unirradiated sample at the same temperature. The determination of *in situ* bi-directional spectral reflectance of unirradiated standard samples has been completed for the range of temperatures from 70°F to 440°F for the visible region of the spectrum. This data is presented in Figure 4-1. The same measurements for the range -300°F to 70°F and also the infrared portion of the spectrum for the full temperature range will be reported in the forthcoming addendum. For a given sample, the bi-directional reflectance data for 70°F in vacuum are normalized with

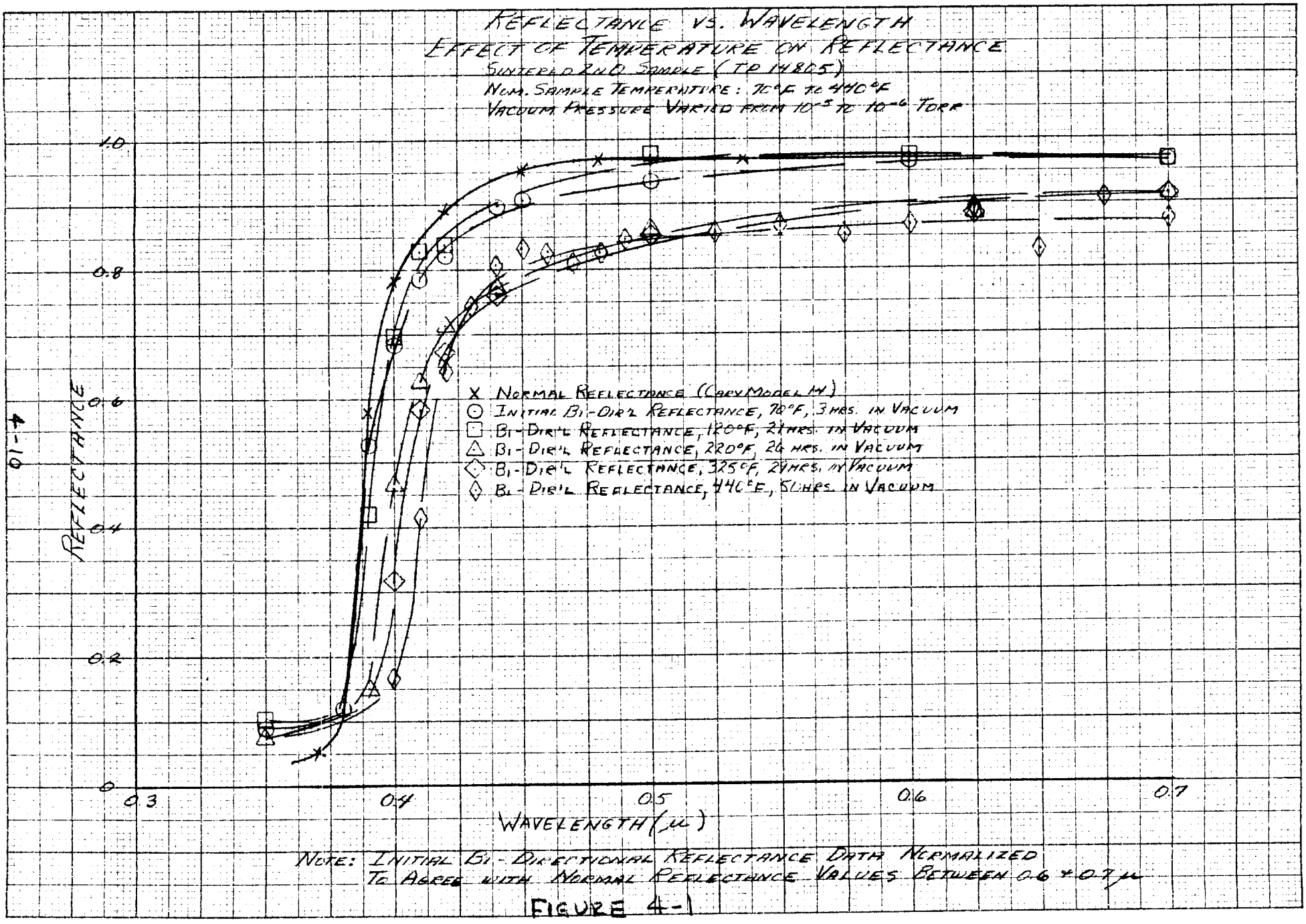

NOTE: INITIAL Bi-DIRECTIONAL REFLECTANCE DATA NORMALIZED TO AGREE WITH NORMAL REFLECTANCE VALUES BETWEEN 0.6 & 0.7 μ

FIGURE 4-1

respect to the initial normal reflectance measured on the Cary spectrophotometer by setting them equal at 0.6 microns (except where otherwise indicated). All bi-directional data taken in the same test are subsequently adjusted by the same multiplying factor. See Appendix C for a more detailed explanation.

Referring to Figure 4-1 it is clear that there is a definite shift of the absorption band edge toward longer wavelengths and a decrease of the visible reflectance due to increasing temperature. The wavelength of the true absorption band edge is observed to be only a function of sample temperature. In situ bi-directional reflectance measurements have shown that neither vacuum nor ultraviolet irradiation have an effect on the band edge during or after irradiation except to the extent that sample temperature is affected. In fact, the band edge location may serve as a convenient check for sample temperature measurements. It can be seen in Figure 4-1 that a small band edge shift produces a large percentage change in spectral or bi-directional reflectance at a wavelength in the region of the edge. The observed temperature-dependence of the band edge is similar to that reported in Ref. 33.

Exposure at 500°F

After evaluating the magnitude of the effect of temperature and vacuum on the spectral reflectance of unirradiated zinc oxide, an ultraviolet exposure test was performed on a sample maintained at 490°F ± 20°F. The chronological variation of spectral reflectance up to the termination of the 54 hour irradiation period is shown in Figure 4-2. The variation of spectral reflectance from the end of exposure to the final measurement with the Cary Spectrophotometer is shown in Figure 4-3. All of the bi-directional reflectance data on both Figures 4-2 and 4-3 are normalized with respect to the initial Cary reflectance curve at 0.65 microns.

FIGURE 4-2
REFLECTANCE VS. WAVELENGTH
ULTRAVIOLET DAMAGE HISTORY (0 TO 54 HRS)

SINTERED ZnO SAMPLE (TP14861)
NOMINAL SAMPLE TEMP: 500°F DURING IRRADIATION
IRRADIATION SOURCE: A-H6 (1KW), 3.5" FROM SAMPLE
VACUUM PRESSURE VARIED FROM 10^{-5} TO 2×10^{-7} TORR.

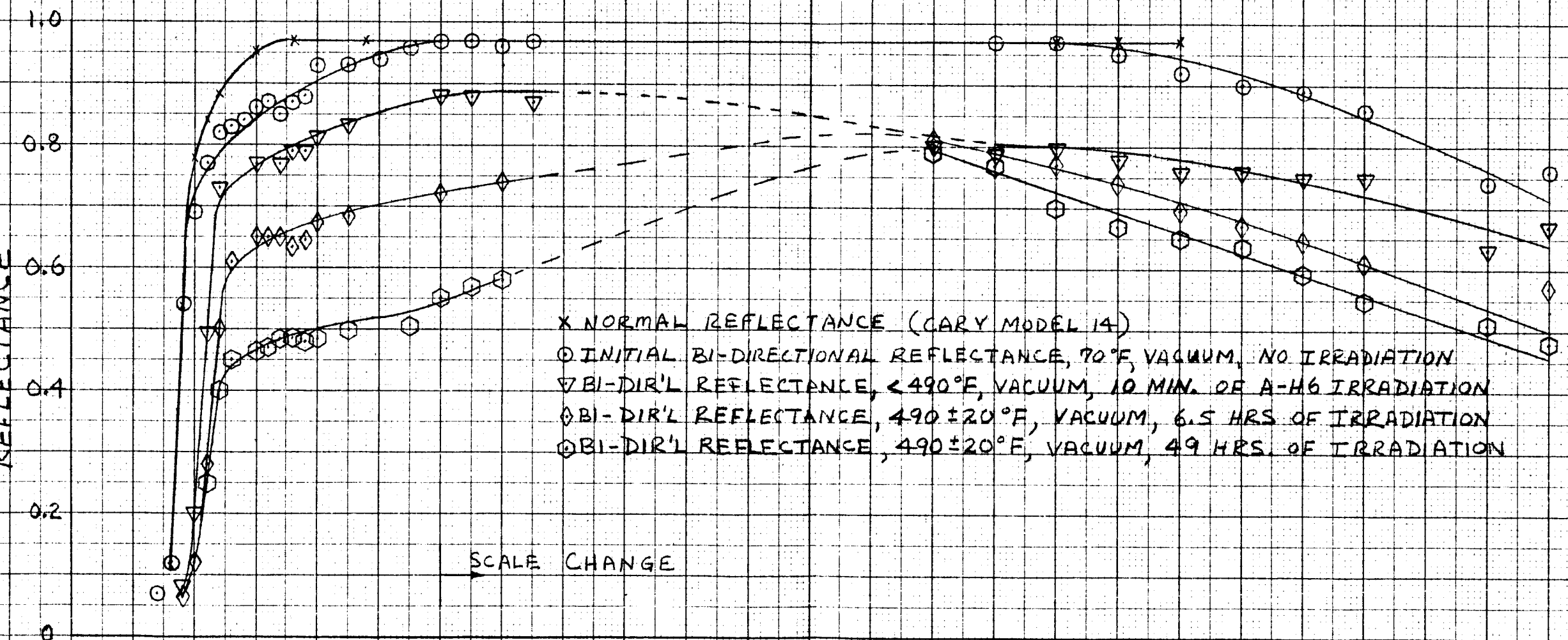

X NORMAL REFLECTANCE (CARY MODEL 14)
⊙ INITIAL BI-DIRECTIONAL REFLECTANCE, 70°F, VACUUM, NO IRRADIATION
▽ BI-DIR'L REFLECTANCE, <490°F, VACUUM, 10 MIN. OF A-H6 IRRADIATION
◇ BI-DIR'L REFLECTANCE, 490±20°F, VACUUM, 6.5 HRS OF IRRADIATION
⬡ BI-DIR'L REFLECTANCE, 490±20°F, VACUUM, 49 HRS. OF IRRADIATION

NOTE: BI-DIRECTIONAL REFLECTANCE DATA NORMALIZED TO AGREE WITH NORMAL REFLECTANCE VALUES AT 0.65 MICRONS.

FIGURE 4-3
REFLECTANCE VS. WAVELENGTH
HISTORY OF RECOVERY FROM DAMAGE (54 TO 95 HRS.)

SINTERED ZnO SAMPLE (TP 1486)
NOM. SAMPLE TEMP. : 500°F TO 70°F
IRRADIATION SOURCE : A-H6 LAMP

VACUUM PRESSURE VARIED FROM 10^{-5} TO 2×10^{-7} TORR

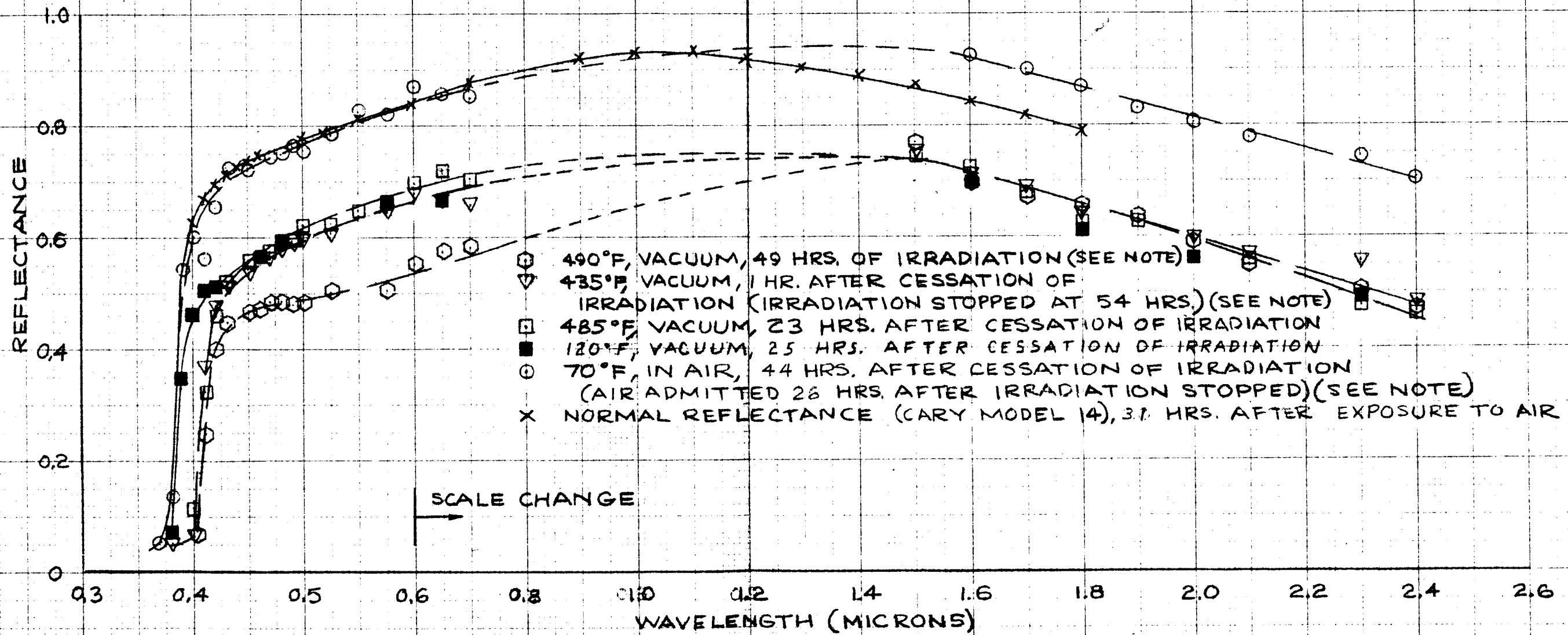

NOTE: BI-DIRECTIONAL REFLECTANCE DATA NORMALIZED TO AGREE WITH NORMAL REFLECTANCE VALUES FOR UNIRRADIATED SAMPLE AT 0.65 MICRONS.

The initial bi-directional reflectance at 70°F in vacuum is lower than the Cary reflectance in the regions 0.4 to 0.6 microns and 1.6 to 2.4 microns. This departure from the Cary measurement is repeatedly observed (also see Figure 4-1) for bi-directional reflectance measurements taken in vacuum, but not for those taken in air. Checks have been made to ensure that these departures were not associated with mechanical displacement of the optical system during pump-down. It is probable that this observation is related to the desorption of oxygen from the zinc oxide, and is not instrumental.

Ten minutes after initiation of ultraviolet irradiation, a full reflectance spectrum was measured. Referral to Figure 4-2 indicates that the band edge has not fully shifted, so the sample has not quite reached steady state temperature. The visible reflectance has decreased from the room temperature values. However, comparison of this data to that for a 440°F sample in Figure 4-1 indicates that this decrease is largely if not completely due to the increased temperature under irradiation. The spectral dependance of the infrared reflectance ten minutes after initiation of irradiation is unexpected, in that it does not have the same general form as the remaining infrared reflectance spectra. As yet this is not explained, but may be connected with the rapid change in sample temperature during this run.

The last two bi-directional reflectance spectra show a progressive and definite degradation of sample reflectance with continued irradiation. The total degradation is only slightly greater in the visible range than in the infrared if the lowest reflectance curve (after 49 hours irradiation) is compared to the initial room temperature reflectance. However, the relative rates of degradation in the visible and infrared cannot be meaningfully compared because of the one irregular infrared spectrum discussed above. Further data on degradation rates will be obtained.

After 54 hours of irradiation the lamp was extinguished and "recovery" measurements made. The first post-irradiation spectrum was recorded one hour after stopping irradiation; sample temperature had decreased to 435°F. For the second post-test spectrum, taken 23 hours after the termination of radiation, the sample temperature is approximately that maintained during irradiation (490°F). Note that there has been no recovery in the infrared region (1.4 to 2.4 microns), but there appears to have been significant recovery in the visible and very near infrared. Furthermore, the visible recovery occurred primarily during the first hour after irradiation ceased.

The final spectrum in vacuum, taken 25 hours after irradiation is terminated and after the sample had cooled to room temperature, is essentially identical to those taken one hour (at 435°F) and 23 hours (at 490°F) after termination of irradiation. The only significant change is the shift in the band edge, which is due to the decrease in sample temperature from 490°F to 120°F. This spectrum does indicate that the significant decrease in visible reflectance due to increasing temperature shown in Figure 4-1 is not reversible after zinc oxide has been irradiated in vacuum. These data do not demonstrate that the irradiation is a causitive factor in producing this irreversibility, however. More data for samples irradiated at elevated temperature is required to explain the nature of this observed recovery of reflectance.

From these three spectra, it appears that very little reflectance recovery occurs in vacuum, at temperatures from 490°F to 70°F, for many hours after the termination of irradiation, except for a very fast initial increase in the visible reflectance.

After 26 hours in vacuum and comparative darkness, the damaged sample (having reached room temperature) was re-exposed to air. Fifteen hours later the bi-directional reflectance was measured. After an additional six hours the final normal reflectance was measured on the Cary spectrophotometer. These final two spectra indicate that significant recovery of spectral reflectance

has occurred upon re-exposure of the sample to air. The total recovery is generally uniform in the visible and infrared, however insufficient data was obtained to determine if there were different recovery rates in the visible and infrared during the first moments of exposure to air.

The fact that the final infrared reflectance measured as bi-directional reflectance was higher than the normal reflectance measured on the Cary was certainly not expected. Further tests will be performed to clarify this behavior.

Additional Damage Recovery Data

In addition to the data presented in the preceding paragraphs, there is more evidence to substantiate the occurrence of recovery of optical properties when irradiated zinc oxide is re-exposed to air. Data on static ultraviolet tests presented in Section 4.4 and especially Figure 4-6 show the effect of long post-irradiation periods in air on the spectral reflectance of standard particulate samples irradiated in vacuum.

Further important data are provided in the ultraviolet irradiation tests of a room temperature sample with in situ reflectance measurements. The data are shown in Figure 4-4. The second set of in situ data taken after air admission are normalized with respect to the Cary normal reflectance at 1.6 μ. The lowest in situ reflectance curve was obtained one-half hour after admission of air to the chamber. The next higher was obtained three hours later, the Cary less than one hour after that and the final bi-directional reflectance curve eight days later.

"Recovery" of approximately uniform magnitude occurred between the first and second in situ spectra at all wavelengths longer than the band edge. The Cary reflectance is no higher in the infrared, but significant additional

FIGURE 4-4

REFLECTANCE VS. WAVELENGTH
RECOVERY IN AIR (73 TO 272 HRS.)

SINTERED ZnO SAMPLE (TP 14707)
IRRADIATION SOURCE: A-H6 LAMP, 3.5" FROM SAMPLE
NOMINAL SAMPLE TEMP: 150°F DURING IRRADIATION
VACUUM PRESSURE VARIED FROM 2×10^{-6} TO 3×10^{-7} TORR.

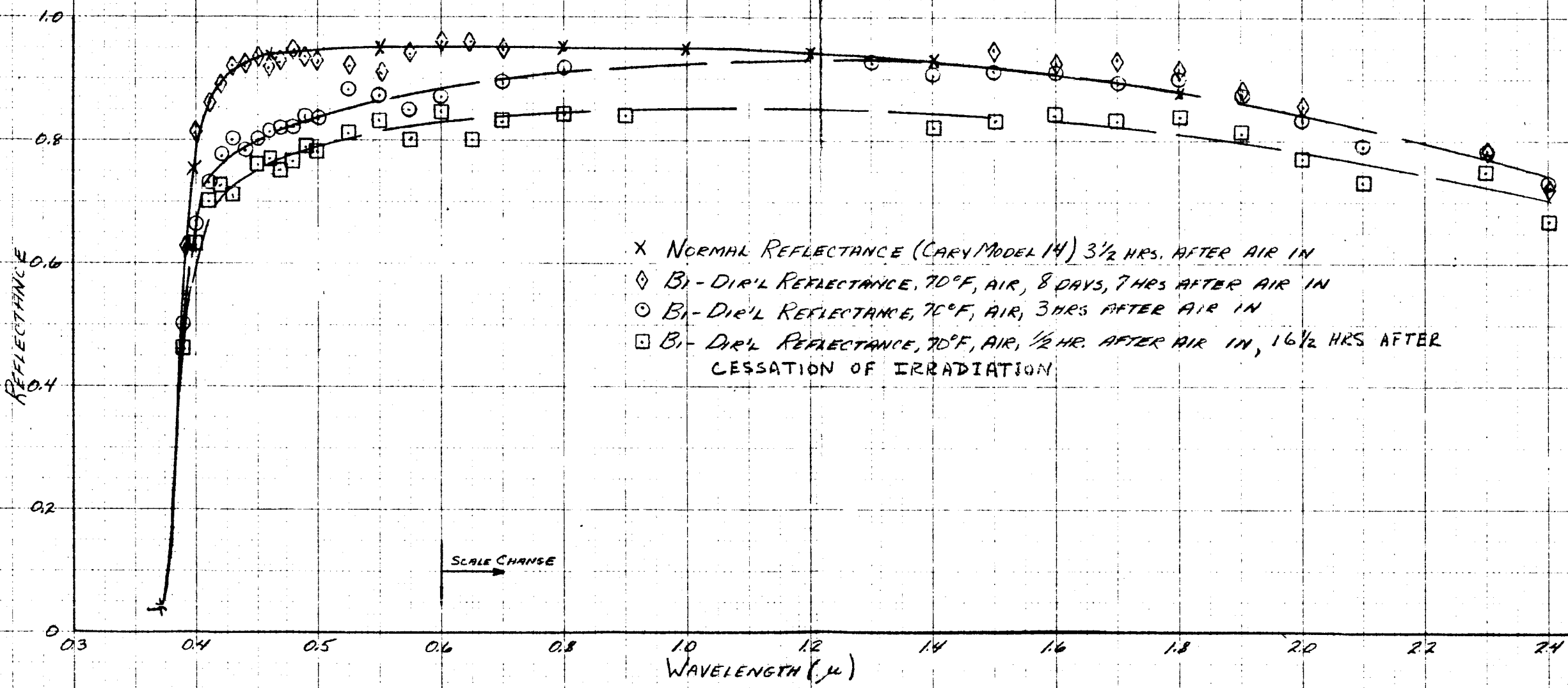

× NORMAL REFLECTANCE (CARY MODEL 14) 3½ HRS. AFTER AIR IN
◇ BI-DIR'L REFLECTANCE, 70°F, AIR, 8 DAYS, 7 HRS AFTER AIR IN
⊙ BI-DIR'L REFLECTANCE, 70°F, AIR, 3 HRS AFTER AIR IN
⊡ BI-DIR'L REFLECTANCE, 70°F, AIR, ½ HR. AFTER AIR IN, 16½ HRS AFTER CESSATION OF IRRADIATION

NOTE: FINAL BI-DIRECTIONAL REFLECTANCE DATA NORMALIZED TO AGREE WITH NORMAL REFLECTANCE VALUES BETWEEN 1.6 AND 1.8 MICRONS.

recovery has occurred in the visible. The final bi-directional reflectance spectra on the same sample, in air, affirms the change in character of the spectral reflectance between the second in situ and the Cary reflectance curves. This requires further investigation; it may be attributable to the intense tungsten source in the Cary used to illuminate the sample. This source will tend to bleach the ultraviolet degradation in zinc oxide. In taking the normal reflectance data, the Cary spectrophotometer scans from 1.8 microns to 0.3 microns. The bleaching effect of the tungsten source will therefore tend to affect the visible data (which is measured last) more than the infrared. This could explain the apparent large difference between the bi-directional and Cary data in the visible region. The fact that the Cary curve was reproduced eight days later by the bi-directional reflectance data indicates that no further significant bleaching occurred after exposure to the tungsten lamp in the Cary.

The implications of this effect on general pre- and post-test spectral reflectance measurements to evaluate environmental degradation are potentially far-reaching. The impact on procedures used in this zinc oxide study is not great, because the post-test Cary measurements are regarded as qualitative. The use of post-test reflectance measurements allows exposure of the sample to too many potential causes for damage recovery; such measurements are clearly inadequate for the generation of quantitative data on radiation damage of zinc oxide. In situ measurements are mandatory.

4.4 STATIC ULTRAVIOLET IRRADIATION TESTS

Ultraviolet irradiation tests without in situ optical property measurements are termed "static" tests in this report; information on sample behavior is based on before-test and after-test examination of the sample. These tests are performed with the apparatus described in Appendix C. Static tests were performed on particulate zinc oxide samples, under various test conditons, throughout the last eight months. Before proceeding to presentation of the data, a few comments qualifying the value of static exposure techniques are in order.

The in situ bidirectional reflectance data presented in Section 4.3 indicate that significant post-test "recovery" from ultraviolet damage, as measured by decrease in sample reflectance, occurs upon exposure of the damaged samples to air. Through prompt post-test measurement of reflectance with the Cary or Beckman spectrophotometer, the effect of such "recovery" on evaluation of the damage is minimized. In practice, the elapsed time between opening the vacuum chamber to air and the measurement of the last of a series of samples has been no longer than one hour. It must be kept in mind however, that in this first hour of exposure to air, it is very likely that measurable recovery occurs. Valid qualitative data are gained, but precise quantitative data are difficult to obtain. As an example, two samples were prepared and irradiated under nominally identical conditions. One (TP-14872AB) suffered a 12 percent decrease in spectral reflectance at 0.45μ, the other (TP-14507AA) a 8 percent decrease. The first post-test measurement was performed within one hour after exposure to air, and the second within two hours after exposure to air. A probable explanation for the apparently different behavior of the two samples is the different time that each sample was allowed to recover in air before being measured. Nevertheless, through static tests valuable information has been obtained of the influence of sample preparation and ultraviolet exposure parameters on the behavior of particulate zinc oxide during irradiation. With these qualifications in mind, it is now appropriate to review the results of the static tests.

The basic parameters considered in the static tests have been the preparation conditions (forming pressure and sintering atmosphere) and the exposure conditions, (pressure, sample temperature and irradiation spectrum). The data presented is representative of each condition. All of the tests have been repeated with more than one sample. A full tabulation of test samples and test conditions are presented in Table 4-1. Unless otherwise specified, the test parameters of the static exposures are:

(1) Irradiance Source: A-H6 (PEK Labs Type) Lamp
(2) Distance of Sample from Lamp: 3.9 inches
(3) Sample Temperatures from 100 to 125°F
(4) Pressures of 2×10^{-7} Torr except during initial ultraviolet exposure, when sample and chamber wall "outgassing" causes pressures as high as 1×10^{-5} Torr.

Standard Samples

Figure 4-5 shows the spectral reflectance of a "standard" particulate zinc oxide sample from 0.3 to 20 microns. A standard sample is prepared by forming at 10,000 psi in air for 1 minute and then sintering at 600°C in air for 15 minutes (Section 4.2). The spectral reflectance of these standard samples before irradiation was found to be highly repeatable, that is within 1 percent in the range 0.3 to 1.8μ throughout the program. For wavelengths larger than 1.8μ particulate zinc oxide is significantly transparent, so the reflectance is affected by sample thickness (Ref. 20). Two different sample thicknesses are depicted to show this effect. Spectral reflectance for samples prepared under the same forming and sintering condition of SP-500 zinc oxide are identical to these reflectance curves for the interval 0.3 to 1.8 microns. Comparative measurements were not taken at longer wavelengths.

Standard Samples - Standard Exposure

Standard samples and samples made of SP-500 zinc oxide exposed to ultraviolet irradiation in vacuum for 67 hours underwent decreases in reflectance as shown in Figure 4-6. It can be seen that the reflectance decrease is a maximum near

FIGURE 4-5

NORMAL SPECTRAL REFLECTANCE
OF PARTICULATE ZINC OXIDE (UNIRRADIATED)

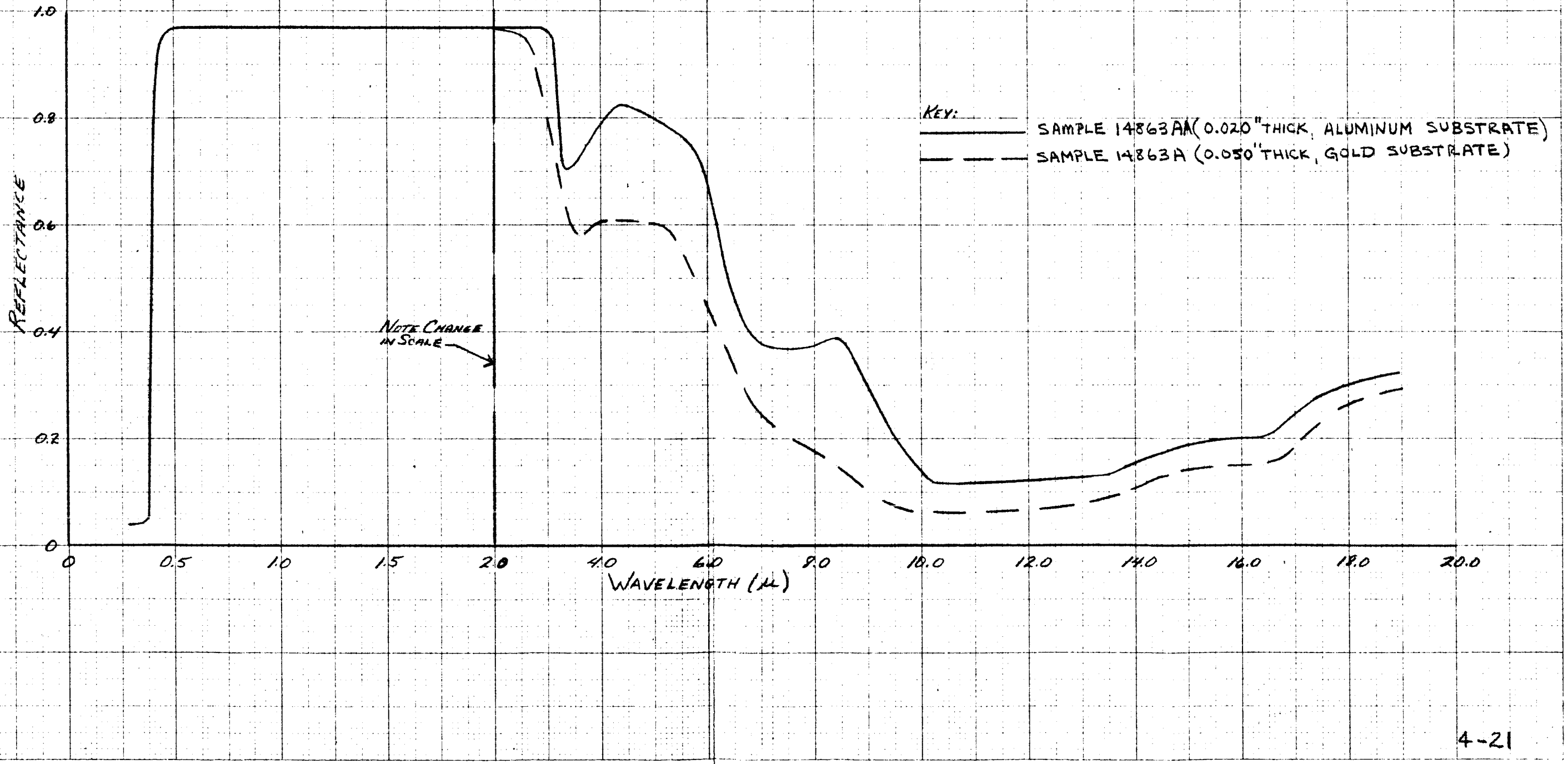

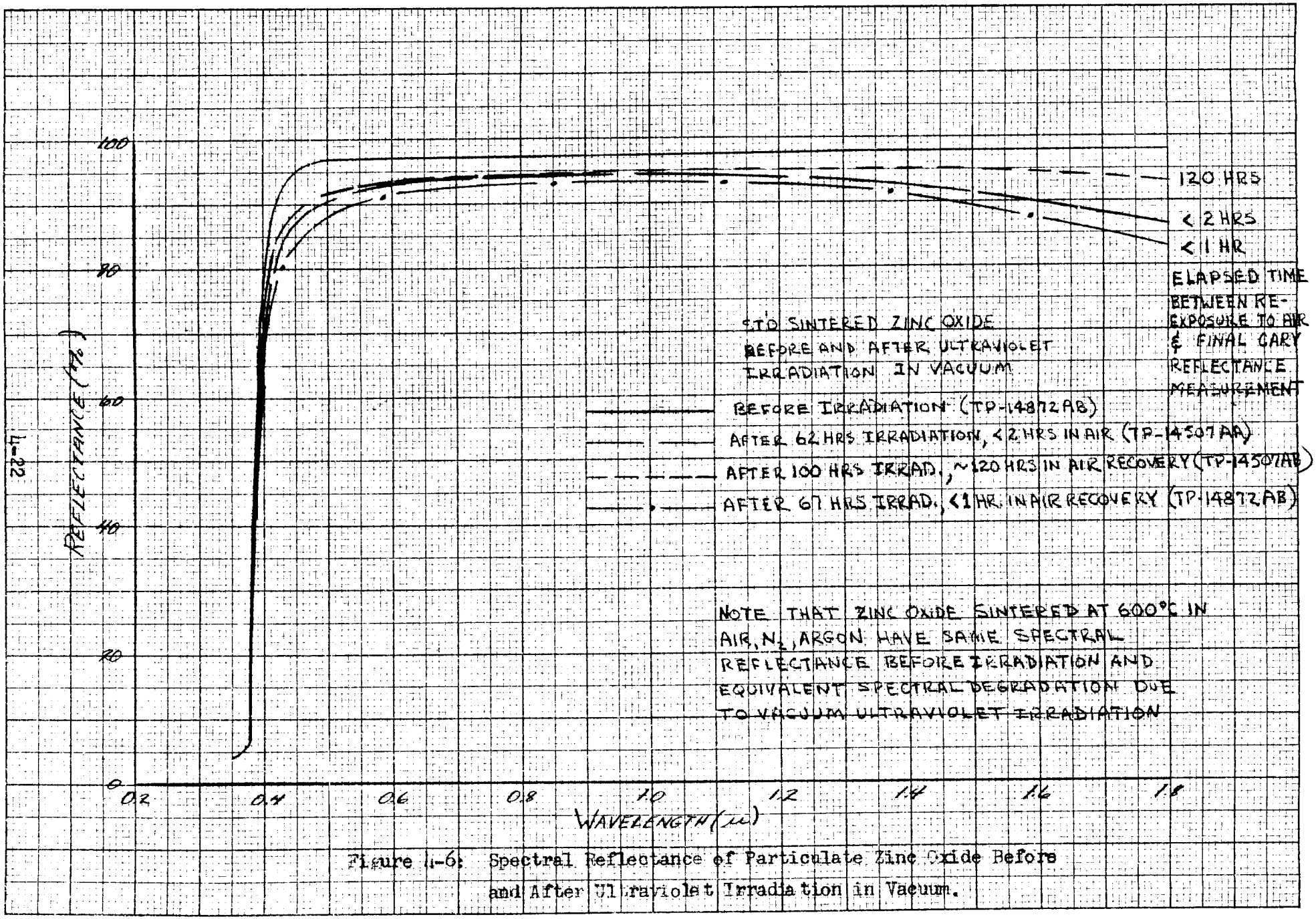

Figure 4-6: Spectral Reflectance of Particulate Zinc Oxide Before and After Ultraviolet Irradiation in Vacuum.

the absorption band edge at 0.4 microns. The decrease is less in the visible and near infrared region, but becomes greater in the region of 1.5 to 1.8 microns. Data on the Beckman to 2.6 microns shown in Figure 4-10 shows the decrease in reflectance becomes still larger in the region 1.8 to 2.6 microns. Three post-test reflectance curves are presented to show the range of variation in measured reflectance due to sample variation and more importantly to "recovery" time in air between cessation of exposure and final measurement. Tests are underway to evaluate the variation in degradation due to a range of sample irradiances. These tests will be covered in a forthcoming addendum to this report.

Standard Sample - Filtered Exposure

Standard samples were irradiated in vacuum simultaneously with those reported above, but behind selective wavelength filters. The normal transmission characteristics before and after the test are shown in Figure 4-7. One filter (microsheet) transmits radiation of wavelength longer than 0.3 microns. The other (approximately equivalent to Corning filter #3-73) transmits radiation of wavelength longer than 0.4 microns, that is radiation less energetic than the band gap energy for zinc oxide. The effects of this selective wavelength irradiation are shown in Figure 4-8. As expected, the samples protected by the 0.4 micron cut-on filter showed relatively slight damage increasing in the near infrared. It is significant that the samples protected by the 0.3 micron cut-on filter show less damage than the unprotected samples in the visible region, but more in the infrared. The implications of this are discussed in Section 6.

Standard Samples - Exposed in Air

Standard samples exposed to 88 hours of ultraviolet in ambient air did not show any change in spectral reflectance. Consequently, no data on this test are presented in graphical form.

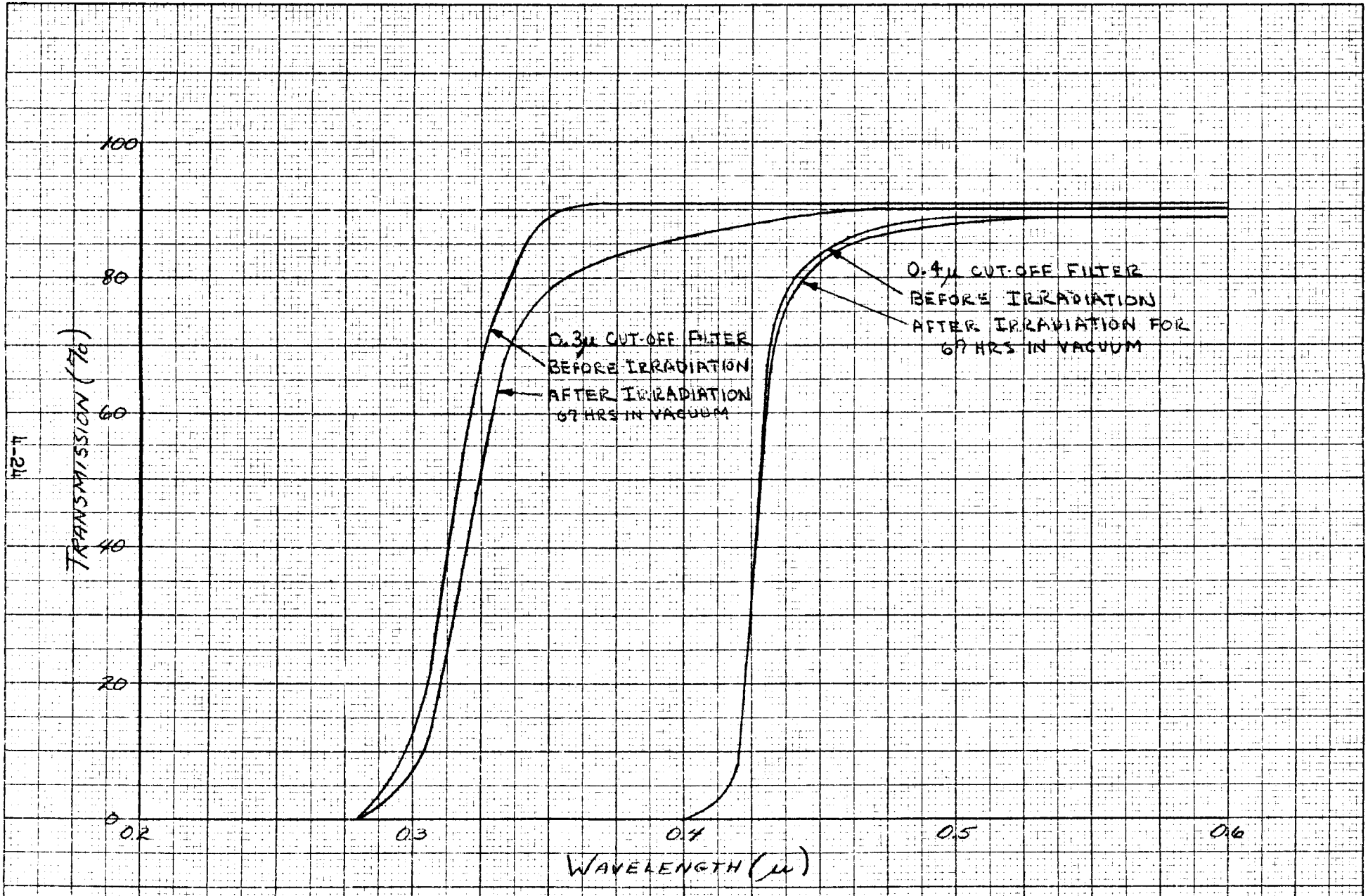

Figure 4-7: Normal Spectral Transmission of Selective Wavelength Filters Before and After Ultraviolet Irradiation in Vacuum.

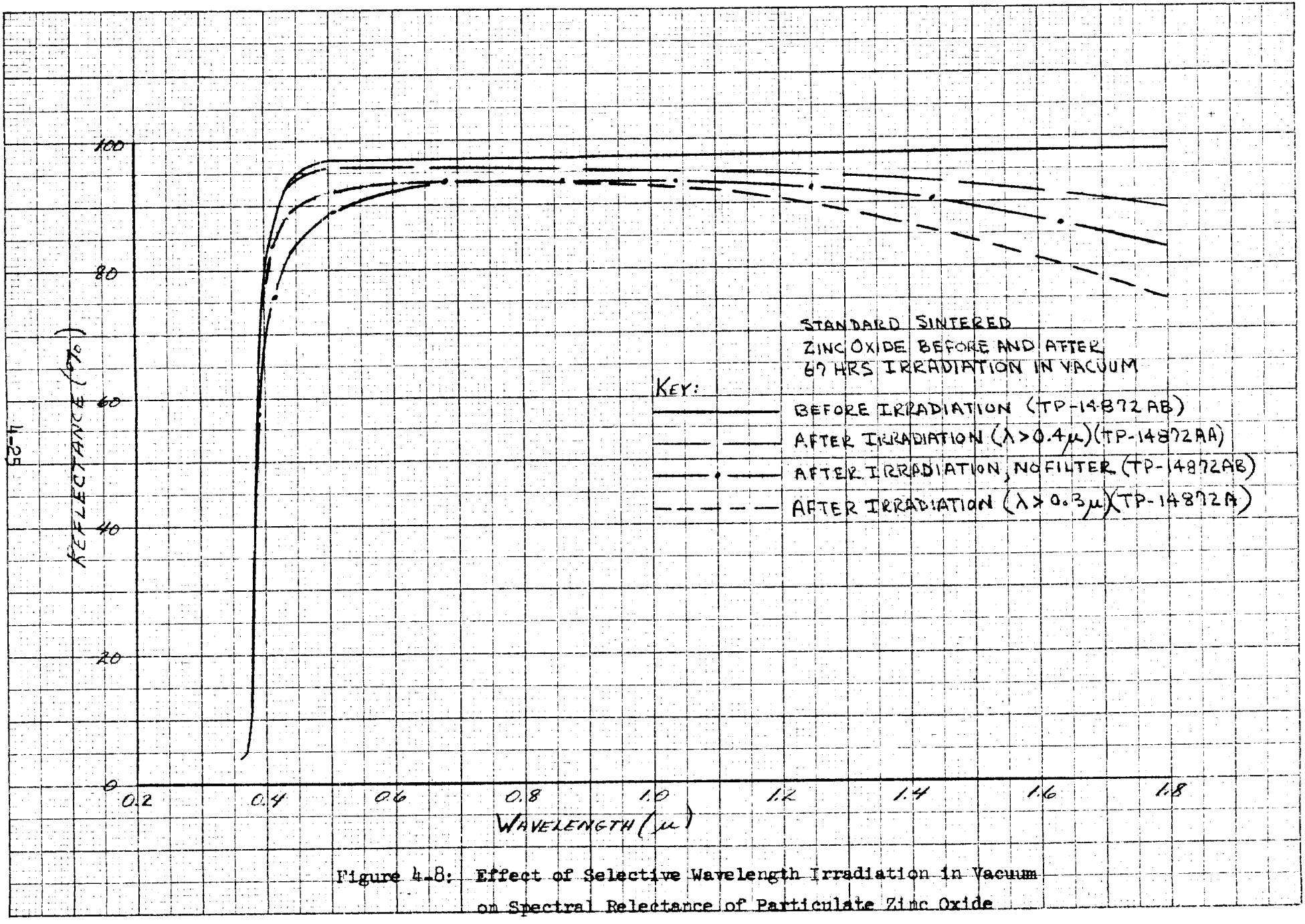

Figure 4-8: Effect of Selective Wavelength Irradiation in Vacuum on Spectral Relectance of Particulate Zinc Oxide

Effects of Sample Forming Pressure

The effect of forming pressure on the spectral reflectance of irradiated samples is shown in Figure 4-9. Samples were pressed at pressure from 10,000 psi to 100,000 psi, in air, and sintered at 600°C in air. The reflectance of the same samples after 100 hours of irradiation in vacuum is shown in Figure 4-10. Note that the decreases in reflectance due to increased forming pressure and to ultraviolet radiation are in the same spectral regions. The magnitude of the spectral reflectance decrease was found difficult to reproduce consistently because of the large variations in local pressure on any sample at high forming pressures. Consequently, depending on the exact small region of the sample viewed by the Beckman, the effect of pressure and ultraviolet varied considerably. However, these variations were generally small compared to the overall trend shown in Figures 4-9 and 4-10.

Effects of Sintering Atmosphere

Particulate samples prepared at a forming pressure of 10,000 psi and sintered at 600°C in various atmospheres were exposed to ultraviolet irradiation in vacuum and in air. Those samples sintered in air, nitrogen and argon exhibited: (1) the same initial spectral reflectance, (2) the same magnitude of spectral reflectance degradation when irradiated in vacuum, and (3) no degradation when irradiated in air. Therefore, Figure 4-6 is representative of all these conditions. On the other hand, samples sintered at 600°C in a residual air presure of 10^{-2} to 10^{-3} Torr exhibited markedly different characteristics. When irradiated for 88 hours in air, the vacuum sintered samples showed a marked increase in reflectance in the visible region, but only a slight increase in the infrared.

These results are shown in Figure 4-11. Similar samples sintered at approximately 10^{-3} Torr and irradiated in vacuum for 67 hours showed only a slight increase in reflectance at all wavelenghts. This result is not surprising, considering the relative lack of oxygen in the vacuum irradiation test (See Section 6). These results are presented in Figure 4-12. The vacuum sintered

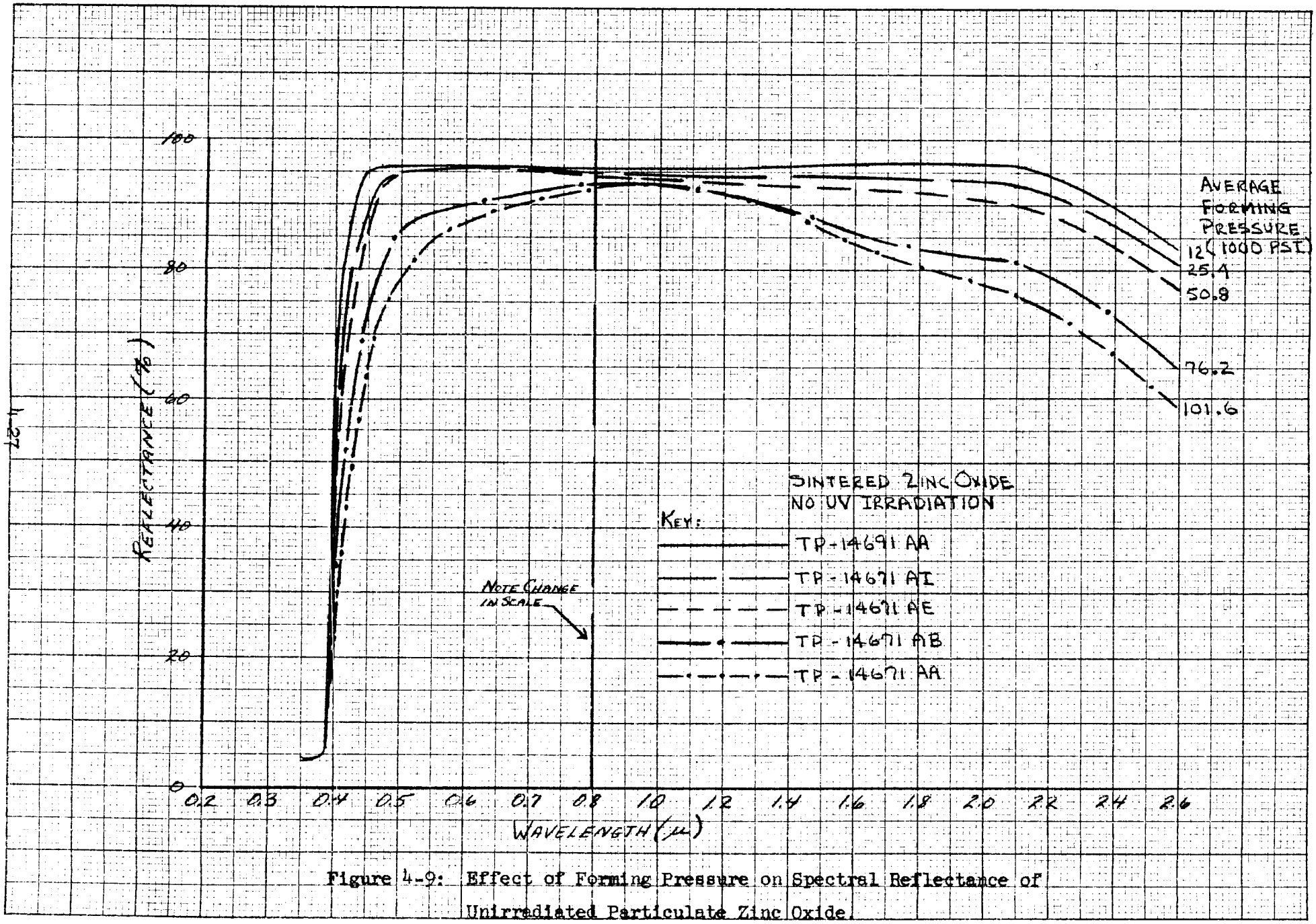

Figure 4-9: Effect of Forming Pressure on Spectral Reflectance of Unirradiated Particulate Zinc Oxide.

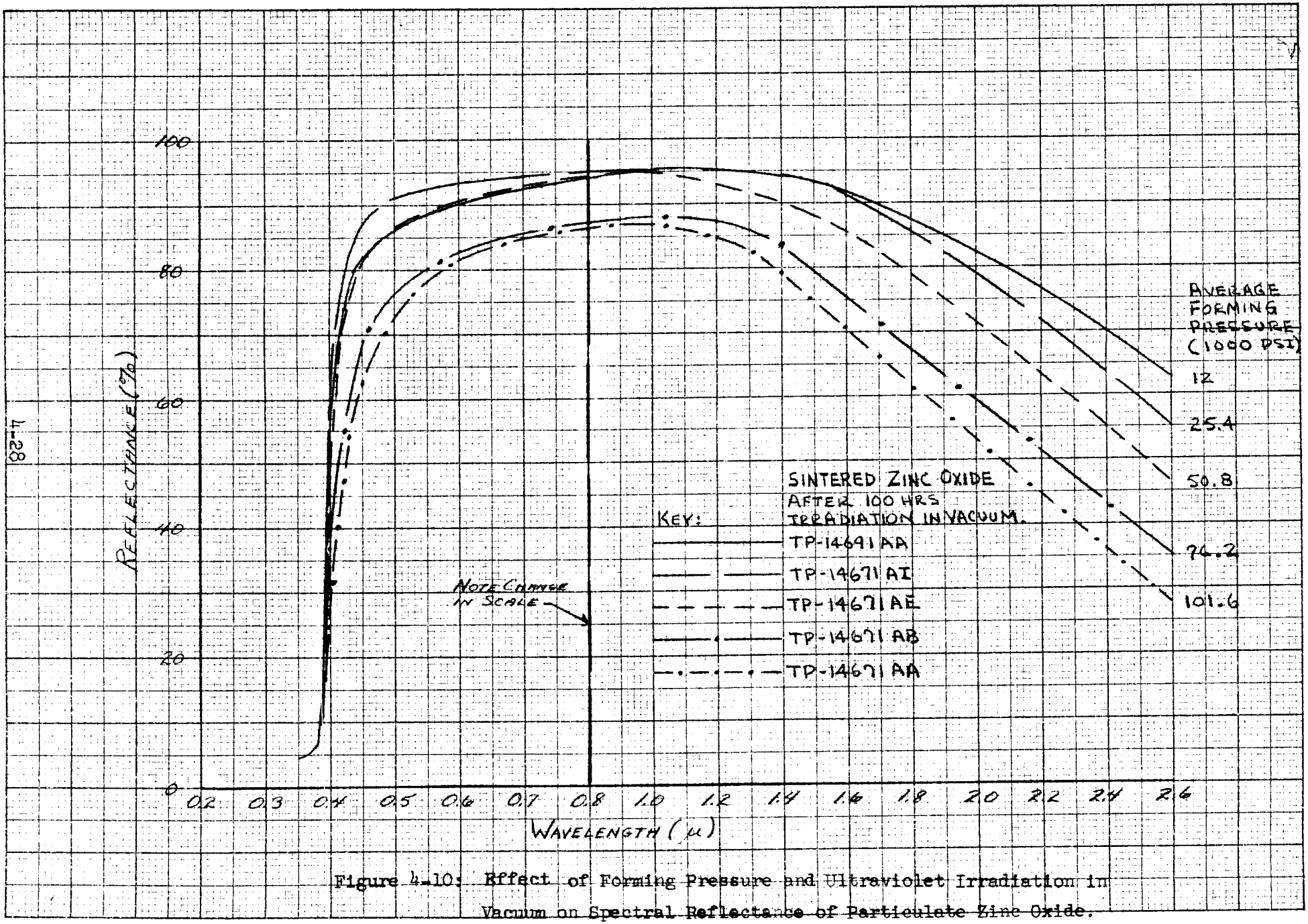

Figure 4.10: Effect of Forming Pressure and Ultraviolet Irradiation in Vacuum on Spectral Reflectance of Particulate Zinc Oxide.

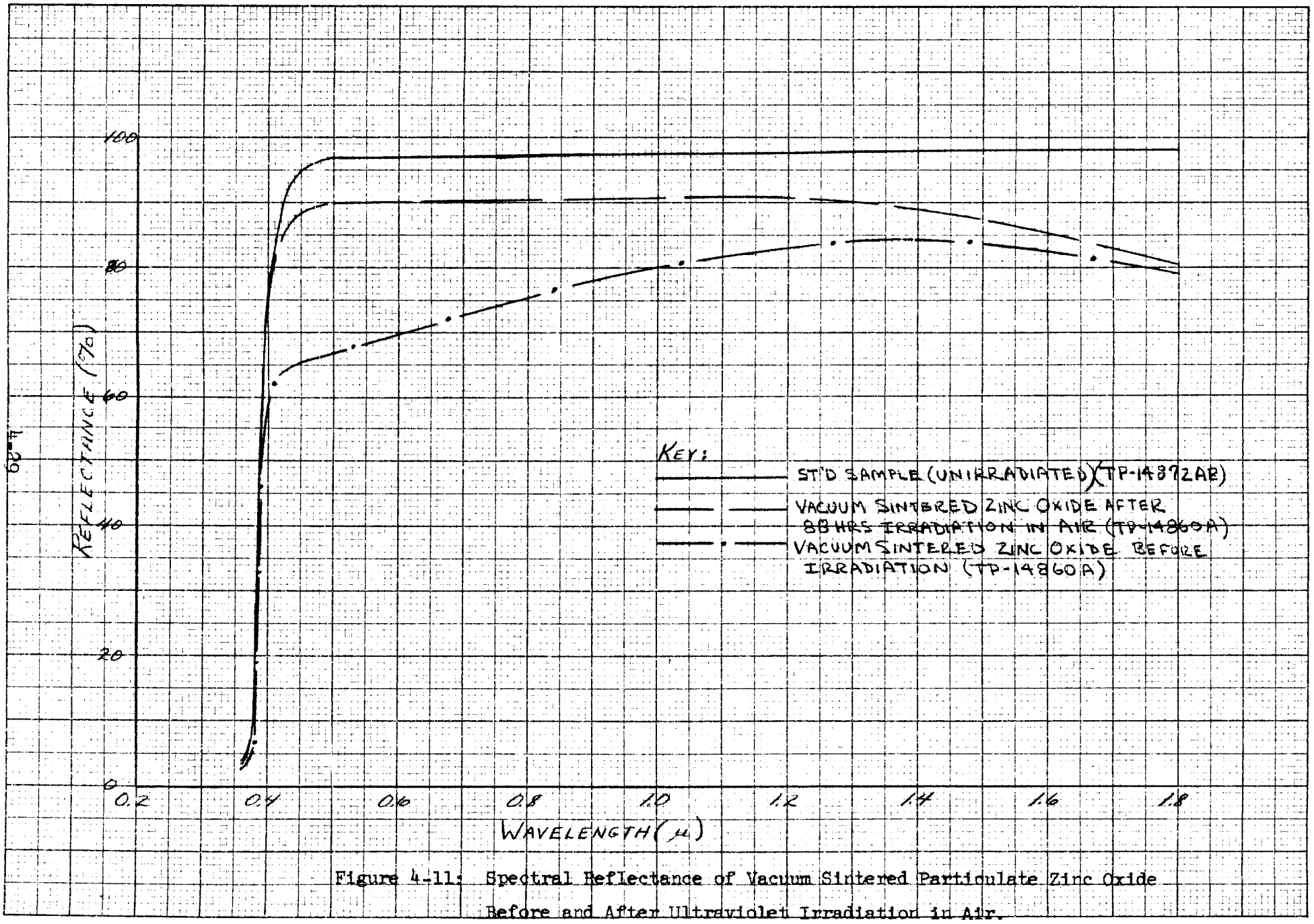

Figure 4-11: Spectral Reflectance of Vacuum Sintered Particulate Zinc Oxide Before and After Ultraviolet Irradiation in Air.

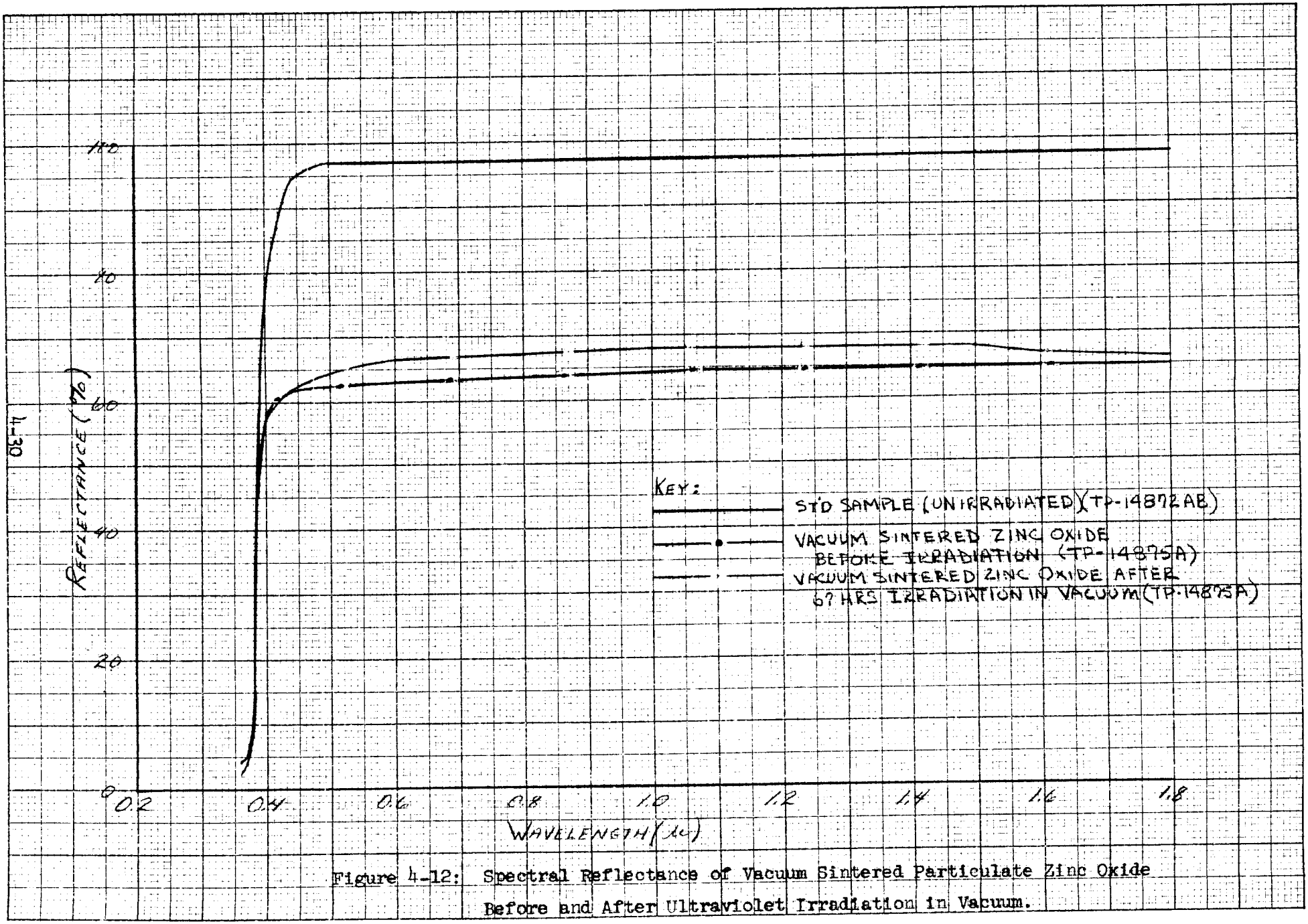

Figure 4-12: Spectral Reflectance of Vacuum Sintered Particulate Zinc Oxide Before and After Ultraviolet Irradiation in Vacuum.

samples for which spectral reflectance data is presented in Figures 4-11 and 4-12 have different spectral reflectances before irradiation. The sample presented in Figure 4-11 has higher reflectance throughout the infrared region than that presented in Figure 4-12. At this time no particular significance can be attached to these differences. Although all vacuum sintered samples were prepared in nominally identical fashion, it is recognized that sintering oven pressure variations and temperature gradients through each sample can have marked effects. Variations in surface appearance, not only between samples but on the same sample, have consistently occurred.

Cu/ZnO Samples

Samples prepared by co-precipitating copper and zinc oxide as described in Section 3.1, were irradiated for 67 hours in vacuum. The pre-and post-test spectral reflectance data are presented in Figure 4-13. The effect of the 0.1% copper doping is to lower the initial reflectance throughout the visible and infrared. However, the ultraviolet stability of copper doped samples is markedly better than for the pure zinc oxide. For comparison with the copper doped sample spectral reflectance two undoped zinc oxide spectral reflectance curves are presented. One is of the standard sample, and the other is for undoped, precipitated zinc oxide prepared in identical fashion to the copper doped sample. The ultraviolet irradiation of the undoped, precipitated sample has not been performed as yet. The results of this test will be included in the final report.

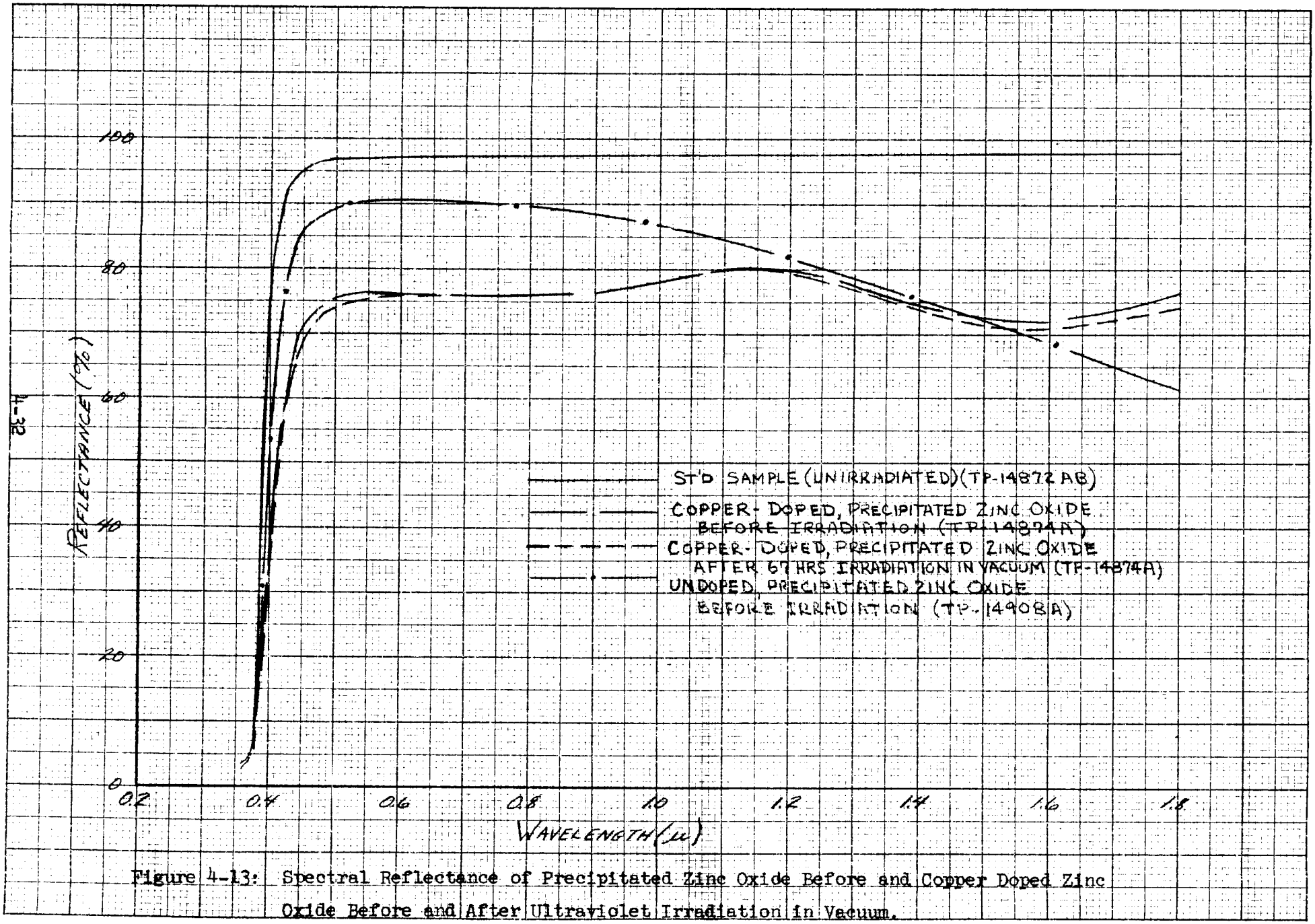

Figure 4-13: Spectral Reflectance of Precipitated Zinc Oxide Before and Copper Doped Zinc Oxide Before and After Ultraviolet Irradiation in Vacuum.

Section 5

BAND STRUCTURE STUDIES

A thorough understanding of the electronic energy band structure (Ref. 21) of a crystal is a necessary prerequisite for the detailed interpretation of many important transport and optical properties. We have, therefore, initiated theoretical band structure studies of ZnO to complement the experimental program.

To the best of our knowledge, no serious attempt has previously been made to elucidate the electronic band structure of ZnO. We thus feel that our efforts will prove to be both useful and unique. Although the results to be presented here are of a preliminary nature, a number of interesting inferences can be made on the basis of this work.

The initial attempt to determine the band structure of ZnO was based on the pseudopotential method, (Ref. 22). The essential feature of this approach is that it provides a parametrized form of $E(\underline{k})$ throughout the entire Brillouin zone. The correct band structure is then obtained by adjusting the parameters so that certain features of the calculated band structure agree with experiment. At certain points of the zone, for instance, one might choose to fit experimentally determined band gaps, or individual band slopes or curvatures.

Our pseudopotential calculation was carried out for several points of high symmetry in the Brillouin zone using five parameters and an average of about twenty plane waves. Proceeding on this basis, it was not possible to obtain an energy band scheme in agreement with the relevant experimental data. This was initially somewhat puzzling, since in the case of the

column IV semiconductors only three pseudopotential parameters are needed to obtain excellent results. The key to this difficulty is likely to be found in some recent work by Falicov and Golin, (Ref. 23). In a paper reporting on an investigation of the band structure of the group-V semimetals, these authors made an interesting speculation concerning the construction of pseudopotentials. If their procedure is adapted to the wurtzite-type crystals, it would imply that approximately fifteen pseudopotential parameters are needed in this case. The parametrization of the band structure is thus very complex for wurtzite-type crystals. Furthermore, because of the paucity of experimental band parameters for ZnO, there is clearly insufficient information available to fit such a large number of parameters. The pseudopotential calculation was therefore temporarily put aside for a more promising method. However, we did gain a great deal of physical insight into the ZnO band structure problem in the course of this initial study.

In particular, it became evident that the band structure of ZnO should be quite similar to that of ZnS. Both compounds crystallize in the wurtzite structure, have nearly the same c/a ratio, and 16 valence electrons per unit cell. Furthermore, sulfur is adjacent to oxygen in column VI of the periodic table and both elements have only s and p valence states occupied. The direct band gaps at $\underline{k} = (000)$ are similar in ZnS and ZnO (3.94 and 3.44 e.v. at 0 ^{o}K respectively), and exciton studies of Dietz, Hopfield and Thomas (Ref. 24) have given a band edge structure for ZnO at $\underline{k} = (000)$ which is identical to that determined for ZnS by the exciton studies of Wheeler and Miklosz[3] (Ref. 25). This latter work is also in agreement with the band edge ordering calculated for ZnS by Herman and Skillman (Ref. 26) using the orthogonalized-plane-wave (OPW) method.

During the course of his early investigation of ZnS, Herman studied the behavior of the energy bands when all of the core energy levels are shifted by a common amount - the so-called "core shift". The core shift was

originally intended as a diagnostic device; however, it can be used to great advantage to relate the band structures of similar systems. Stated briefly, certain energy band levels are extremely sensitive to changes in the crystal potential while other levels are relatively insensitive. As one proceeds in a systematic fashion through a series of closely related crystals, it is the shifts of the sensitive levels which provide the most significant changes in the electronic properties throughout the sequence. As an example, Phillips (Ref. 27) has shown that the band structure of Si can be obtained from that of Ge by application of a suitable core shift to the band structure of Ge. Thus, given a band structure and the knowledge of how the important valence and conduction bands vary as a function of the core shift we have, in fact, an "adjustable" band structure which can be chosen to determine other, closely related band structures. This describes the "method of corresponding states."

We have carried out this core shift procedure and have succeeded in obtaining the band structure of ZnO from that of ZnS thereby. The results of this calculation, given in Fig. 5-1, were obtained by using that core shift yielding the correct direct gap at $\underline{k}$ = (000). Of interest here is the relative flatness of the upper valence bands, the presence of a subsidiary conduction band minimum at K, and the presence of a valence band maximum at H. The nearly parallel conduction and valence bands along the A-H axis should give rise to a marked increase in the optical absorption at $\sim$ 5.5 - 6.0 e.v.

The reliability of our results, of course, can be no better than that of the ZnS calculation used as a basis for this work. The photoemission studies of Kindig and Spicer (Ref. 28) on CdS add to our confidence here. For many of the same reasons already noted, the band structure of CdS should be similar to both that of ZnS and ZnO. These authors have shown that the valence and conduction band densities of states are in good agreement with Herman's ZnS calculation. We do expect, however, that a self-consistent band structure calculation may lead to results which differ from Fig. 5-1 in some respects.

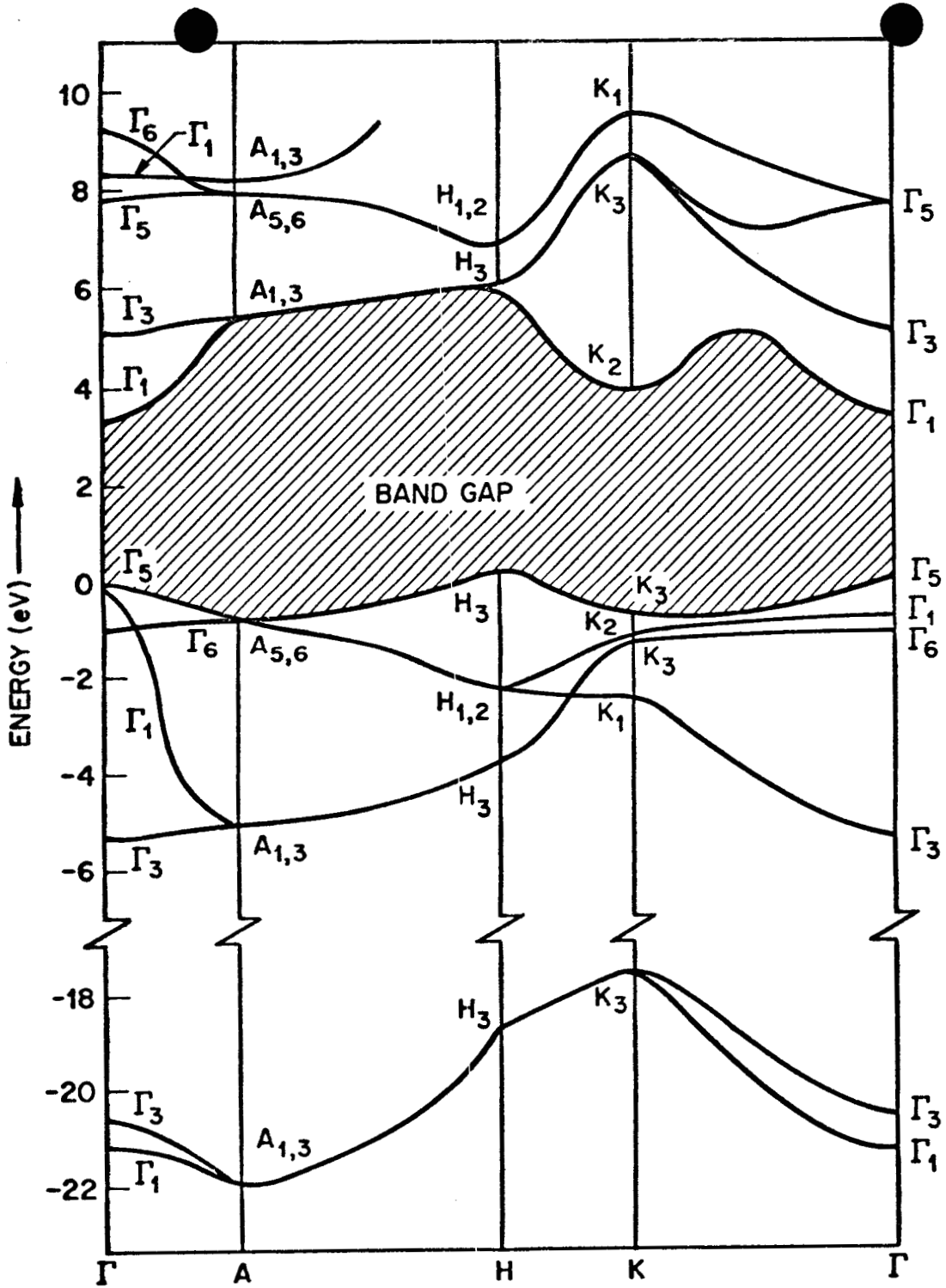

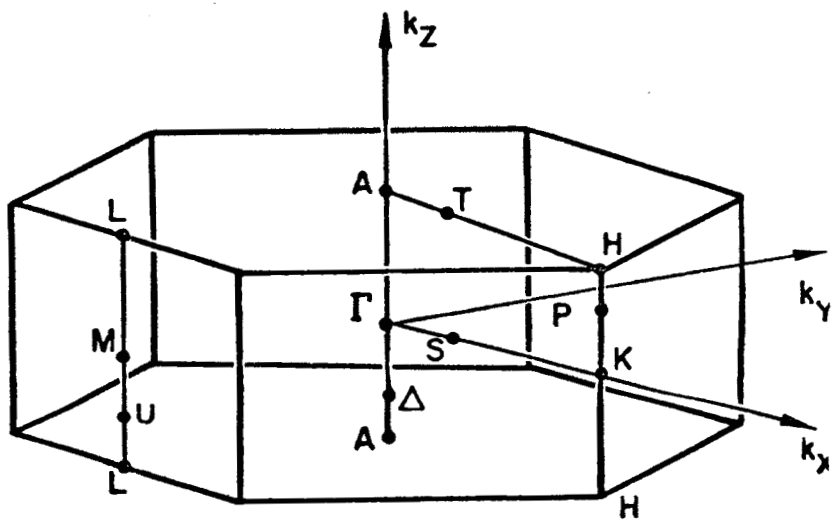

THE FIRST BRILLOUIN ZONE SHOWING LINES AND POINTS OF SYMMETRY

Figure 5-1

Energy Band Structure of ZnO Along the Γ-A-H-K Directions

For the sake of comparison, the free electron (or "empty lattice") band structure (Ref. 29) for wurtzite-type crystals is given in Fig 5-2. This represents the band structure in the limit of zero crystal potential. As the crystal potential is "turned on" on its true value, the free electron bands evolve into the actual band structure as shown in Fig. 5-1.

Another interesting comparison is given in Fig. 5-3. Here we have compared the energy levels at the center of the zone (Γ) as given by three different methods: the free electron model, our preliminary results for the band structure, and a tight binding model (to be discussed below). In the left hand column, we have taken the set of plane waves corresponding to each degenerate eigenstate and have formed linear combinations (designated by Γ_i) transforming as the irreducible representations of the group of the wave vector $\underline{k}$ = (000)(Ref. 30). In this way, it is shown how the free electron levels split as the crystal potential is "turned on" and the correspondence between the free electron and actual band structures at is established.

In the right hand column, we have assumed that the electronic wave functions are simply the orbitals of the constituent neutral atoms. The energy levels were obtained from the work of Herman and Skillman (Ref. 31). This would serve, for instance, as the starting point for a linear-combination-of-atomic-orbitabls (LCAO) calculations, (Ref. 32) As in the case of the plane wave states, we have taken the atomic orbitals corresponding to each degenerate eigenstate and have determined linear combinations transforming as the irreducible representations of the group of the wave vector $\underline{k}$ = (000). In explanation of the notation used here, $[4s, Zn]_2$ identifies the 4s states of the two (subscript) Zn atoms in the unit cell.

In both the free electron and tight binding cases, states having the same irreducible representation will be mixed as the crystal potential is "turned on". The lowest conduction band is thus a mixture of Zn 4s-orbitals and O 2p-orbitals as is the second highest valence band. The highest

Figure 5-2 Wurtzite Free Electron Band Structure

Free electron band structure for close-packed hexagonal or wurtzite-type crystals, drawn for the ideal c/a ratio. The heavy lines denote the positions of the highest valence band and lowest conduction band for crystals having 16 valence electrons per unit cell. The dots denote the degeneracy of each band (not including spin degeneracy) and the shaded region shows the band gap.

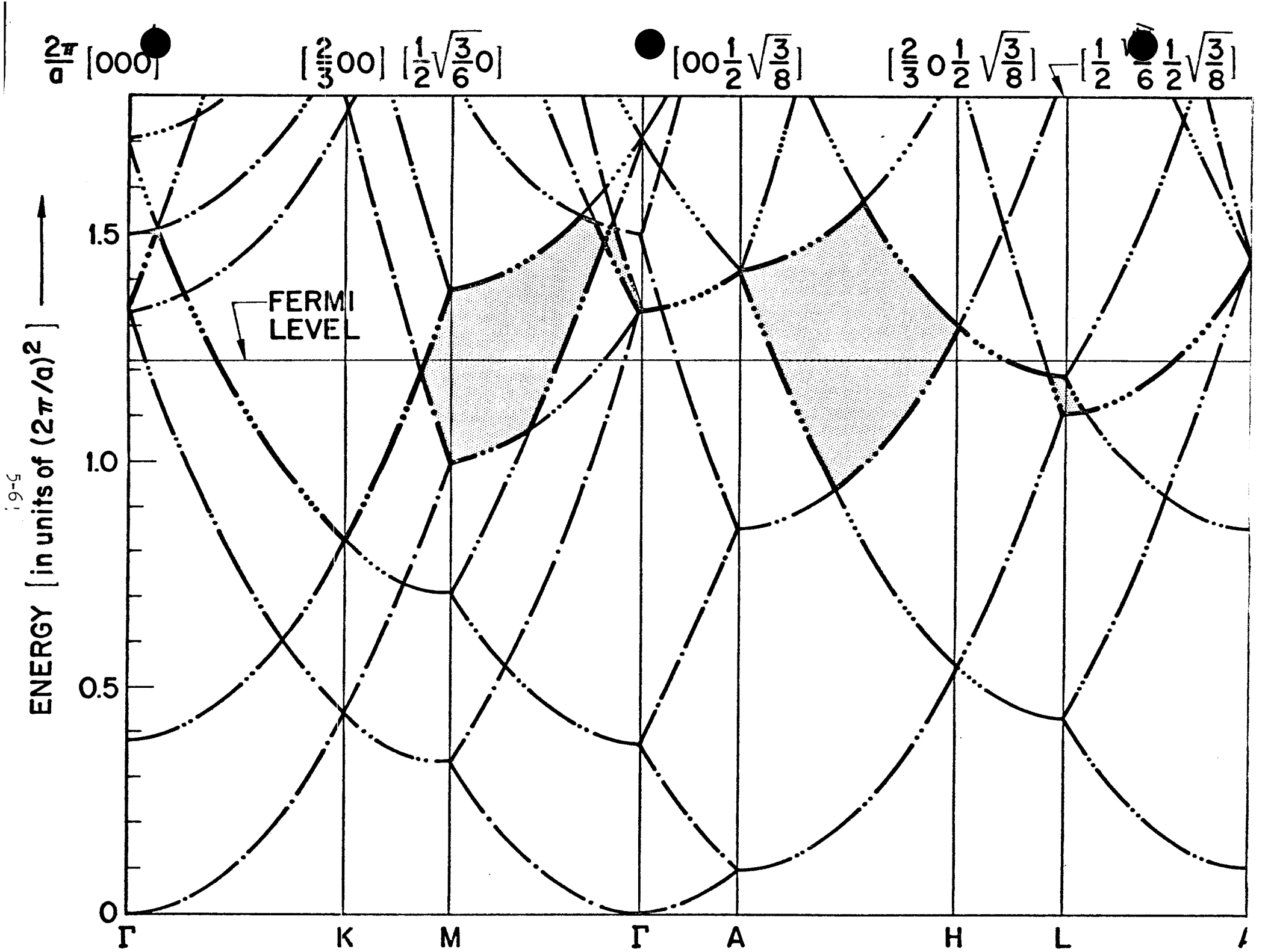
$\frac{2\pi}{a}$ [000]
$[\frac{2}{3}00]$ $[\frac{1}{2}\sqrt{\frac{3}{6}}0]$
$[00\frac{1}{2}\sqrt{\frac{3}{8}}]$
$[\frac{2}{3}0\frac{1}{2}\sqrt{\frac{3}{8}}]$
$[\frac{1}{2}\sqrt{\frac{1}{6}}\frac{1}{2}\sqrt{\frac{3}{8}}]$
ENERGY [in units of $(2\pi/a)^2$]
1.5
1.0
0.5
0
FERMI LEVEL
Γ
K
M
Γ
A
H
L

Figure 5-2

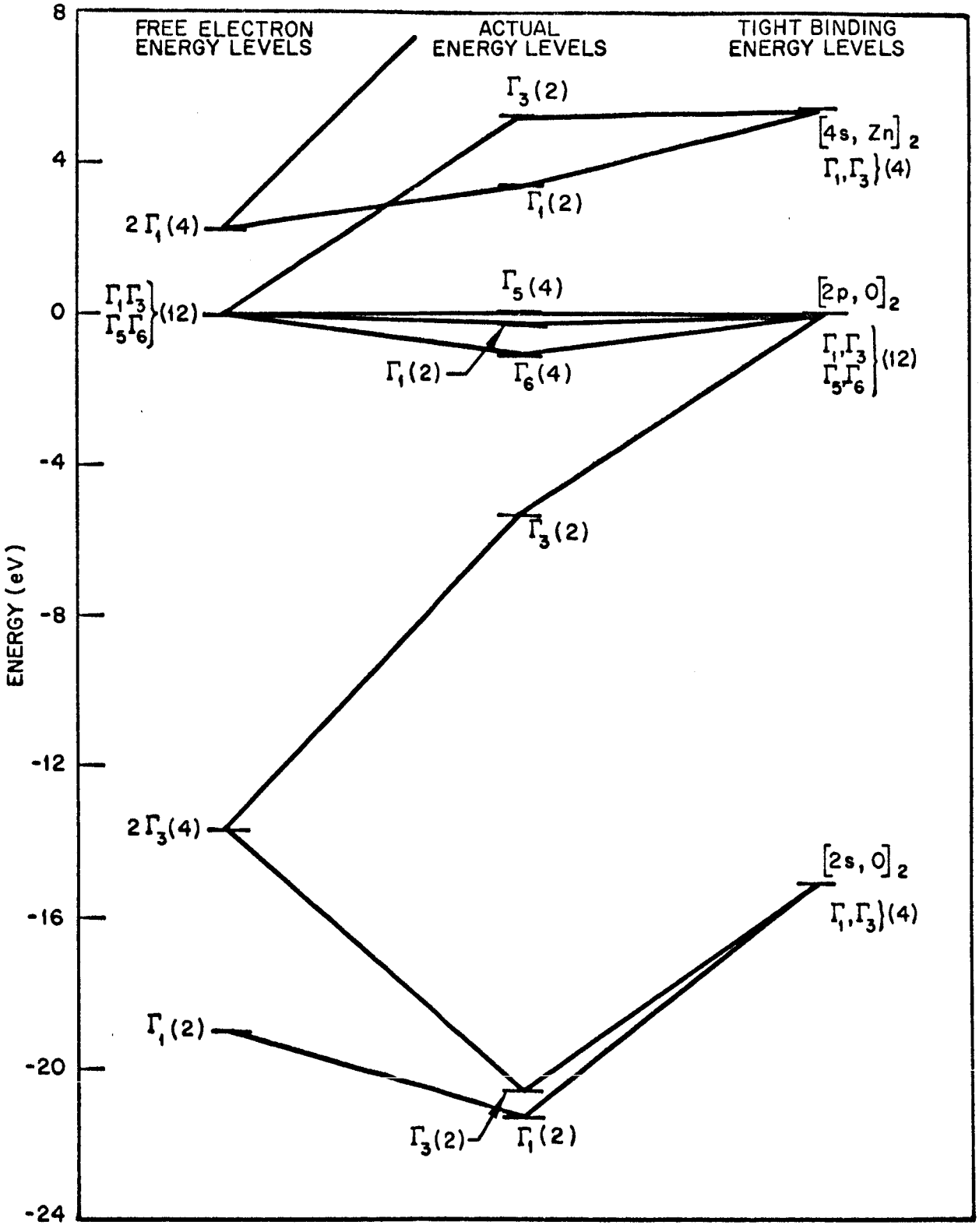

Figure 5-3 Comparison of Band Structure Models at Center of Brillouin Zone

Comparison of the energy levels as given by the free electron, tight binding, and "actual" band structure models at $k = (000)$. The top of the valence band has been chosen as the zero energy for all three models. Numbers in parentheses denote the degeneracy of the levels, including spin degeneracy.

valence band arises from O 2p-orbitals.

Our assignment of an atomic orbital character to the various bands is subject to the following limitations. In the first place, we have neglected all states of higher (or lower) energy than those indicated. We can therefore expect that the energy bands of interest (subject to the rules of group theory) will contain small admixtures of these states. Secondly, the 3d levels of Zn, which lie between the oxygen 2s and 2p levels, have for the sake of simplicity been treated as core rather than valence states. Actually, the 3d orbitals fall into a class that is between true "core states" (virtually no nearest neighbor overlap) and "valence states" (significant overlap). Finally, the atomic character of the bands will vary somewhat as $\underline{k}$ varies over the Brillouin zone.

The energy band structure of ZnO has been examined in a preliminary manner on the basis of four different theoretical models: the method of pseudopotentials, the method of weak binding, the method of tight binding, and the method of corresponding states. The pseudopotential method was used to gain some physical insight into the nature of the band structure. While it was found that insufficient experimental information was available at present to make possible a detailed band calculation on the basis of the pseudopotential method, the work we carried out led us to the conclusion that the band structures of ZnO and hexagonal ZnS were probably closely related, and that the former could be deduced from the later by the method of corresponding states. Starting from an earlier study of the band structure of hexagonal ZnS by Herman and Skillman, and making suitable adjustments in scale, an energy band model for ZnO was derived. The plausibility of the derived model was then tested by the method of weak binding (nearly-free-electron model) and by the method of tight binding (LCAO model). These tests indicated that our derived band structure for ZnO was probably a good first estimate. Further work in this area may prove to be quite valuable because of the crucial role that the energy band structure can play in estimating the energy levels of both surface states and bulk defect state. In order to put this work on a firmer theoretical

foundation, carrying out detailed first-principles self-consistent energy band calculations for ZnO using the method of orthogonalized plane waves in the near future is under consideration.

Section 6
DISCUSSION

During the course of this program, the primary characterization of the solar-radiation-induced damage to zinc oxide has been made in terms of the changes in optical properties of the samples. The relationships existing between the zinc oxide employed in this work and the material employed in thermal control paints is of particular interest. Although no binder materials were included with the pressed and sintered samples, the reflectance spectra were found to be quite similar, over the wavelength range of 0.27μ to 2.5μ, to those of zinc oxide paints. This observation, in connection with the findings that the average particle sizes of the original zinc oxide powder and the sample compacts were approximately the same, indicates that the sample preparation procedures did not alter the properties of the material to an appreciable extent. Therefore, it is to be expected that, exclusive of binder effects and pigment-binder interactions, the damage processes observed in this study are similar to those occurring in zinc oxide paint systems. The relative simplicity of the pure pigment system has led to a better understanding of those processes characteristic of the pigment, without the added complexities of pigment-binder interactions.

Throughout the course of the experimental studies, one overriding trend in the data has been apparent: <u>most of the changes in the optical properties of zinc oxide appear to be connected with the loss and gain of oxygen by the crystal</u>. This is borne out not only by the results of irradiation in vacuum and air, but also by the changes in optical properties induced by sintering in vacuum. Evidence in support of this point lies in the observation that both the ultraviolet-radiation-induced damage and mechanically-induced damage can be reversed by exposure to air. These results emphasize the need for <u>in situ</u>

measurements of sample reflectance, since recovery and bleaching effects greatly limit the quantitative significance of post-exposure reflectance measurements.

A major portion of the effort in this program has been devoted to development of the in situ bi-directional reflectance measurement and ultraviolet exposure apparatus, and to learning the strengths and limitations of this new analytical tool. Excessive quantitative importance should not be attributed to the preliminary in situ data accumulated to date; however, the trends and qualitative behavior observed are extremely significant. Further exposures with in situ measurements will play a crucial role in the construction and evaluation of a model for the mechanisms of optical damage. Because of the complications involved in observation of the spectral and temporal dependence of recovery, in situ measurements are mandatory for accurate determination of the kinetics of damage and recovery. In situ tests afford much greater flexibility than static tests involving only pre- and post-test property measurements. For instance, conditions can be altered during the course of a run as a result of data being obtained. In addition, the in situ tests provide a means for observing behavior of samples when in the simulated orbital environment, and thus are the best practical means for observing phenomena predicted on the basis of a postulated damage model.

Of particular importance in diagnosing the degradation effects in ZnO are the characteristics of the degradation observed in various spectral regions. In most of the degradation observed, a "gray" absorption occurs throughout the spectral range studied (0.4 – 1.8 μ). This absorption is very likely due to a surface layer of Zn in some form. Such a deposit has been observed in the vacuum chamber and is an expected consequence of the degradation process. In addition to this "gray" absorption, additional damage-induced absorption occurs in the 0.4 – 0.6 micron ("visible") region and in the 1.0 – 2.6 micron ("infrared") region.

Samples damaged by ultraviolet irradiation in vacuum, and by vacuum sintering both develop marked absorption in the visible and infrared regions, as well as exhibiting the generalized lowering of reflectance throughout the spectral range studied. Samples damaged mechanically by means of high forming pressures also exhibit damage in the same regions, which is further enhanced by irradiation. The qualitative similarity among the various types of damage strongly suggests one common underlying cause, which appears to be the presence or absence of oxygen.

The first experiments to be discussed are those involving filtering of the damaging radiation source. Two filters were used, a yellow filter and a pyrex filter. The yellow filter cut off radiation below 0.40 μ and has a 50 percent transmission near 0.425 μ, and the pyrex filter cut off radiation below 0.28 μ with a 50 percent transmission at 0.32 μ (see Sec. 4.4).

The yellow filter removes all radiation with energy greater than the band gap, and in this case only damage in the infrared was produced. The pyrex filter passes significant amounts of radiation with energy greater than the band gap, and in this case visible damage occurred and increased infrared damage was observed. The unfiltered radiation produced increased visible damage but less infrared damage in comparison to the results of the pyrex filter. The lack of visible absorption in the 0.4 μ filter run and its subsequent increase with increasing intensity of band gap radiation in the other filter runs indicate that this damage requires band gap radiation. Because band gap radiation is absorbed very near the surface (<0.1 μ) the visible absorption is presumably associated with damage generated near the surface.

Since the yellow filter only passes radiation with energies less than the band gap, this radiation is rather penetrating, and the infrared damage resulting from this radiation must, therefore, be generated in the bulk of the particles. By penetrating radiation is meant radiation which can penetrate deeply into

the bulk of the particles because of its relatively low absorption coefficient. This experiment only shows that the damage is generated throughout the bulk of the particles. The resulting infrared absorbing species may not necessarily, on the basis of this experiment, reside throughout the particle.

In comparison to the yellow filter, the pyrex filter passes a greater amount of radiation less than the band gap (penetrating radiation) in addition to passing radiation of energy greater than the band gap. Apparently this increased penetrating radiation increases the infrared damage. The relatively large change in infrared dmage produced by radiation between the absorption edge and 0.425 microns would indicate that the radiation producing the infrared damage is rather near the absorption edge in energy.

The relative decrease in the infrared absorption with no filtering is presumably the result of a self-filtering action which comes about from the increased visible damage for this case. The lack of the "gray" absorption in the yellow filter run and its appearance in the other runs indicates it also required band gap radiation.

The next important series of experiments are those involving the ultraviolet irradiation in air of vacuum sintered samples which show recovery in the visible region, but not in the infrared, after exposure. Because the visible absorption observed in vacuum sintered samples and samples degraded by ultraviolet radiation are similar, the disappearance of visible absorption by bleaching a vacuum sintered sample would indicate that this visible absorption and its elimination is primarily a surface phenomenon. Also the lack of bleaching in the infrared would indicate that the infrared damage is located in the bulk; its bleaching would presumably require a much longer time because of the requirement for a diffusion process.

The next related series of experiments we wish to discuss involve the time dependence of the ultraviolet-induced degradation and its recovery both in the visible and infrared regions; these are the ultraviolet exposures performed

with in situ bi-directional reflectance measurements (Sec. 4.3). Both the 500°F and 100°F exposures show that in the visible region, the time dependence of the ultraviolet damage is characteristic of the time dependence observed in the slow photoconductive process, which is due to the adsorption and desorption of oxygen. In the 500°F exposure, the damage in the visible region appeared to have a rapid partial recovery in vacuum upon cessation of irradiation. After this fast behavior, no further recovery in vacuum was observed. This effect is presumed to be connected with the rapid return of residual oxygen to the surface upon removal of the incident radiation. This again is similar to the slow photoconductive process. The infrared absorption in the 500°F exposure, like the visible absorption, increases and reaches a saturation level during irradiation; however, no essential change was observed in vacuum when the irradiation was stopped. It must be noted that the comments on sample damage recovery are based on limited data; further evidence is required before any final conclusions are in order. However, if this recovery pattern is firmly established, then it supports the thesis that the visible damage occurs close to the surface, whereas the infrared damage is more of a bulk phenomenon. Recovery was observed to some extent in both the visible and infrared regions upon exposure of the samples to air. The kinetics of this process will be more closely followed in the future tests; we would expect that admission of air to the degraded systems would result in a more rapid recovery in the visible than in the infrared because of the postulated requirement of a diffusion process for the latter.

The last experiments to be mentioned have just been initiated; these are the studies of particulate samples of copper-doped zinc oxide (see Sec. 4.1). These studies were based on consideration of certain aspects of the damage model (Sec. 2.6), and on the observed behavior of single crystals doped with copper and lithium. On the basis of conductivity measurements, it has been shown that the Fermi level can be depressed by 1 ev or more through doping with group I acceptor impurities (i.e., lithium or copper) (Sec. 3.1). Lowering of the Fermi level by a sufficient amount may lead to an emptying of the

surface states, and consequently to stabilization of the surfaces of the ZnO particles by reduction of the field-aided drift of optically injected holes toward the surface. It might therefore be possible that copper or lithium doping of ZnO would result in a retardation of the solar-radiation-induced optical damage. The available data on the copper-doped particulate samples were shown in Fig. 4-13; the copper-doped samples exhibited a marked reduction in damage, as compared to that incurred by "standard" samples (Fig. 4-6). These data must be interpreted with caution, since (1) the data relating to the behavior of undoped ZnO prepared in the same manner as the doped samples are not yet available, and (2) the initial absorptance of the doped sample was considerably higher than that of the "standard" samples. The data can be more meaningfully evaluated after the undoped precipitated samples are run.

In Section 2.6 on the working degradation model, the possible impurity mechanisms which give rise to the observed visible and infrared damage were discussed. On the basis of the existing knowledge of ZnO and the experiments carried out here on particulate samples to date, it has not been possible to clearly define the specific impurity transitions giving rise to the observed absorptions. However, some of the experiments outlined in Section 7 have been specifically designed to help resolve some of these questions.

The work reported herein is continuing, in an attempt to resolve many of the questions raised by the foregoing discussion; the work leads toward the formulation of a complete, coherent model of the optical damage in ZnO caused by solar radiation.

Section 7

CONCLUSIONS AND RECOMMENDATIONS

7.1 CONCLUSIONS

- The initial reflectance spectra of the pressed and sintered particulate samples were quite similar to those of zinc oxide-pigmented thermal control paints, over the wavelength range 0.27 to 2.5 μ.
- Solar-radiation-induced reduction in reflectance of the particulate samples over the same wavelength range was similar to that observed for zinc oxide paints.
- Most of the zinc oxide optical property changes observed in this program appear to be connected with the loss and gain of oxygen by the ZnO.
- Solar-radiation-induced reduction in reflectance spectra of particulate samples essentially recovers upon exposure to air.
- The solar-radiation-induced reduction in the reflectance for visible energy is apparently initially generated near the surface, whereas reduction in infrared reflectance appears to be more of a bulk phenomenon.
- The effects in the particulate sample reflectance spectra produced by (1) solar-radiation in vacuum, (2) high sample forming pressure, and (3) sintering in vacuum all appear to have the same origin.
- Sintering in vacuum appears to produce free zinc at the surface of the particulate samples.
- A working model for solar-radiation-induced damage to the optical properties of zinc oxide has been formulated.

- The information available on diffusion rates in zinc oxide and the complex diffusion conditions near the surface prevent quantitative prediction of the time dependence of the damage processes.
- A band structure for zinc oxide was derived in a preliminary manner by the method of corresponding states.
- Ultraviolet exposures with in situ bidirectional reflectance measurements play a crucial role in the construction and evaluation of a model for the mechanism of optical damage to zinc oxide.

7.2 RECOMMENDATIONS FOR FUTURE WORK

The following studies are considered necessary for confirmation, refinement and completion of the working model for solar-radiation-induced damage to the optical properties of zinc oxide.

Work selected from these topics will be initiated during the remaining portion of this program.

- Further studies of the kinetics of degradation and recovery of particulate samples, using the ultraviolet exposures with in situ bidirectional reflectance measurements.
- Further studies of the dependance of damage on irradiation wavelength (L. Hering studies), with in situ measurements on particulate samples.
- Further studies of the dependeance of damage on sample temperature, with in situ measurements, with particular emphasis on the rate processes as a function of temperature in order to clarify the role of diffusion in the damage process.
- Studies of damage recovery in the dark, and with filtered illumination, at various oxygen pressures using in situ measurements of particulate samples.
- Irradiate a single crystal of zinc oxide in the attempt to produce measurable optical damage.

- o Electron spin resonance experiments on single crystals to help establish the detailed nature of the defect states giving rise to the optical absorption observed in ultraviolet degraded ZnO.
- o Experiments designed to gain information pertinent to the surface barrier heights, surface charge density and the location of the surface states in energy. As an example, this would include external photoeffect measurements on metal-ZnO surfaces and surface field effect measurements.
- o Extend the Cu and Li doping studies of both particulate and single crystals with particular emphasis on the photo desorption-adsorption process via studies of the slow photoconductive process.
- o Perform a detailed first-principle self-consistent energy band calculation for zinc oxide using the method of orthogonalized plane waves; perhaps the greatest importance of these calculations will be the acquisition of information leading to the characterization of surface and impurity states.
- o Extend the capability of the in situ bi-directional reflectance measurements farther into the infrared, to allow observation of optical behavior beyond 2.4μ during exposure tests.

Section 8
REFERENCES

1. Lockheed Missiles & Space Co., Thermophysics Design Handbook, Report 8-55-63-3, Sunnyvale, Calif., Jul 1963

2. Lockheed Missiles & Space Co., Thermal Radiative Control Surfaces for Spacecraft, by R. E. Gaumer and L. A. McKellar, LMSC-704014, Sunnyvale, Calif., Mar 1961

3. R. L. Olson, L. A. McKellar, and J. V. Stewart, "The Effects of Ultraviolet Radiation on Low α_s/ϵ Surfaces," Symposium on Thermal Radiation in Solids, Sponsored by NASA, NBS, and USAF/ASD, held in San Francisco, Calif., Mar 4-6, 1964

4. R. L. Olson, L. A. McKellar, and W. E. Spicer, The Energetics of Ultraviolet Radiation Damage to White Surfaces, Lockheed Missiles & Space Co., Report (in preparation), Sunnyvale, Calif., Mar 1964

5. Coatings for the Aerospace Environment, A Symposium sponsored by WADC, WADC TR 60-773, Wright Air Development Center, Wright-Patterson Air Force Base, Ohio

6. R. E. Gaumer, F. J. Clauss, M. E. Sibert and C. C. Shaw, "Materials Effects in Spacecraft Thermal Control," Proceedings of WADD Conference on Coatings for Aerospace Environment, Dayton, Ohio, Nov 1960; WADD TR 60-773.

7. W. F. Carroll, "Development of Stable Temperature Control Surfaces for Spacecraft – Progress Report No. 1," JPL Technical Report No. 32-340, Jet Propulsion Laboratory, Pasadena, Calif., Nov 1962

8. G. A. Zerlaut, Y. Harada, and E. H. Tompkins, "Ultraviolet Irradiation in Vacuum of White Spacecraft Coatings," Symposium on Thermal Radiation of Solids, sponsored by NASA, NES, and USAF/ASD, held in San Francisco, Calif., Mar 4-6, 1964

9. H. H. Hormann, "Improved Organic Coatings for Temperature Control in a Space Environment," ASD-TDR-62-917, Aeron. Systems Division, USAF, Feb 1963

10. James H. Weaver, "Anodized Aluminum Coatings for Temperature Control of Space Vehicles," ASD-TDR-62-918, Aeron. Systems Division, USAF, Feb 1963

11. N. Z. Searle, J. H. Daniel, R. C. Hirt, P. A. Mullen, and W. J. Stehman, "Pigmented Surface Coatings for use in the Space Environment," Report No. ML-TDR-64-314, Air Force Materials Laboratory, Wright-Patterson AFB Ohio, Nov 1964

12. E. R. Streed and C. M. Beveridge, "The Study of Low Solar Absorptance Coatings for a Solar Probe Mission," Symposium on Thermal Radiation in Solids Sponsored by NASA, NBS, and USAF/ASD, held in San Francisco, Calif., Mar 4-6, 1964

13. J. A. Parker, C. B. Neel, and M. A. Golub, "Experimental Development of a Technique for the Correlation of Flight and Ground Based Studies of the Ultraviolet Degradation of Polymer Films," NASA, TM X-54-015, National Aeronautics and Space Administration, Dec 1963

14. J. S. DeWitt, C. W Litton, and T. C. Collins, Bull. Am. Phys. Soc., Vol 10, No. 3, p. 331, March 1965

15. A. R. Hutson, Physical Review, Vol. 108, No. 2, p. 222, 15 Oct 1957

16. G. Heiland, "Surface Properties of Zinc Oxide," International Summer Course on Solid Stage Physics, Ghert (1963)

17. P. H. Kasai, "Electron Spin Resonance Studies of Donors and Acceptors in ZnO," Phys. Rev., 130, 989-995 (1953)

18. G. Heiland, "Surface Conductivity of Semiconductors and its Variation by Adsorption, Transverse Electric Fields, and Irradiation," Disc. Far. Soc., 28, pp. 168-182 (1959)

19. J. J. Lander, "Reaction of Lithium as a Donor and Acceptor in ZnO," J. Phys., Chem., Solids, 15, 324, 1960

20. H. E. Brown, ed., Zinc Oxide Rediscovered, The New Jersey Zinc Co., New York, N.Y., 1957

21. Frank Herman, Proc. IRE,43, 1703 (1955). This, together with reference 29, forms an excellent introduction to energy band theory and related topics.

22. L. Kleinman and J. C. Phillips, Phys. Rev. 116, 880 (1959)
M. H. Cohen and V. Heine, Phys. Rev., 122, 1821 (1961)
F. Bassani and V. Celli, Phys. Chem., Solids 20, 64 (1961)
David Brust, Phys. Rev., 134, A1337 (1964)

23. L. M. Falicov and Stuart Golin, Phys. Rev., 137, A871 (1964)

24. R. E. Dietz, J. J. Hopfield, and D. G. Thomas, J. Appl. Phys. 32, 2282 (1961)

25. R. G. Wheeler and J. C. Miklosz, Proceedings of the International Conference on Semiconductor Physics, Paris, 873 (1964)

26. F. Herman and S. Skillman, Proceedings of the International Conference on Semiconductor Physics, Prague, 20 (1960)

27. J. C. Phillips, Phys. Rev., 125, 1931 (1962)

28. N. B. Kindiz and W. E. Spicer, to be published

29. F. Herman, Rev. Mod. Phys., 30, 102 (1958)

30. L. P. Bouckaert, R. Smoluchowski, and E. P. Wigner, Phys. Rev., 50, 58 (1936). G. F. Koster, Solid State Physics, Vol. 5, F. Seitz and D. Turnbull (eds.), Academic Press, New York, 1957

31. F. Herman and S. Skillman, Atomic Structure Calculations (Prentice-Hall, Inc., Englewood Cliffs, New Jersey, 1963)

32. F. Bloch, Z. Physik 52, 555 (1928)
J. C. Slater and G. F. Koster, Phys. Rev., 94, 1498 (1954)

33. H. E. Brown, ed., Zinc Oxide Rediscovered, The New Jersey Zinc Co., New York, N. Y., 1957

Appendix A

A PARTIAL BIBLIOGRAPHY OF RESEARCH ON ZINC OXIDE

The published literature on the semiconducting properties of zinc oxide is very extensive (for example, one article by Heiland, Mollwo and Stockmann quotes 130 references), and there is also a large literature on catalysis at ZnO surfaces. Much information on the above subjects exists also in the form of unpublished reports (such as the University of Pennsylvania reports during the 1950's).

Additionally, there is a large body of information (both in published and in report form) on the degradation of zinc oxide paints due to electromagnetic or particulate radiation. This information has not been specifically included in this abbreviated literature bibliography, but instead enough of the published papers on zinc oxide as a material so that results which shed light on damage mechanisms will have been reported in at least one paper.

Some of these papers relate to the electrical and optical properties of single crystals, or to impurity diffusion rates in single crystals. Others are concerned with the properties of ZnO in powdered or microcrystalline form, and there are four review papers which attempt to cover the whole field.

Review Articles

G. Heiland, E. Mollwo and F. Stockmann, Solid State Physics Vol. 8, (Academic Press, 1959), pp. 191 – 323.
"Electronic Processes in Zinc Oxide"

(A very exhaustive and well documented survey article of results on both powdered and monocrystalline zinc oxide, with 130 references up to 1959. Describes the electrical and optical properties, adsorption phenomena, impurity diffusion, luminescence.)

G. Heiland, International Summer Course on Solid State Physics, Ghent (1963)
"Surface Properties of Zinc Oxide"

(Notes associated with lectures given by Heiland at this summer school in Belgium. Contains nothing brand new, but gives a useful summary of information about processes on the ZnO surface up to 1963, field effect measurements, adsorption, etc.)

E. Scharowsky, Z. Phys. 135, pp, 318 – 330 (1953)
"Optical and Electrical Properties of ZnO Single Crystals with Zn Additions"
(In German)

(The foundation paper of ZnO single crystal work – essentially Scharowsky's thesis in which he describes how crystals are grown from a vapor phase reaction. Crystals were heated in Zn vapor at various temperatures and he shows how excess zinc in the lattice provides conduction electrons and produces the famous "b" optical absorption between 0.37 and 0.65 microns.)

E. E. Hahn, J. Appl. Phys. 22, pp. 855 – 863 (1951)
"Some Electrical Properties of Zinc Oxide Semiconductor"

(This is probably the earliest general review paper we should take note of. There had been much earlier work on zinc oxide – notably the work of Carl Wagner and his group before World War II – but Hahn essentially brings us up to date to 1950 with the situation on ZnO pressed powders, the n-type conduction, the high resistance at intergranular contacts due to upturned bands.)

F. F. Kenshtein (Th. Wolkenstein).
"The Electronic Theory of Catalysis on Semiconductors," MacMillan Co., N.Y., 1963. (Translated from Russian)

(An excellent review and an extended version of concepts in his many papers on the subject.)

H. E. Brown, ed., Zinc Oxide Rediscovered,
The New Jersey Zinc Company, New York, 1957.

(Extensive review of selected properties and commercial uses of zinc oxide.)

Single Crystals – Electrical Properties

G. Mesnard and C. Eymann, Comptes Rendus 258, pp. 3672 – 3675 (1964)
"Electronic Properties of Zinc Oxide Single Crystals Containing Acceptor Elements." (In French)

(Reports on ZnO single crystals grown by the flux method – using a lead fluoride flux – rather than the conventional Scharowsky vapor phase approach. Crystals can be grown with up to 1 percent of acceptor elements such as lithium, sodium, and copper. Such crystals are still not p-type, but have extremely small free electron densities, reduced infrared absorption, but a fundamental absorption edge displaced towards longer wavelengths.)

A. R. Hutson, J. Phys. Chem. Solids 8, pp. 467 – 472 (1959
"Electronic Properties of ZnO"

(A paper given at the 1958 Rochester conference. Uses thermoelectric and magnetoresistance data in combination with existing Hall effect and conductivity data to elucidate the conduction band structure in ZnO. Finds that there should be at least 12 conduction band valleys of relatively small mass anisotropy!)

G. Heiland, J. Phys. Chem. Solids 6, pp. 155 – 168 (1958)
"Field Effect and Photoconductivity in ZnO Single Crystals." (In German)

(Uses field effect and photoexcitation to study electron mobility in the surface layer of ZnO crystals treated in hydrogen to create an N+ surface layer. Tries to measure electron lifetime from functional dependence of steady state and chopped photoresponse, while gas coverage is maintained nominally constant.)

A. R. Hutson, Phys. Rev. 108, pp. 222 – 230 (1957)
"Hall Effect Studies of Doped Zinc Oxide Single Crystals"

(A useful review of the temperature dependence of density and mobility of free electrons in ZnO crystals, to be used in conjunction with other papers.)

Single Crystals – Optical Properties

D. G. Thomas, J. Phys. Chem. Solids 10, pp. 47 – 51 (1959)
"Infrared Absorption in Zinc Oxide Crystals"

(Comments on lattice absorption bands at 10.1 and 11.5 microns, uses lithium and indium doped single crystals to show how superimposed free carrier absorption is linear in free electron density, varies as cube of wavelength from 1 to 6 microns.)

R. Arneth, Z. Physik 155, pp. 595 – 608 (1959)
"On the Absorption of ZnO Crystals in the Infrared" (In German)

(Displays infrared results in good agreement with above reference. Also shows how additions such as zinc or copper lead to additional near ultraviolet and visible absorption on the low energy side of the "pure crystal" intrinsic absorption edge.)

Single Crystals – Surface Effects

G. Heiland, Disc. Far. Soc. 28, pp. 168 – 182 (1959)
"Surface Conductivity of Semiconductors and its Variation by Adsorption, Transverse Electric Fields and Irradiation"

(A review of University of Erlangen work, particularly field effect experiments, on ZnO and other semiconductors. The discussion involving Heiland and F. S. Stone brought up the point as to whether any proof exists that oxygen from the lattice itself as opposed to adsorbed oxygen is evolved on irradiation – methinks the strongest evidence here lies in Collins and Thomas paper, Phys. Rev. 112.)

G. Heiland, Z. Phys. 142, pp. 415 – 432 (1955)
"The Surface Electrical Conductivity of Zinc Oxide Crystals" (In German)

(Concerned with the change of conductance of single crystals due to change in the surface condition following irradiation. Used 1 KeV electrons as well as ultraviolet photons for irradiation.)

D. F. Anthrop and A. W. Searcy, J. Phys. Chem. 68, 2335 – 2342 (1964)
"Sublimination and Thermodynamic Properties of ZnO."

(Mass spectrometric study of sublimination of ZnO. Resolves the problem of the anomalous rate of sublimative of ZnO in the presence of Zn vapor.)

E. Kh. Enikeev, C. Z. Roginsky and J. H. Rufov, Proc. International Conf. on Semiconductor Phys., Prague 1960.
"Study of the Influence of the Adsorption of Gases on the Work Function of Semiconductors."

(Relates the work function and activation energy of adsorption and desorption of oxygen on ZnO as a function of surface coverage and Li and Zn doping.)

Th. Wolkenstein, Disc Faraday Soc. 31, 209 – 218 (1961).

(The problem of ionizing radiation in the adsorptive and catalytic properties of a semiconductor is formulated within the framework of the electron theory of chemisorption and catalysis. Discusses band-bending and bulk parameters of a semiconductor in relation to the above effects.)

G. Heiland, J. Phys. Chem. Solids 22, pp. 227 – 234 (1961)
"Photoconductivity of Zinc Oxide as a Surface Phenomenon"

(Discusses field effect and photoconductivity measurements on single crystals in terms of the motion of motion of mobile carriers in a surface channel, and the trapping and recombination of electrons and holes. The data appears open to several interpretations.)

H. J. Krusemeyer, J. Phys. Chem. Solids 23, pp. 767 – 777 (1962)
"The Influence of Light, Oxygen and Nitrogen on the Field Effect Mobility of Zinc Oxide Crystals."

(Suggests that a result of optical absorption in the fundamental region is the transfer of oxygen lattice ions to adsorption sites – from which they can presumably later desorb.)

T. Wolkenstein and I. V. Karpenko, J. Appl. Phys. 33, pp. 460 – 465 (1962)
"On the Theory of the Photoadsorptive Effect on Semiconductors"

(Establishes a rather complicated criterion for adsorption or desorption of oxygen upon illumination which appears to be able to reconcile the various experimental observations of Fujita, Terenin, Barry and Stone, and Barry.)

R. J. Collins and D. G. Thomas, Phys. Rev. 112, pp. 388 – 395 (1958)
"Photoconduction and Surface Effects with Zinc Oxide Crystals"

(Remarks that the surface photoconduction in single ZnO crystals is too large to be explained by photo-desorption of adsorbed oxygen. Argues that actual photolysis must occur – light produces hole electron pairs, holes move to surface and discharge lattice oxygen, leaving a zinc-enriched surface region.)

H. J. Krusemeyer, Phys. Rev. 114, pp. 655 – 664 (1959)
"Surface Potential, Field Effect Mobility, and Surface Conductivity of ZnO Crystals"

(Measurements on single crystals suggest that the bulk diffusion length for holes exceeds 10^{-5} cm, and that the quantum efficiency of the hold trapping process at the surface is approximately unity for a neutral surface.)

D. G. Thomas and J. J. Lander, J. Phys. Chem. Solids 2, pp. 318 – 326 (1957)
"Surface Conductivity Produced on Zinc Oxide by Zinc and Hydrogen"

(Studies the additional conductance of single crystals of ZnO caused by adsorption of zinc or hydrogen. Zn is adsorbed at room temperature and the additional conductance is a surface effect, with evidence of impurity band conduction.)

Single Crystals-Diffusion Studies

W. J. Moore and E. L. Williams, Disc. Far. Soc. 28, pp. 86 – 93 (1959)
"Diffusion of Zinc and Oxygen in Zinc Oxide"

(A quite small diffusion coefficient for zine, governed by an activation energy of 165 K cal, is found by using radioactive tracer techniques with single crystals. A mechanism based on thermally produced Frenkel defects is suggested. Radioactive techniques for oxygen yield a diffusion coefficient which is even smaller than for zinc. Vigorous discussion following presentation of this paper at an Ottawa symposium brought out the diversity of views on how zinc can propagate through the ZnO lattice.)

D. G. Thomas, J. Phys. Chem. Solids 3, pp. 229 – 237 (1957)
"Interstitial Zinc in Zinc Oxide"

(ZnO single crystals heated in zinc vapor, and the temperature dependence of the interstitial zinc solubility and diffusion coefficient inferred from the added conductivity. This method implies much faster diffusion than radioactive methods suggest.)

D. G. Thomas, J. Phys. Chem. Solids 9, pp. 31 – 42 (1959)
"The Diffusion and Precipitation of Indium in Zinc Oxide"

(Indium coated on ZnO single crystals is dissolved and diffused in at temperatures from 800–1300 C. This precipitates out on dislocations at lower temperatures when the solubility limit is surpassed, at rates indicating dislocation densities ranging from 10^6 to 10^7 cm^{-2}.)

Single Crystals-Doped

G. Bogner and E. Mollwo, J. Phys. Chem. Solids 6, pp. 136 – 143 (1958)
"On the Production of Zinc Oxide Single Crystals with Definite Additions"
(In German)

(Describes adaptation of the Scharowsky method for making doped single crystals of ZnO. Shows how the conductivity increases with indium

addition and decreases with copper addition, and how doping affects the infrared free carrier optical absorption.)

H. Rupprecht, J. Phys. Chem. Solids 6, pp. 144 – 154 (1958)
"On the Concentration and Mobility of Electrons in Zinc Oxide Single Crystals with Definite Additions." (In German)

(Conductivity and Hall effect measured and analyzed for the indium- and copper-doped crystals of Ref. 14.)

J. J. Lander, J. Phys. Chem. Solids, 15, 324 (1960)
"Reaction of Lithium as a Donar and Acceptor in ZnO."

(Contains recipes for obtaining Li donor and acceptor states in ZnO and discusses the thermodynamic and kinetic aspects of the problem.)

P. H. Kasai, Phys. Rev., 130, 989 – 995 (1963)
"Electron Spin Resonance Studies of Donors and Acceptors in ZnO."

(Identifies levels and gives estimates for them from an analysis of ESR experiments on Li and Zn doped polycrystalline ZnO.)

Powders – Surface Effects

Y. Fujita and T. Kwan, Bull. Chem. Soc. Japan, 31, pp. 379 – 380 (1958)
"Photodesorption and Photoadsorption of Oxygen on Zinc Oxide"

(Report direct observations of gas – presumably oxygen – given off by ZnO powder in vacuum under ultraviolet illumination.)

D. B. Medved, J. Chem. Phys. 28, pp. 870 – 873 (1958)
"Photodesorption in Zinc Oxide Semiconductor"

(Also reports evolution of gas – presumably oxygen – by ZnO powder on U.V. illumination. Compares simultaneous curves of gas evolution and photoconductivity as a function of time.)

D. B. Medved, J. Phys. Chem. Solids, 20, 255 – 267 (1961)
"Photoconductivity and Chemisorption Kinetics in Sintered ZnO Semiconductor"
(Relates the "slow photoconductivity process to the chemisorption process which obeys the Elovich rate equation.)

S. R. Morrison, Advances in Catalysis VII (Academic Press, 1955), pp. 259 – 301
"Surface Barrier Effects in Adsorption, Illustrated by Zinc Oxide."
(Explains time-dependent events in ZnO as the consequence of chemisorption with electron transfer across the surface potential barrier as the rate-determining step. Suggests that ionization of surface states is the primary rather than secondary result of absorption of light.)

H. J. Gerritsen, W. Ruppel and A. Rose, Helv. Phys. Acta 30, pp. 504 – 512 (1957)
"Photoproperties of Zinc Oxide with Ohmic and Blocking Contacts"
(Studies fast and very slow photoconductive response for the finely divided powders of Ruppel et al.)

T. I. Barry and F. S. Stone, Proc. Roy. Soc. A.255, pp. 124 – 144 (1960)
"The Reactions of Oxygen at Dark and Irradiated Zinc Oxide Surfaces"
(Adsorption techniques including use of 18O used to keep track of oxygen on and off the surface of zinc oxide with a large surface to volume ratio. Results suggest that U.V. irradiation usually results in photodesorption, but that oxygen photoadsorption can occur when the ZnO has a large zinc excess – a not unreasonable result but one in direct conflict with Terenin et al.)

T. I. Barry, Proc. 2nd Int. Cong. Catalysis (Paris, 1960) pp. 1449 - 1457
"The Adsorption of Oxygen on Zinc Oxide. The Effect of γ Radiation."
(The kinetics of oxygen chemisorption on ZnO surfaces studies as a function of temperature, and two processes separated, interpreted as chemisorption of O^- at low temperatures and of $O^=$ above 200 C. Gamma radiation produces desorption of oxygen adsorbed at low temperatures, but there are complications when oxygen is pre-adsorbed at higher temperatures.)

W. Ruppel, H. J. Gerritsen and A. Rose, Helv. Phys. Acta 30, pp. 495 – 503 (1957)

"An Approach to Intrinsic Zinc Oxide"

(Studies extremely finely divided zinc oxide powder, which can have an apparent resistivity of up to 10^{17} ohm cm. The grain size of about 10^{-5} cm resulted in enormous effects of adsorbed oxygen.)

S. R. Morrison and P. H. Miller, Jr., J. Chem. Phys. 25, pp. 1064 – 1065 (1956)

"Adsorption of Oxygen on Zinc Oxide"

(Measures directly the volume of oxygen adsorbed by powdered ZnO. The variation of this with the prior time-temperature-oxygen pressure history is suggestive of the ready diffusion of interstitial zinc away from and towards the surface at about 500 C.)

P. H. Miller, Jr., Photoconductivity Conference (Wiley, 1956), pp. 287 – 297

"The Role of Chemisorption in Surface Trapping"

(A report to the Atlantic City conference on the work of the University of Pennsylvania group up to 1954. Reviews the experiments of Melnick and Medved on very slow and non-exponential decay of photoconductance in pressed powders in the light of Morrison's model for surface barrier and adsorption effects.)

E. Mollwo, Photoconductivity Conference (Wiley, 1956), pp. 509 – 528

"Electrical and Optical Properties of ZnO."

(Reviews the work of Scharowsky and Heiland. Discusses both the rapid and the slow photoconductive response observable in pressed sintered layers.)

D. A. Melnick, J. Chem. Phys. 26, pp. 1136 – 1146 (1957)

"Zinc Oxide Photoconduction, an Oxygen Adsorption Process"

(Much concerned with the very slow and non-exponential decay of photoconductance in pressed powders, and its interpretation on the basis of Morrison's model.)

A. Terenin and Yu. Solonitzin, Disc. Far. Soc. 28, pp. 28 – 35 (1959)
"Action of Light on the Gas Adsorption by Solids"

(Results suggest that photodesorption of oxygen occurs when ZnO with zinc excess is illuminated with U.V., but that oxygen photosorption occurs if the ZnO has excess oxygen!)

Powders – Optical Properties

V. N. Filimonov, Optika i Spektr. 5, pp. 709 – 711 (1958)
"Electronic Absorption Bands of ZnO and TiO_2 in the Infrared Region of the Spectrum" (In Russian)

(Describes how infrared absorption by ZnO powder increases under ultraviolet irradiation in vacuum, and how it decreases again when oxygen is admitted to the system.)

Thin Films

V. K. Miloslavskii and N. A. Kovalenko, Optika i Spektr. 5, pp. 616 – 617 (1958)
"Absorption by Zinc Oxide in the Infrared Region of the Spectrum" (In Russian)

(Measurements of infrared optical transmission for sputtered films of ZnO apparently with a large excess of zinc, showing a strong absorption peak at 5 microns which is attributed to an impurity band.)

Catalysis

F. Romero-Rossi and F. S. Stone, Proc. 2nd Int. Cong. Catalysis (Paris 1960), pp. 1481 – 1496.
"The ZnO-Photosensitized Oxidation of Carbon Monoxide"

(Is involved with the effect of dopants such as Li and Cr in ZnO on the adsorption and photoadsorption characteristics of the surface. Results are discussed relative to oxygen adsorption.)

Appendix B
BI-DIRECTIONAL REFLECTANCE APPARATUS

B.1 INTRODUCTION

Evaluation of the effects of the space environment on the optical properties of materials generally consists of exposing materials to the simulated environment, and characterizing material behavior by pre- and post-exposure optical property measurements. This technique allows use of standard optical instrumentation in the performance of the measurements, and therefore permits selection of the measuring technique best suited to definition of the operational parameters required of the optical material. For surfaces used to control spacecraft temperatures, the solar absorptance can be obtained from spectral reflectance data measured with either an integrating sphere or Coblentz hemisphere. However, such "static" test data (i.e., with pre- and post-test measurements only) cannot account for possible post-exposure recovery of the damaged material during the period preceding the measurements. Exposure to ultraviolet or high-energy radiation in vacuum generally reduces the solar reflectance of white paints; this damage is known to recover upon exposure of the irradiated specimens to air. Previous work at LMSC also indicated that white metallic oxide pigments without a surrounding paint binder might recover quite rapidly. Furthermore, such recovery could occur in vacuum upon cessation of irradiation. It is evident that precise information on ultraviolet degradation of these materials can only be obtained by optical property measurements performed in vacuum and during irradiation, i.e., in situ.

This Appendix describes the apparatus developed to obtain in situ data, and gives a synopsis of the operating principles and procedures. A more complete exposition of the measurement technique, together with a full uncertainty analysis, will be set forth in the Final Report. Since this apparatus is being used primarily to observe changes in spectral properties, reproducability and resolution are the essential performance parameters. These parameters are presented in Section B.3 of this Appendix.

The apparatus measures an approximation of bi-directional spectral reflectance, which can be defined as follows. Consider a differential surface element irradiated with essentially unidirectional, monochromatic energy. The bi-directional reflectance gives the fraction of that energy that is reflected in a given direction. Proper integration of the bi-directional spectral reflectance over the hemispherical space above the surface element will give the spectral reflectance of the surface for the specified unidirectional irradiation. For a true measurement of bi-directional reflectance, the directions, areas, and solid angles involved in both sample irradiation and signal detection must be accurately specified and controlled. In the present apparatus, due primarily to the nature and dimensions of the light pipes used, such control is not achieved; however, it is not necessary for the purposes of this study. For convenience the data obtained will be referred to as bi-directional reflectance, since that term most nearly describes the property measured.

Conceptually, the apparatus consists of a vacuum enclosure with a sample table inside. The chopped radiation source for the reflectance measurements is external to the vacuum chamber; its radiation passes through a light pipe which penetrates the chamber walls and illuminates the sample at an angle of incidence of 45° (Fig. B-1). The energy reflected specularly from the sample enters another light pipe and passes out the opposite side of the chamber to a monochromator. After passing through the monochromator the dispersed signal is detected; the detected signal is amplified and filtered in frequency

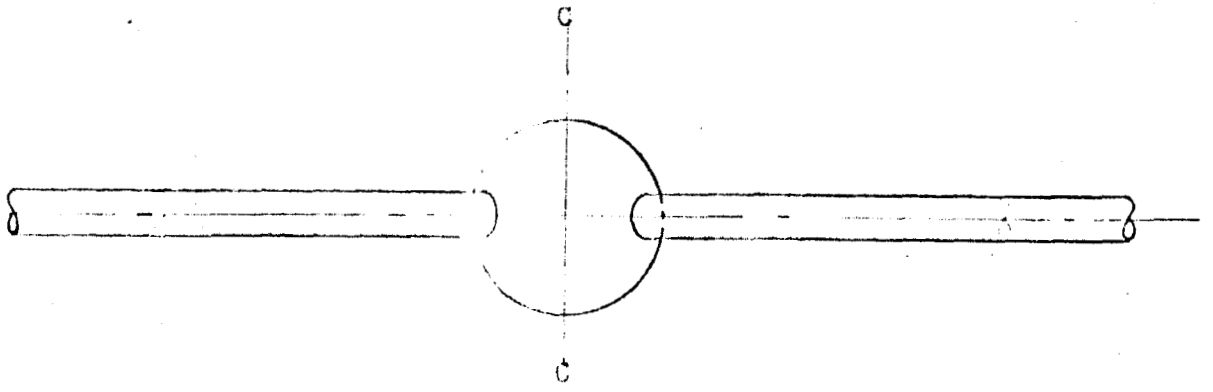

PLAN VIEW

Sample may be repositioned by rotation around axis C for non-specular measurements

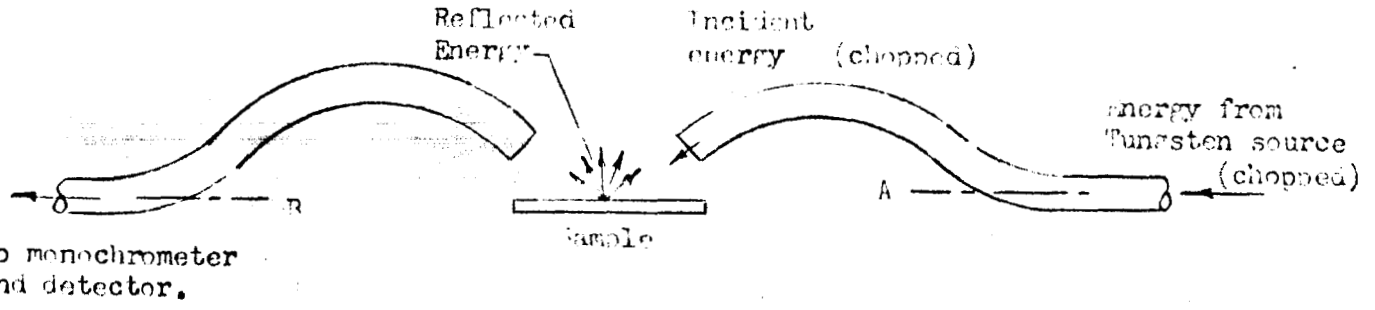

SIDE VIEW

Light-pipes are repositioned by rotation around axis A or B for non-specular or transmission measurements.

FIG. B-1

Schematic of Light-Pipe Geometry in Position for Specular Bi-directional Reflectance Measurement

and phase, corresponding to the chopper frequency and phase.

The intense source of damaging ultraviolet and visible radiation is also external to the vacuum chamber, and is incident on the sample through a high-purity quartz window in the top of the chamber.

The reflected signal, $I(\lambda)$, is compared to a reference signal, $I_o(\lambda)$, obtained by allowing the two light pipes to "look" directly at each other. The ratio of these is then normalized such that the initial bi-directional reflectance, obtained in air before ultraviolet irradiation, agrees with the normal spectral reflectance, $\rho(\lambda)$, measured with the Cary Model 14 spectrophotometer and associated integrating sphere. This normalization is based on one selected wavelength, λ_N. The final bi-directional reflectance (BDR) data, as reported herein, are therefore given by the following expression (written for the wavelength λ):

$$BDR\ (\lambda) = \frac{I(\lambda)}{I_o(\lambda)} \left[\rho(\lambda_N) \quad \frac{I_o(\lambda_N)}{I(\lambda_N)} \right]$$

Provision is made for (1) rotation of the sample table about an axis lying in the face of the sample and normal to the plane of the light pipes, and (2) rotation of the receiving light pipes out of the plane of incidence of the of the incoming reflectance source energy (See Fig. B-1). As a result, through proper manipulation of the light pipes and the sample table the following measurements can be made: (1) bi-directional reflectance for the non-specular case; and (2) direct beam transmission measurements for angles of incidence from 45° to 90°.

B.2 DESCRIPTION OF APPARATUS

The apparatus is shown in Fig. B-2. In the center of the picture is the cylindrical vacuum chamber, with an electronic high vacuum pump mounted below it.

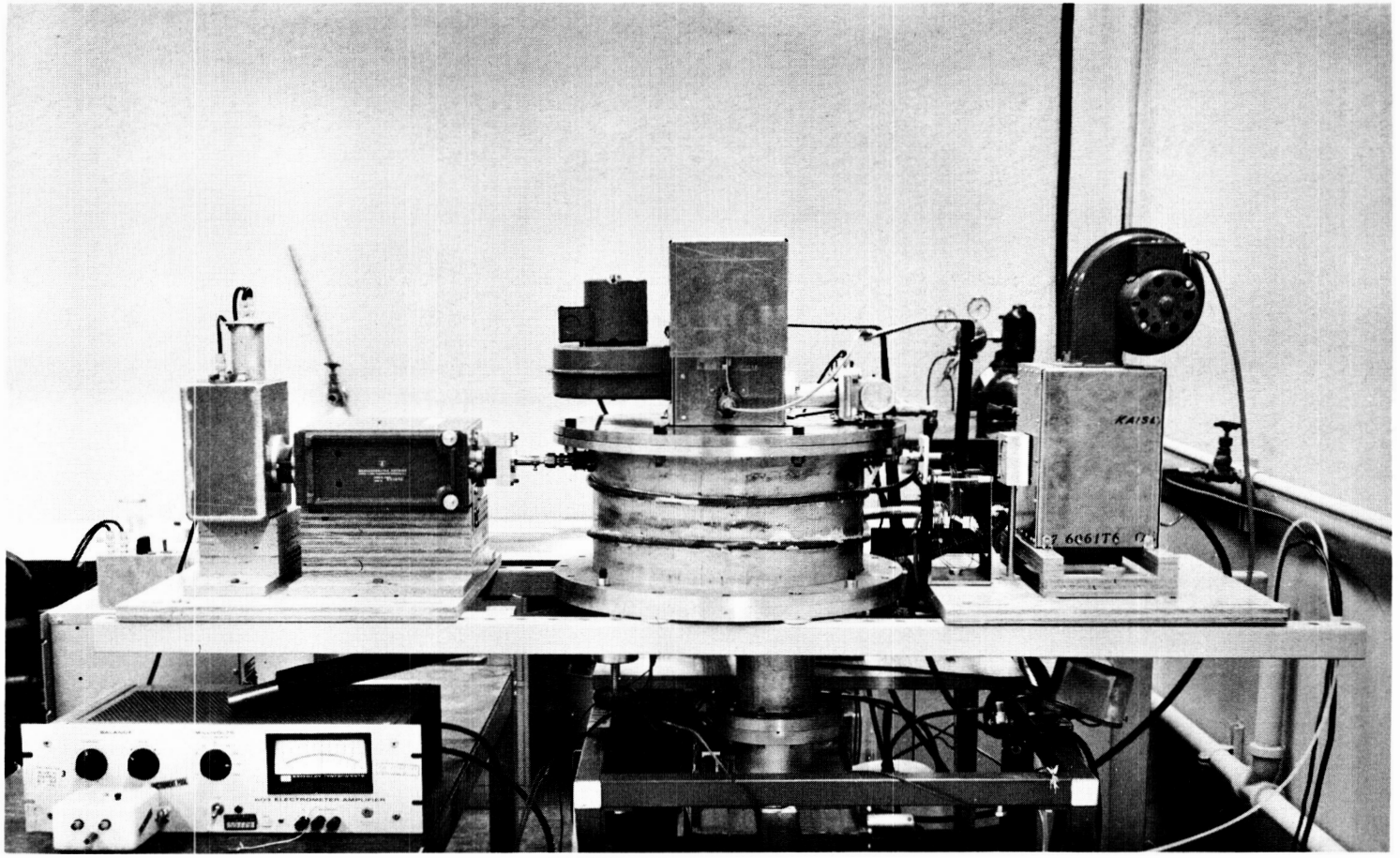

Figure B-2

Ultraviolet Radiation-High Vacuum Exposure Apparatus
for In Situ Measurement of Bi-directional Reflectance

On top of the chamber are mounted the ultraviolet irradiation source and its convection-cooled housing, with an automatic lamp-intensity monitor. The housing is constructed to accommodate xenon, mercury-xenon or mercury-argon ultraviolet arc lamps, either air or water-cooled. Ultraviolet radiation enters the chamber through a four-inch diameter, one-half inch thick Suprasil (Engelhard Industries, Inc.) window located on the center of the removable top plate.

The samples are mounted on a horizontal three-inch-diameter stainless steel table located two inches below the Suprasil window. A detail of the sample table is shown in Fig. B-3. The table has attached cooling coils and an electric resistance heater for temperature control over the range -320°F to 600°F. The table can be translated to extract samples from the region of ultraviolet illumination or to locate alternate samples for in situ optical measurements. These movements can be accomplished while the chamber is maintained under high vacuum.

In situ measurements of sample transmittance and bi-directional reflectance can be performed with the ultraviolet source on or off, and under vacuum or ambient pressure conditions. The measurements are performed essentially as described in Section B.1. The sample table and the ends of the light pipes are shown in Fig. B-3. A schematic of the light pipe geometry is shown in Fig. B-1. The light pipes and the sample table are rigidly supported both inside and outside the chamber to minimize the possibility of system misalignment during chamber pump-down or return to atmospheric pressure. The light pipes and the sample table supporting arm both pass through the chamber walls inside flexible stainless steel bellows.

The source for the reflectance (or transmittance) measurements is the 1000 watt tungsten lamp shown at the right of Fig. B-2. The output of this lamp is focused at the end of one light pipe (at right in figures) and interrupted by a twenty C.P.S. synchronous-motor-driven chopper. Energy reflected from the sample and striking the end of the second light pipe (at left) is

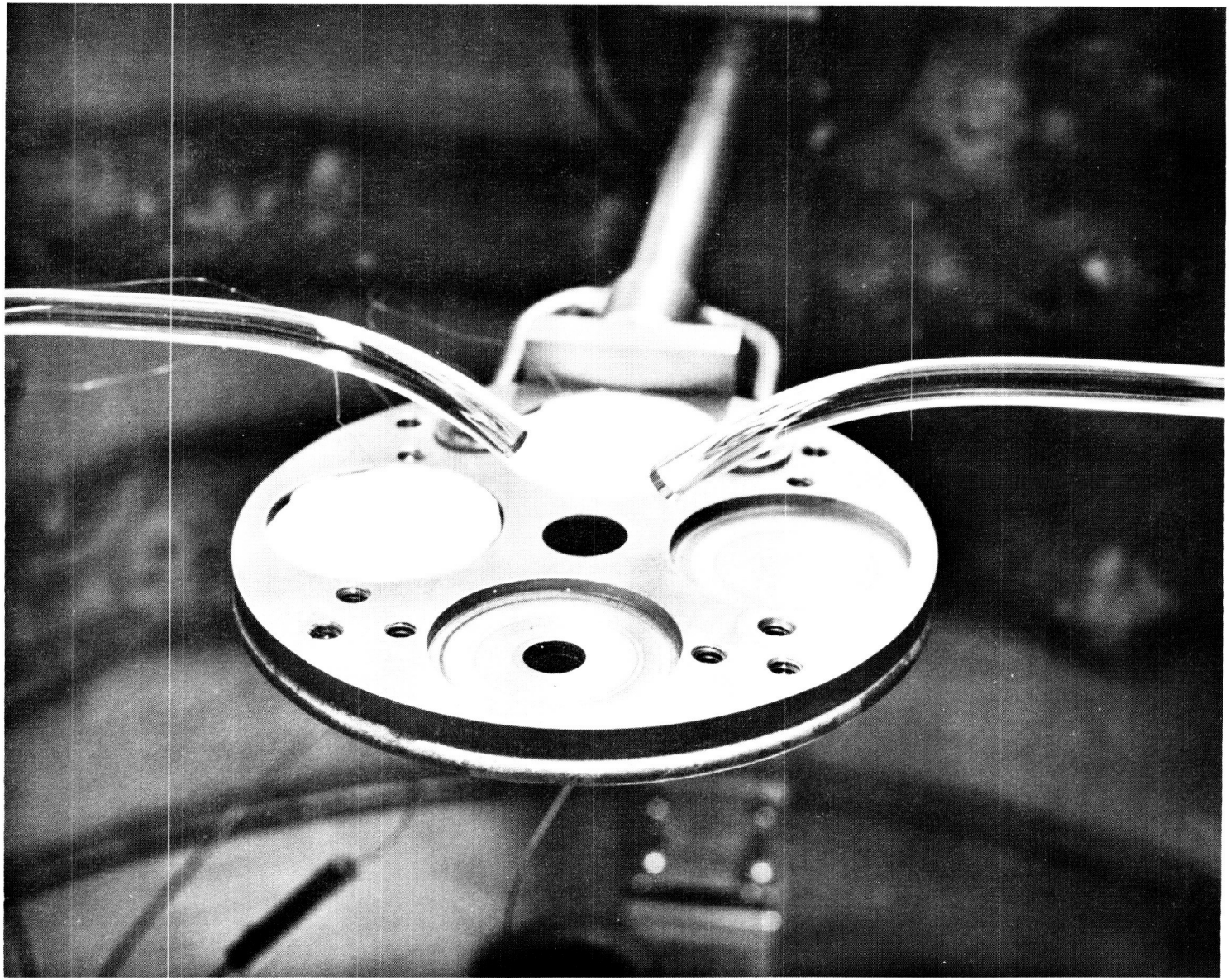

Figure B-3
Detail of Water-cooled Sample Table and Quartz Light
Pipes for In Situ Measurement of Bi-directional Reflectance

collected and transmitted to a collimating lens, then passed through a monochromator. The dispersed signal is finally measured by a photodetector. The photodetectors used are a RCA7200 photomultiplier for the range 0.3 to 0.7 microns and a Kodak lead sulphide photoresistor for the range 0.7 to 2.4 microns. The monochromator is a Baush and Lomb Grating Monochromator with interchangeable gratings and variable slits, which can be used over the range 0.18 to 3.2 microns. The monochromator and detector housings are shown at the left side in Fig. B-2. The output of the detector is amplified by a narrow frequency band, phase sensitive amplifier (Princeton Applied Research Lock-In Amplifier Model JB-5) and recorded on a milliampere chart recorder.

Incorporation of the narrow band amplifier in conjunction with the mechanical light chopper permits the measurement of only the reflected energy which originates from the tungsten source. The high-intensity ultraviolet irradiation (damage source), which is predominantly direct current with a significant 120 cycle harmonic, is reflected from the sample and measured by the detector. However, this background does not affect the amplifier output signal level.

B.3 MEASUREMENT PROCEDURE

The bi-directional spectral reflectance is determined by measuring the spectral energy reflected from the sample, $I(\lambda)$, with the light pipes on the positions shown in Figs. B-1 and B-2. Then one pipe is rotated about its axis so as to directly view the other pipe with the sample table withdrawn. The transmitted spectral energy, $I_o(\lambda)$, is measured and the ratio of the first measurement to the latter is proportional to the bi-directional reflectance. This ratio as such has no absolute units; it is normalized at a particular wavelength with respect to the normal spectral reflectance measured with an integrating sphere. (See Section B.1). The resulting quantity is referred to as bi-directional reflectance in this report. For a test during which a series of bi-directional reflectance spectra are desired, only the initial spectrum is normalized to be equal to the normal reflectance spectrum. The succeeding spectra are <u>in situ</u>

measurements of the degradation in reflectance. See Figs. 4-1 through 4-3 for examples of results of this procedure.

The procedure for determining bi-directional reflectance outlined in the preceding paragraph accounts for any degradation in transmittance of the optical components, detector sensitivity, or tungsten lamp output. It does not account for mechanical movement of optical components due to changes in structural loading induced by chamber pump down or return to atmospheric pressure. These changes are minimized by proper apparatus design and checked by monitoring either the reference signal (I_o) or the reflectance of a mirror during chamber pressure changes.

The sample temperature must be known during irradiation, so that the changes in optical properties due to ultraviolet degradation and those due to temperature change can be segregated. To illustrate, the magnitude of the effect of temperature only on the reflectance of zinc oxide is shown in Fig. 4-1.

Procedures to determine sample temperature and restrict sample temperatures within desired limits have been developed. Direct measurement, by use of fine guage thermocouples embedded in the samples, is not adquate nor appropriate because: (1) the exact magnitude of direct heating of the thermocouple by the incident A-H6 energy is difficult to determine for each thermocouple, and (2) thermocouples are a potential source of sample contamination.

Sample temperature is determined by calculation of the energy balance for the sample, using experimentally determined values of incident radiant flux, sample spectral reflectance and sample-to-sample-table contact conductance. The thermal conductivity of standard zinc oxide samples is approximately 0.6 Btu/in.-hr ^{o}F as reported by Kingery in American Ceramic Society Vol. 37, 1954. Therefore, for the heat exchange rates typical for these tests, the temperature difference through these samples is less than 10^{o}F for typical thickness of 0.10 in.

Sample temperature is given by the equation:

$$\epsilon\sigma\left(T_s^4 - T_c^4\right) + K(T_s - T_{st}) = \int W_\lambda \alpha_\lambda \, d\lambda \qquad (1)$$

where

T_s = sample surface temperature
T_c = effective chamber temperature
T_{st} = sample table temperature
σ = Stephan-Boltzmann constant
ϵ = sample emittance
W_λ = spectral irradiance of sample by A-H6 lamp
α_λ = spectral absorptance of zinc oxide
K = sample-to-sample-holder contact conductance

This equation can be used because (1) the dominant radiation absorbed by the sample is ultraviolet energy which is absorbed close to the sample surface, and (2) the total temperature drop through the sample is less than 10°F.

Incident radiant flux is determined with an Eppley radiometer and monitored for successive runs with a filtered phototube. ϵ and α_λ are determined from total normal reflectance data over the region 0.3 to 20 microns, obtained with the Cary spectrophotometer and a Hohlraum reflectometer with associated spectrophotometer. α_λ is corrected for damage with the <u>in situ</u> measurements.

Clearly, if K is very large then $T_s \rightarrow T_{st}$, and the problem is a trivial one of measuring the sample table temperature. Unfortunately the standard sintered samples are not flat, and they are brittle. Therefore contact area between sample and sample table is meager and contact pressure is necessarily small to minimize sample breakage. The best method to increase contact conductance employs a thin layer of unsintered zinc oxide powder in the sample

recess, on which the sample is pressed with a stainless steel frame. This method removes the possibility of contamination due to adhesives or conductance pastes. Repeatable thermal contact conductances are provided, and the sample-to-sample table temperature gradient is less than 100°F for all sample holder temperatures in the range -320 to +500°F, and for irradiation intensities typical for the AH-6 at a distance of 3.5 inches.

The contact conductance was measured by installing instrumented standard zinc oxide samples and heating the sample table to approximately 500°F in several steps with the AH-6 off. At each steady state condition, the sample and sample table temperatures are recorded, and the radiation heat transfer computed. The contact conductance is given by:

$$K = \frac{\epsilon\sigma\left(T_s^4 - T_c^4\right)}{\left(T_{st} - T_s\right)} \qquad (2)$$

Several evaluations have repeatedly given conductance values in the range 0.3 to 0.4 Btu/in.^{2}-hr-°F. Using the mean of the above conductance values for all samples installed in this fashion, the sample temperature is computed with an expected error of less than ±20°F for the range -320°F to 500°F.

A detailed analysis of the uncertainties in this equipment is underway, and will be presented in the final report. The reproducibility of the bi-directional reflectance data is within ±5 percent. Spectral resolution of about 10 Å is achieved for wavelengths between 0.3 and 0.8 microns; in the range between 0.8 and 2.4 microns the resolution is approximately 50 Å.

B.4 APPLICATION OF DATA

In this program, the "bi-directional reflectance" data taken on this apparatus are being used to infer changes in absorptance. There are two possible

objections to this procedure, which will be reviewed below. On the macroscopic scale, radiation striking an object can do three things: (1) be transmitted, (2) be reflected, or (3) be absorbed.

One possible objection is related to the sample opacity; transmitted energy would be interpreted as absorption. However, for the sample thicknesses used in this program (0.070 in.), the transmittance is less than one percent for the wavelength range from 0.3 to 2.0 microns.

The second possible objection is that bi-directional reflectance is not a measure of all energy reflected from the sample; changes in bi-directional reflectance can be caused by changes in either total absorption or the directional distribution of the reflected energy. In general, this may be a valid objection. However the situation must be considered in light of the particular samples under study.

The samples are composed of zinc oxide particles with an average particle diameter of 0.3 microns; they reflect solar radiation through the process of back-scattering. The standard sintered zinc oxide samples are observed to be nearly diffuse reflectors in the range 0.3 to 2.4 microns. For all but highly grazing angles it has been found that the bi-directional spectral reflectance of standard zinc oxide samples is directly proportional to the total normal spectral reflectance over the range 0.3 to 2.4 microns. This is to be expected for diffuse samples. The real question is: what happens to the directional behavior of the samples when they are damaged. It is highly unlikely that the ultraviolet-induced damage causes changes in the real part of the index of refraction, or in particle size. The damage produces changes in the absorption index. Now these samples are composed of particles which are nearly the same size as the wavelength of light being considered, and which have an indices of refraction which are several orders of magnitude larger than their absorption indices. In such systems, the direction of light

scattering is controlled primarily by the particle size and the refractive index. Consequently, the damaged samples are expected to have the same directional behavior as the undamaged samples, i.e., highly diffuse. When this has been checked by appropriate rotation of the light pipes (see Sec. B.1), it has been found to be the case.

Consequently, for the study of particulate zinc oxide samples, measurements of change in bi-directional reflectance are valid indications of changes in sample absorption.

Appendix C

STATIC ULTRAVIOLET EXPOSURE APPARATUS

The static ultraviolet exposure chamber is shown in Figure C-1. The test chamber is a water-cooled stainless steel bell jar 14 inches high and 14 inches in diameter. The 1" diameter samples are mounted on a water-cooled, semi-cylinder copper sample holder concentric with the ultraviolet source and at a distance of 3.9 inches which results in nominal irradiances of 5 "suns" of ultraviolet energy. A flux density of one "sun" of ultraviolet energy is herein defined as the flux density of extraterrestrial radiation at one astronomical unit from the sun, in the wavelength interval from 2000Å to 4000Å. At these flux densities the sample temperatures were maintained between 100°F and 125°F for all ultraviolet tests in this chamber. Thermal contact conductance between the sample and the water-cooled copper sample holder was controlled with individual mounting frames which pressed the back face of the sample against the copper. Vacuums are established prior to initiation of ultraviolet exposure with cryogenic sorption roughing pumps and an electronic high vacuum pump to avoid potential oil contamination problems. The chamber pressure is typically 2×10^{-7} Torr in the last portion of an exposure period and before the lamp is started. At the beginning of the exposure period the pressure typically rises to 1×10^{-5} Torr, because of the relatively high initial "out gassing" of zinc oxide under irradiation.

The source of ultraviolet energy is a 1 KW AH-6 (PEK Labs Type C) high pressure mercury-argon capillary arc lamp. Approximately 35 percent of the lamp's radiant output is in the interval from 2000Å to 4000Å. The lamp's total output is in the interval 2000Å to 26,000Å. The lamp is water-cooled and has a quartz water jacket and velocity tube. This assembly is lowered into a quartz envelope

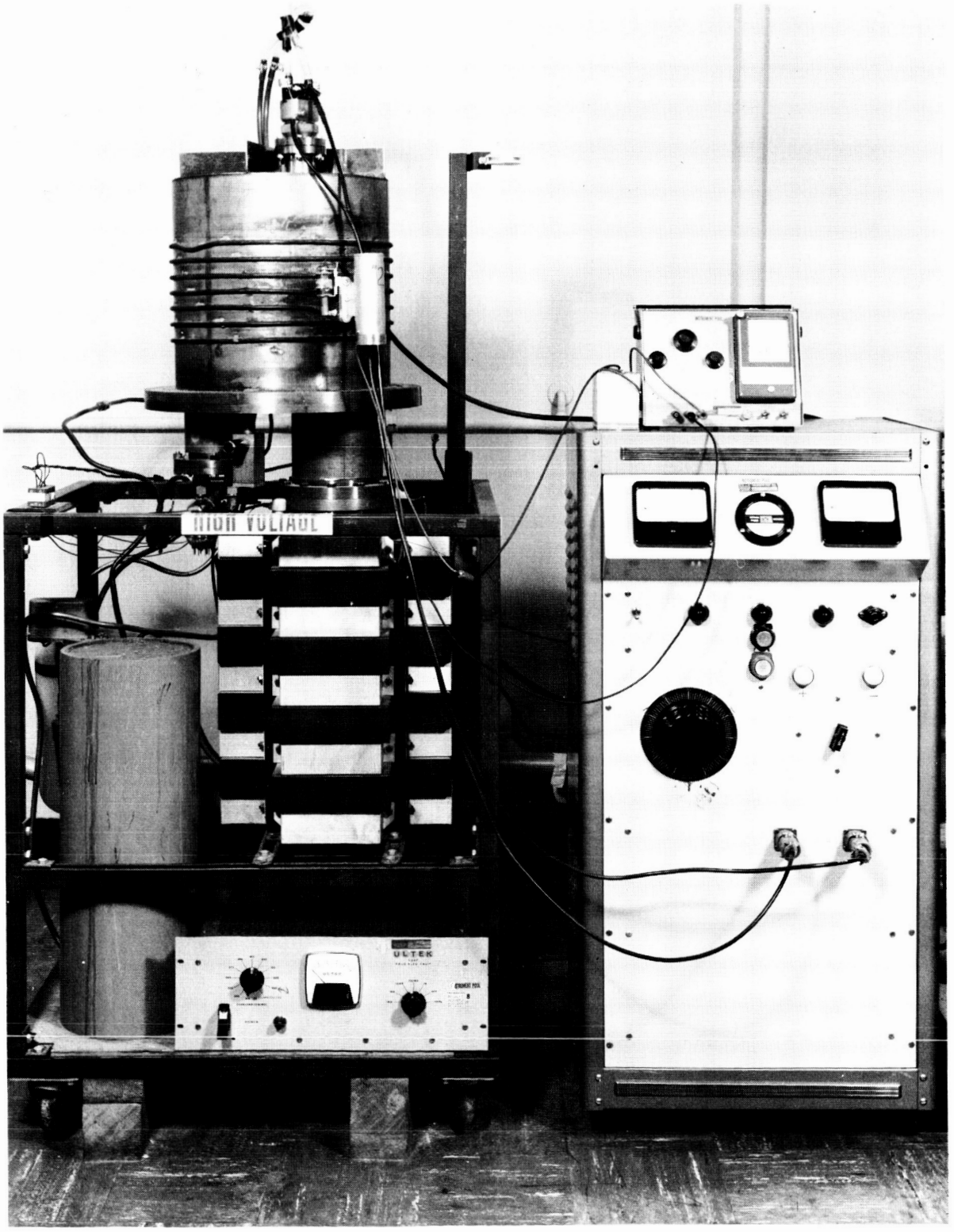

Figure C-1

Ultraviolet Radiation - High Vacuum Exposure
Apparatus

extended into the exposure chamber from the top. The assembly can be withdrawn to change lamps without disturbing the established vacuum. Unless a lamp ruptures, it is run for 100 hours, and then replaced. Each test is begun with a new lamp. This procedure is followed because the AH-6 output decreases with time more in the 2000 – 3000Å interval than in the 3000 – 4000Å interval. Therefore, for materials which are degraded primarily by energy of wavelengths less than 3000Å, an old lamp will produce less degradation than a new lamp for the same total ultraviolet exposure, expressed in sun-hours. Some control over this effect is achieved through following this standard replacement procedure.

The ultraviolet intensity is monitored external to the vacuum chamber with a calibrated RCA 935 phototube in conjunction with a Corning 7-54 filter, which transmits only the near ultraviolet output of the lamp. The output of the phototube is automatically measured and recorded for a few minutes each hour with a recording microammeter. The intervening quartz window and 7-54 filter are periodically checked for degradation in spectral transmittance and cleaned or replaced as necessary. When desired, a Corning 0-54 filter is used to compare the intensity in the 2000 to 3000Å region to that in the 3000 to 4000Å region as a measure of the relative degradation of lamp output in the shorter wavelength regions.

The effect of ultraviolet radiation on the optical properties is evaluated by measuring the spectral reflectance immediately before and after irradiation with a Cary Model 14 spectrophotometer and integrating sphere in the range 0.3 to 1.8 microns. In some cases a Beckman DK-2 spectrophotometer and integrating sphere were used to extend the infrared measurement range from 1.8 microns to 2.6 microns. Both instruments effectively measure spectral near-normal reflectance.

Appendix D

PHOTOCONDUCTIVITY

The photoconductive response of Li doped ZnO was measured by a method first used by Haynes and Hornbeck in 1953[1]. This experimental procedure was later recommended as a standard by the IRE.[2] It involves a small sample at the semiconductor with end contacts connected to a constant current source. A flash of light, generated either electronically or with a mechanical chopper, is focused on the sample and the changes in conductivity of the sample are measured as changes in the voltage across the sample.

For accurate lifetime measurements, the following experimental parameters are recommended:

(a) Peak conductivity modulation of about 10 percent.

(b) The electric field across the sample should not be too large, to avoid sweeping the carriers away and altering their distribution or so small as to let diffusion effects predominate.

(c) The elimination of photovoltaic effects at the end contacts by masking.

(d) Ohmic contacts.

(e) Provision for background illumination to saturate those traps close to the valence band or to optically pump these traps close to the conduction band.

(f) Rapid decay of the light source.

---

(1) Haynes, J. R. and Hornbeck, J. A., Phys. Rev. 90 (1953), 152 – 153

(2) IRE Standards, Proc. Inst. Radio Engr., N.Y. 49 (1961), 1293 – 1299

The experimental arrangement, as used in ZnO, is illustrated in the block diagram of Fig. D-2. The light source and associated electronics consisted of a high voltage (10 kilovolts) power supply, the Abtronic Point Light Source which was an air discharge spark gap and the Abtronic Time Delay Generator. The light source had a decay time of 0.5 microseconds. The purpose of the Time Delay Generator was to delay the light flash for a few microseconds after the time base of a Tektronic 581 oscilloscope had been triggered.

The sample was mounted in a Sulfrian double dewar, fitted with appropriate windows to allow for the illumination of the sample. As well as being able to cool the sample, it was also possible to heat the sample above room temperature by means of a heater incorporated into the dewar. The leads from the sample went through a vacuum seal to a cathode follower (for impedance matching) and the output from the cathode follower went to a Tektronic 581 oscilloscope. A 90 volt D.C. battery was used as the constant current source and was connected across the sample. The light was focused on the sample by using a focusing bellows and a condensing lens. When background illumination was required it was provided by a 6 volt D.C. tungsten lamp which was positioned to illuminate the sample. Provision was also made for filtering the background illumination.

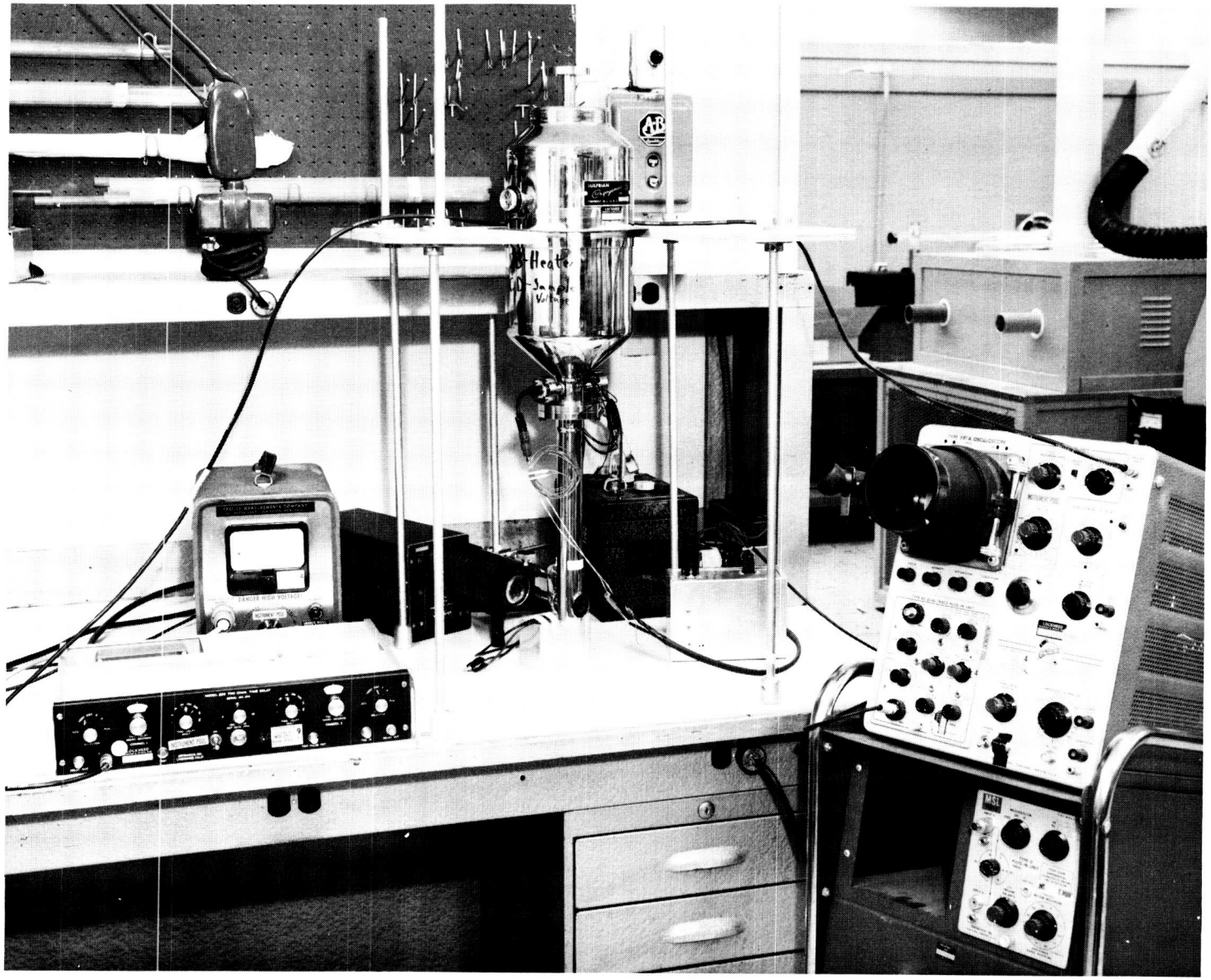

Apparatus for Transient Photoconductivity Measurements
on Zinc Oxide Single Crystals

Figure D-1

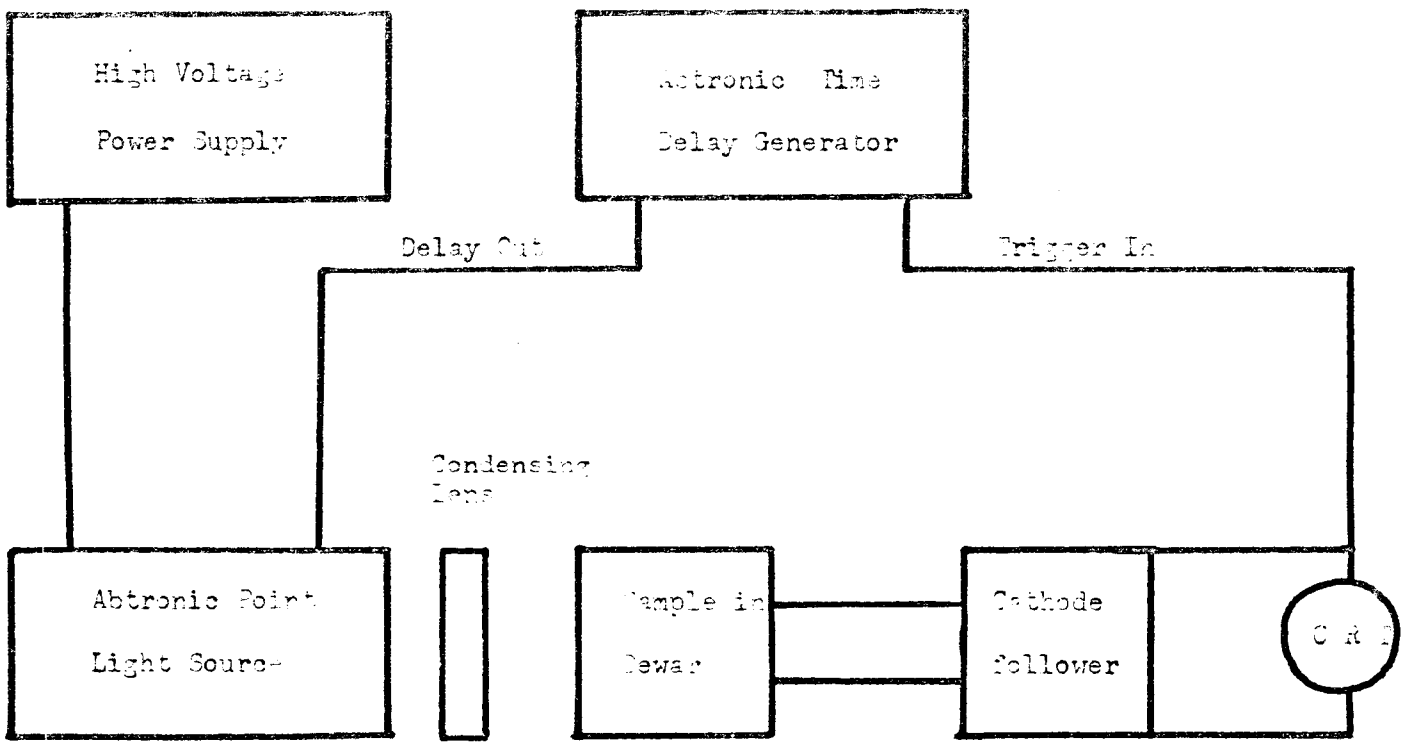

D-2 Experimental arrangement for measuring Photoconductivity